UNIVERSITY OF CALIFORNIA,
IRVINE

Ion-channel transporter complexes

DISSERTATION

submitted in partial satisfaction of the requirements
for the degree of

DOCTOR OF PHILOSOPHY

in Pharmacology

by

Daniel Loerch Neverisky

Dissertation Committee:
Professor Geoffrey W. Abbott, Chair
Professor Frederick J. Ehlert
Professor Olivier Civelli

2016

Chapter I from KCNQ1, KCNE2, and Na+-Coupled Solute Transporters Form Reciprocally Regulating Complexes That Affect Neuronal Excitability
BY GEOFFREY W. ABBOTT, KWOK-KEUNG TAI, DANIEL L. NEVERISKY, ALEX HANSLER, ZHAOYANG HU, TORSTEN K. ROEPKE, DANIEL J. LERNER, QIUYING CHEN, LI LIU, BOJANA ZUPAN, MIKLOS TOTH, ROBIN HAYNES, XIAOPING HUANG, DIDEM DEMIRBAS, ROBERTO BUCCAFUSCA, STEVEN S. GROSS, VIKRAM A. KANDA, GERARD T. BERRY
SCI. SIGNAL.04 MAR 2014 : RA22

DEDICATION

To Mom and Dad

TABLE OF CONTENTS

LIST OF FIGURES

CURRICULUM VITAE

Daniel Loerch Neverisky

2011	B.A. in Psychology, Whittier College
2011-2012	Research Assistant, University of California, Irvine
2012-2016	Ph.D. in Pharmacology, University of California, Irvine

PUBLICATIONS

KCNQ2 forms co-regulatory complexes with sodium-dependent *myo*-inositol transporters **2016**
D.L. Neverisky, G.W. Abbott. (*in preparation*)

Ion channel-transporter interactions **2016**
Critical Reviews in Biochemistry and Molecular Biology
D.L. Neverisky, G.W. Abbott.

KCNQ1, KCNE2, and Na+-Coupled Solute Transporters Form Reciprocally Regulating Complexes That Affect Neuronal Excitability **2014**
Science Signaling
G. W. Abbott, K.-K. Tai, D. L. Neverisky, A. Hansler, Z. Hu, T. K. Roepke, D. J. Lerner, Q. Chen, L. Liu, B. Zupan, M. Toth, R. Haynes, X. Huang, D. Demirbas, R. Buccafusca, S. S. Gross, V. A. Kanda, and G. T. Berry

ABSTRACT OF THE DISSERTATION

Ion channel-transporter complexes

By

Daniel Loerch Neverisky

Doctor of Philosophy in Pharmacology

University of California, Irvine, 2016

Professor Geoffrey W. Abbott, Chair

All living cells require membrane proteins that act as conduits for the regulated transport of ions, solutes and other small molecules across the cell membrane. Here, we discuss the recent discovery of two critical classes of such membrane proteins forming co-regulatory complexes *in vivo* and *in vitro;* namely, voltage-gated potassium channels and sodium-dependent *myo*-inositol transporters of the *SLC5A* family. These ion channels provide a pore that permits rapid, highly selective, and tightly regulated movement of ions down their electrochemical gradient, providing critical effects on cellular excitability and action potential termination. By contrast, the transporters move *myo*-inositol by coupling uphill movement of the substrate to downhill movement of another ion, sodium, to participate in the phosphatidylinositol signaling pathway. It is well known that proteins in each of these classes work in concert with members of the other classes to ensure, for example, ion homeostasis, ion secretion, and restoration of ion balance following action potentials. More recently, evidence is emerging of direct physical interaction between true ion channels and transporters, and regulation of ion channel activity and cellular excitability by *SLC5A* transporter SMIT1. Here, we describe discovery and functional characteristics of novel

members of a new class of the macromolecular channel-transporter complexes that we term “chansporters”, and their diverse effect on each constituent’s function.

In the first part of this dissertation, we discuss our initial discovery of chansporter complexes – that KCNQ1 and SMIT1 reciprocally augment each other’s function and that KCNQ1-associating β-subunit KCNE2 drastically alters function of the complexed transporter as well as channel.

In the second part, we discuss the discovery of the contrasting effect of KCNQ2 on SMIT1 and SMIT2 – unlike KCNQ1, KCNQ2 strongly inhibits *myo*-inositol uptake by the transporters. This effect is demonstrated to be associated with a matched reduction in transporter surface expression, but may also be altered by cellular depolarization and select mutations, suggesting that channel conformation or state may also play a role in altering transporter function. Last, co-immunoprecipitations of truncated KCNQ2 proteins and SMIT1 demonstrate that the pore-forming S5-S6 region of KCNQ2 is required for interaction with SMIT1.

INTRODUCTION

Ion channels constitute a numerous and eclectic class of membrane proteins that are essential for the function of most if not all cell types from the archaebacteria through to the plethora of specialized cells in higher mammals. Ion channels facilitate passive yet often rapid (e.g., tens of thousands of ions per second per channel pore) movement of aqueous ions across the otherwise forbidding barrier of the hydrophobic interior of the plasma membrane that evolved at least partly to prevent such leakage. Thus, ion channels rely on an electrochemical gradient for their activity. This property, together with their often remarkable ion selectivity (K^+ channels can readily permit K^+ movement but are proficient at limiting Na^+ leak, which bears similar charge to K^+ but is slightly smaller), has endowed cells with the ability to communicate on the millisecond timescale using action potentials. Conversely, some ion channels exist in non-excitable cells where their role is to ensure ion and fluid homeostasis or supply the necessary ingredients or conditions for biological functions such as hormone synthesis or mucous secretion. Another class of channels that primarily provides a conduit for water across the plasma membrane are the water channels, or aquaporins[1].

Other types of membrane proteins can also mediate movement of ions or other moieties across cell membranes but do not fall into the category of ion channels, and are referred to as "transporters". The transporters that are perhaps furthest removed conceptually from the channels are the primary active transporters, some of which are also referred to as "pumps". Rather than relying on passive diffusion, the pumps can move molecules such as

ions up an electrochemical gradient because they can utilize energy generated, for example, from hydrolysis of ATP [2,3].

Lying somewhere in the middle of the channels and the pumps are members of the Solute Carrier (SLC) superfamily that comprises facilitative transporters, which as the name suggests facilitate movement of solutes across the cell membrane down an electrochemical gradient ("downhill"), and the secondary active transporters, which can move their cargo uphill by coupling this transport to downhill movement of another solute.

Ion channels, solute carriers and pumps move ions and other solutes in and out of cells, covering a wide range of specificities, transport rates, and biological processes. Many of these functions are crucial production and secretion processes, others are events essential to intercellular communication. One would therefore expect a high degree of crosstalk between the different proteins in these classes. Recently, we and others have discovered a higher degree of crosstalk than expected, with some involving physical interaction between ion channels and transporters, with the formation of what we term "chansporter" complexes.

The majority of the channel-transporter interactions identified to date are between K^+ channels and secondary active transporters that rely on coupling uphill movement of the desired solute to downhill movement of sodium ions (sodium-coupled solute transporters). Here, we first introduce the proteins presently known to participate in chansporter formation based on the work of our studies and other labs in this rapidly growing field.

Kv channels and Ca^{2+}-activated K^+ channels

Voltage-gated potassium channel (Kv) pore-forming (α) subunits are encoded by genes of a 40-member family in humans. Conserved features among Kv α include a six transmembrane domains (S1-S6), a K^+-selective pore region formed by residues between S5 and S6, and a voltage sensor domain (VSD) comprising the S1-S4 segments, which moves in response to changes in membrane voltage (V_m) (Figure 1.1 A). The movement of the VSD controls channel opening by tugging on the intracellular S4-S5 linker region and inducing a conformational change to open the pore and permit K^+ passage [4]. Kv channels are especially well known for their essential functions in numerous excitable cell types including neurons, cardiac myocytes and skeletal muscle [5–7]. KCNQ1, the primary Kv channel discussed in Chapter I, is notable for its diverse functions in tissues including the heart, inner ear, thyroid, stomach, pancreas, lower gastrointestinal tract and choroid plexus [8–12]. KCNQ2 and KCNQ3, the primary Kv discussed in Chapter II, play a critical role in the brain, where they co-assemble to form heterotetramers known as the "M-channel" and pass "M-current", a critical regulator of cellular excitability[6,13].

The *KCNQ1* gene encodes a protein spanning six transmembrane segments, a tetramer of four such proteins forms a functional K^+-selective pore. KCNQ1 is best known for its crucial requirement in maintaining normal cardiac rhythm, arising from its role in repolarizing ventricular and atrial myocytes, responding to cellular depolarization by opening relatively slowly to permit K+ efflux and cellular repolarization to help end each heartbeat. Human KCNQ1 perturbation, e.g. by gene mutation, is associated with cardiac arrhythmias

including Long QT syndrome (LQTS) [14] and atrial fibrillation (AF) [7,15], and has also been associated with extracardiac effects such as increased susceptibility to type II diabetes mellitus (T2DM) [16–18] and gastric cancer [19,20]. In mice, *Kcnq1* gene deletion causes deafness, loss of gastric acid secretion, altered insulin sensitivity, and hypothyroidism [8,21–23]. These extracardiac defects arise from perturbation of the role of KCNQ1 in non-excitable cells such as epithelial cells of the inner ear, stomach and thyroid [8,21]– highlighting the versatility of KCNQ1 and its necessity for many diverse biological processes. KCNQ2 and KCNQ3 share the main topological features of KCNQ1, including a voltage-sensing domain and pore-forming region. Each of these proteins are associated with several forms of epilepsy and neural hyperexcitability[24–27], and, similar to KCNQ1, may also play a role in hearing and cochlear function[28].

Kv α subunits, including members of the KCNQ gene family, can interact with smaller β subunits which drastically alter their function. KCNQ1 is most well-known for its interactions with β subunits of the KCNE family (Figure 1.1A) [29]. Each of the KCNE β-subunits alters KCNQ1 function differently. KCNE1 slows and right-shifts activation, increases conductance and removes inactivation[30–33]; KCNE2 reduces peak outward current but makes KCNQ1 constitutively active [34]; KCNE3 maintains peak outward current and makes KCNQ1 constitutively active[35]; KCNE4 inhibits KCNQ1[36]; KCNE5 slows KCNQ1 activation and right-shifts the channel's voltage-dependence of activation so strongly as to render the channel inactive at physiological membrane potentials [37].

Studies utilizing *Kcne2* knockout mice in particular have revealed the role of heteromeric KCNQ1-KCNE2 channels in supporting function of the thyroid epithelial cell sodium-iodide symporter (NIS) and, in the choroid plexus epithelium, the sodium-dependent *myo*-inositol transporter (SMIT1)[12,38,39]. Investigation into the novel concept of KCNQ-transporter complexes therefore has the potential to greatly improve our mechanistic understanding of KCNQ- and KCNE-linked human diseases as well as the generalizable mechanisms by which ion channels and transporters operate, signal to one another, and are regulated.

Calcium-activated K^+ (K_{Ca}) channels also play a critical role in many realms of physiology, including smooth muscle tone, action potential regulation, and cell metabolism [40,41]. K_{Ca} channels are generally grouped into three categories: large conductance (BK), small conductance (SK), and intermediate conductance (IK) [42]. MaxiK, a member of the BK subfamily of K_{Ca} channels, is a seven transmembrane domain (S0-S6) protein with an extracellular N-terminus and large intracellular C-terminus, and must tetramerize to form a functional channel [43]. MaxiK is involved in diverse protein-protein interactions, with proteins including tubulin [44], and voltage-gated calcium channel Cav2.1 [45].

SLC-superfamily secondary active transporters

Sodium-dependent myo-inositol transporters

Both SMIT1 (*SLC5A3*) and SMIT2 (*SLC5A11*) are large transmembrane proteins of the Solute Carrier Family 5 (*SLC5A*) gene family, and they exhibit similar tissue expression patterns. These proteins, each spanning 14 transmembrane segments (Figure 1.1 B),

function as sodium-coupled symporters and actively transport *myo*-inositol uphill into the cell by coupling to downhill transport of Na^+ ions. SMIT1 is additionally capable of transporting *scyllo*-inositol, L-fucose, L-xylose, L-glucose, D-glucose, α-methyl-D-glucopyranoside, and L-fucosea. SMIT2 transports *myo*-inositol, D-*chiro*-inositol, and D-xylose [46]. The *myo*-inositol transported by each of these proteins functions as a crucial cellular osmolyte, is also a substrate of the phosphatidylinositol 4,5-bisphosphate (PIP_2) signaling pathway [47,48], and may also be converted to phosphatidylinositol (PI) – a crucial membrane component [46] (Figure 1.2). These functions are particularly pertinent to ion channel function, and especially for KCNQ1, because it (and to a greater or lesser degree many other channels) is highly sensitive to changes in both cellular volume and PIP_2 [49,50]. Perturbations to the transporters' functions are therefore predicted to alter PIP_2-dependent processes such as KCNQ1 channel function as well as cellular responsiveness to osmotic stress, and have been implicated in pathologies including Down syndrome [51,52] and bipolar disorder [53–55].

The *myo*-inositol transported by the SMIT proteins serves many important functions within the cell, perhaps the most notable of which occurs after the conversion of *myo*-inositol to PI and PIP_2 by phosphatidylinositol 4-kinase (PI4K), followed by phosphatidylinositol 5-kinase (PI5K). Without PIP_2, many channels and cellular processes effectively shut off, including KCNQ channels, transient receptor potential (TRP) channels, inwardly-rectifying potassium (Kir) channels, plasmalemmal calcium pumps (PMCA), cardiac sodium-calcium exchangers (NCX1), sodium-proton exchangers (NHEx), epithelial sodium channels (ENaC), and ryanodine-sensitive calcium channels (RyR). KCNQ channels, along with

hyperpolarization-activated cyclic nucleotide-gated (HCN) channels, are notable among the voltage-gated channels for their robust responses to PIP_2 [56–58]. PI also plays a critical role in cellular machinery including activation of the Na^+/K^+-ATPase, modulation of catecholamine synthesis by tyrosine hydroxylase, and physical association with alkaline phosphatase and acetylcholinesterase [48], and may also play a cooperative role in the actin cytoskeleton [56].

PIP_2 also plays a prominent role as a secondary messenger. When a Gq-coupled receptor is stimulated, phospholipase C (PLC) is activated and cleaves PIP_2 into constitutive components: inositol(1,4,5)-triposphate (IP3), and diacylglycerol (DAG) (Figure 1.2). DAG and IP3 each play a role in activating protein kinase C (PKC) leading to phosphorylation and altered activity of myriad cellular processes. IP3, then released into the cytosol, is free to bind to IP3 receptors, triggering calcium release from intracellular stores.

Of some level of controversy, inositol status has been implicated in various cognitive disorders. Lithium, valproic acid (VPA), and carbamazepine (CBZ) are each potent mood stabilizers which also alter inositol signaling. Lithium treatment reduces MI concentrations in the brain by 30% and concurrently elevates serum MI levels by 50% [59], and potently inhibits MI synthesis by inhibiting inositol-1 and inositol-4-monophosphatases in a substrate-dependent manner [54]. These findings appear to be consistent with later work demonstrating a lithium-induced reduction in both manic symptoms and MI levels in human brain (anterior cingulate cortex) [53]. VPA also inhibits inositol levels in the brain, although by different mechanism. Here, the treatment inhibits *myo*-inositol-1-phosphate

(MIP) synthase activity, thereby preventing conversion of D-glucose-6-phosphate (G6P) to *myo*-inositol [60]. It comes as no surprise, then, that lithium and VPA are sometimes clinically co-administered in treatment of biopolar disorder [54]. Interestingly, all three of these mood stabilizers (lithium, VPA, and CBZ) inhibit SMIT1 activity and mRNA transcript levels [55,61].

Even though inositol can be synthesized by some tissues, dietary restriction or supplementation of inositol raises/lowers inositol concentrations in most tissues, sometimes to deleterious effect [48]. In the liver, an inositol-deficient diet produces elevated triglycerides and fatty liver [62]. In the intestine, an inositol-deficient high-fat diet produces lipodystrophy and altered gross morphology [63]. Interestingly, each of these syndromes resolved upon addition of inositol to the experimental animals' diets.

Nomenclature of the SMITs can be a source of confusion. Cloned from Madin-Darby canine kidney (MDCK) cells in 1992, SMIT1 was originally known simply as SMIT [64]. In 1994 rkST1 was cloned from rabbit [65], although it was not until nearly a decade later that this protein was renamed to the more suitable "SMIT2" [66]. Last, SMIT1 is purported to have two splice variants titled "SMIT1-2" and "SMIT1-3" each of which exclude the 14th transmembrane segment of SMIT1 and possess differing c-termini [46].

In mice, deletion of the *Slc5a3* gene proves fatal shortly after birth, due to hypoventilation, although the phenotype can be rescued by supplementing the drinking water of both pup and dam with additional *myo*-inositol [67,68]. Interestingly, *SLC5A3* shares exon 1 with

mitochondrial ribosomal protein subunit 6 (*MRPS6*) with the entirety of the *SLC5A3* coding region contained by *MRPS6* exon 2. Deletion of *SLC5A3* does not alter MRPS6 expression, however. The implications of this exon-sharing are not yet clear, although there is some evidence to suggest the presence of a chimeric SMIT1/MRPS6 protein in human tissue [47,69,70].

The sodium-dependent iodide symporter

The Na^+/I^- symporter (NIS), encoded by *SLC5A5*, is a large transmembrane protein containing 13 putative transmembrane segments, an extracellular N-terminal, and a cytosolic C-terminal (Figure 1.1 B). Like other members of the *SLC5A* family, NIS exhibits a high sequence similarity to other members of the *SLC5A* gene family, particularly the sodium-multivitamin transporter (SMVT, *SLC5A6*), with the most distinct sequence differences occurring near the C-terminus. Although the prototypical function of NIS may be associated with the thyroid, the protein is also expressed and functional in the mammary glands, placenta, gastrointestinal (GI) tract [71], and potentially kidney [72,73].

In the thyroid, NIS enables active I^- uptake against the electrochemical gradient and into follicular cells - this process is the rate-limiting step in thyroid hormone (TH) biosynthesis. The I^- is then passed through to the colloid by another channel or transporter, the identity of which is still under debate. Once in the colloid, I^- undergoes oxidation by thyroid peroxidase and is incorporated into the thyroglobulin (Tg) molecule to produce monoiodotyrosine (MIT) and diiodotyrosine (DIT) in a process known as organification. The organified Tg is then resorbed by the follicular cells where, when stimulated by thyroid

stimulating hormone (TSH), the iodinated Tgs are cleaved to form either thyroxine (T_4), generated from a pair of DIT, or triiodothyronine (T_3), produced from one MIT and one DIT molecule (Figure 1.3). These THs are critical for nervous system and lung development, as well as normal metabolic function [74]. Perturbations to NIS function, accordingly, cause hypothyroidism [75]. As discussed in more detail later in this thesis, NIS and KCNQ1 have demonstrated a functional crosstalk whereby KCNQ1-KCNE2 channels regulate iodide uptake through NIS[10,38].

Sodium-dependent GABA transporters

In the brain, the inhibitory neurotransmitter GABA is transported across membranes by GABA transporters (GATs) GAT1, GAT2, GAT3 (Figure 1.1B), and the betain/GABA transporter type 1 (BGT1). At inhibitory neuronal synapses, removal of GABA from the synaptic cleft by GATs acts to terminate the GABA signaling process and is accordingly a critical component of inhibitory neuron regulation [76]. GAT3, a 12 transmembrane domain Na^+/Cl^--coupled transporter preferentially expressed in glia [76–78], is here highlighted for its newly-discovered role in ion channel-transporter complex formation[79].

Figure 1.1. *Membrane topology of channel subunits and transporters*

(**A**) Left, transmembrane topology of KCNQ voltage-gated potassium (Kv) channel a subunits and KCNE b subunits. Kv pore-forming loop pictured between S5-S6. Right, topology of Orai1. Intracellular N- and C-terminals labeled accordingly. (**B**) Upper, transmembrane topology of two SLC5A transporters. (*Left*) Sodium/*myo*-inositol co-transporter SMIT1, with extracellular N and C-terminals labeled accordingly. SMIT1 features a large intracellular loop between segments 13 and 14, as well as two large extracellular loops between segments 6–7 and 8–9. (*Right*) The sodium/iodide symporter NIS. Lower, transmembrane topology of GAT3 (SLC6A11) and a P-type ATPase a subunit such as the gastric H^+/K^+-ATPase. Extracellular N-terminus and intracellular C-terminus are labeled. Note that topology maps are shown for clarity and simplicity. High-resolution crystal structures have been solved for Orai, Kv1.2 (a mammalian relative of KCNQ channels), and vSGLT (a prokaryotic sodium galactose transporter related to mammalian SLC5A transporters). Actual structures may deviate from predicted topologies with respect to, e.g. broken helices and in some cases actual transmembrane disposition.

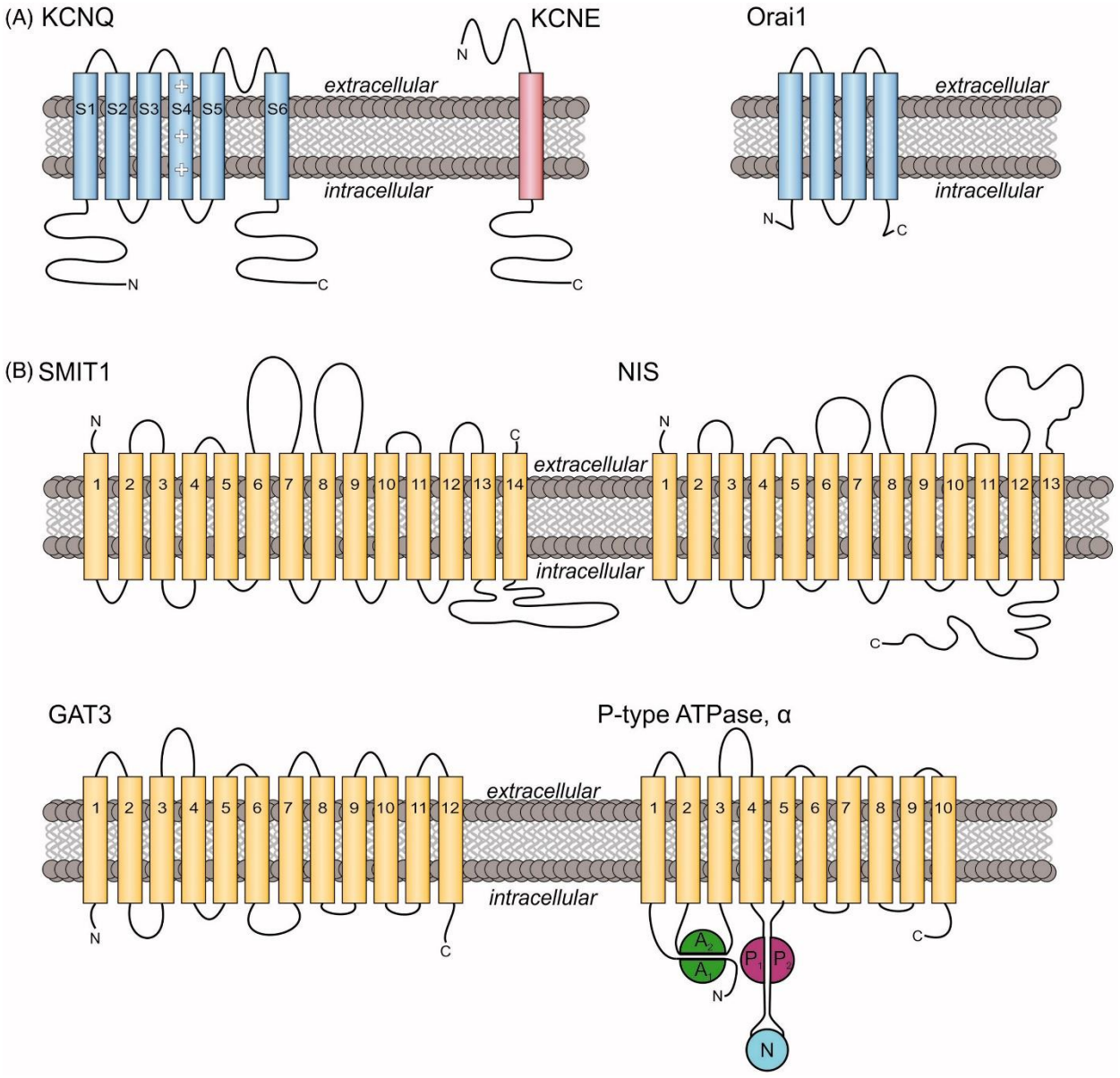
(A) KCNQ
KCNE
Orai1
S1
S2
S3
S4
S5
S6
extracellular
intracellular
N
C
(B) SMIT1
NIS
GAT3
P-type ATPase, α
A2
A1
P1
P2

Figure 1.2. *The myo-inositol pathway in the context of SMIT1 and KCNQ1–KCNE2.*

SMIT1, orange, transports sodium (Na^+) and *myo*-inositol (MI) with a stoichiometry of 2:1. Phosphatidylinositol 4-kinase (PI4K), followed by phosphatidylinositol 5-kinase (PI5K), add phosphates to MI to form phosphatidylinositol 4,5-bisphosphate (PIP2). When activated, commonly by Gq-coupled receptors, phospholipase C (PLC) cleaves PIP_2 into constituent components diacylglycerol (DAG) and inositol(1,4,5)-trisphosphate (IP3). IP3 is then recycled by dephosphorylation to inositol(1,4)-bisphosphate (IP_2) and inositol monophosphate (IP) by Inositol- 1,4 bisphosphate 1-phosphatase (IPP), and back to myoinositol by inositol- 1(or 4)- monophosphatase (IMPase). IP can also be synthesized from glucose 6-phosphate (G6P) by inositol synthase (Ino-1). KCNQ1 (Q1) with and without KCNE2 (E2) can form complexes with SMIT1, although this inter- action is not required for basic SMIT1 function. KCNQ1 gating is heavily regulated by PIP_2.

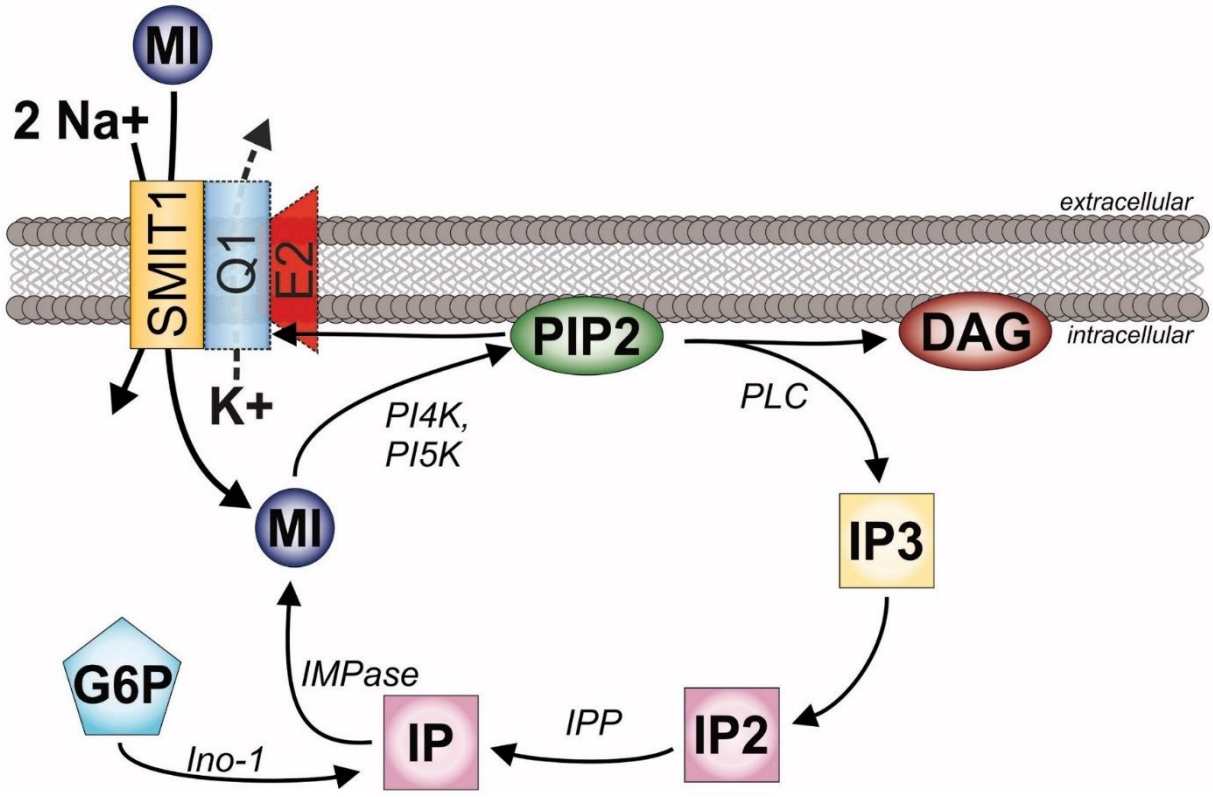
MI
2 Na+
SMIT1
Q1
E2
extracellular
intracellular
PIP2
DAG
K+
PI4K,
PI5K
PLC
MI
IP3
G6P
IMPase
IP
IPP
IP2
Ino-1

Figure 1.3. *Channel-transporter crosstalk in the thyroid*

The sodium-iodide symporter (NIS) transports Na^+ and I^- (purple) into the thyrocyte. This process is facilitated, via an incompletely resolved mechanism, by potassium ion efflux through KCNQ1–KCNE2 (Q1-E2) channels and also involves active transport by the Na^+/K^+-ATPase (Na+/K+). I^- is then passed through to the colloid by another protein (?) whose identity is still under debate. I^- undergoes oxidation by thyroid peroxidase (TPO) and is incorporated into the thyroglobulin (Tg) molecule to produce monoiodotyrosine (MIT) and diiodotyrosine (DIT) by organification. The organified Tg is then resorbed by the follicular cells where, when the thyroid stimulating hormone receptor (TSH-R) is activated, the iodinated Tgs are cleaved to form either thyroxine (T4), generated from a pair of DIT, or triiodothyronine (T3), produced from one MIT and one DIT molecule.

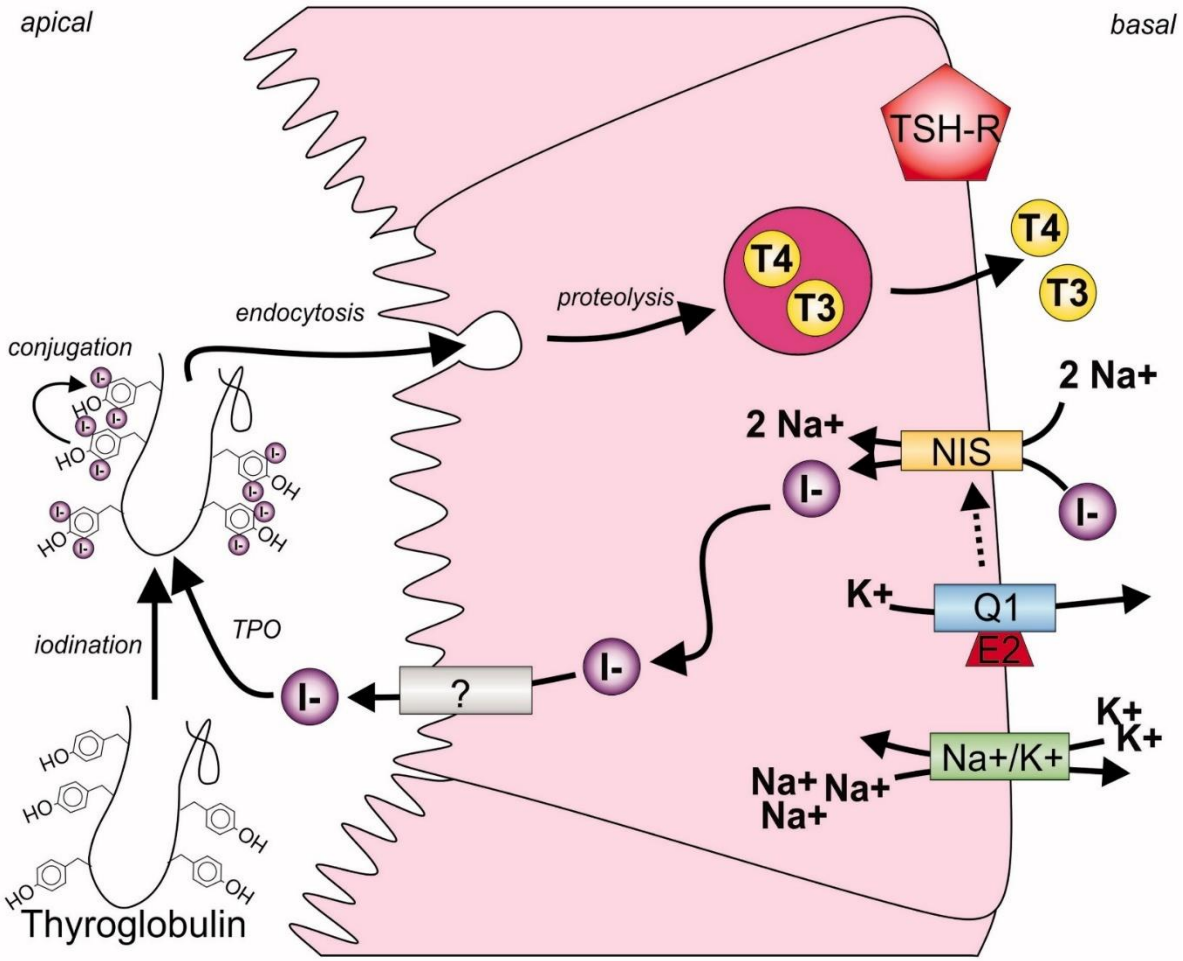
apical
basal
TSH-R
T4
T3
T4
T3
proteolysis
endocytosis
conjugation
2 Na+
2 Na+
NIS
I-
I-
K+
Q1
E2
iodination
TPO
I-
?
I-
K+
K+
Na+/K+
Na+ Na+
Na+
Thyroglobulin

References

1. Morelle, J., Goffin, E. & Devuyst, O. Molecular Physiology of Water Balance. N. Engl. J. Med. 373, 196 (2015).
2. Pedersen, P. L. & Carafoli, E. Ion motive ATPases. I. Ubiquity, properties, and significance to cell function. Trends Biochem. Sci. 12, 146–150 (1987).
3. Pedersen, P. L. & Carafoli, E. Ion motive ATPases. II. Energy coupling and work output. Trends Biochem. Sci. 12, 186–189 (1987).
4. Labro, A. J. et al. The S4-S5 Linker of KCNQ1 Channels Forms a Structural Scaffold with the S6 Segment Controlling Gate Closure. J. Biol. Chem. 286, 717–725 (2011).
5. Abbott, G. W. et al. MiRP2 Forms Potassium Channels in Skeletal Muscle with Kv3 . 4 and Is Associated with Periodic Paralysis. Channels 104, 217–231 (2001).
6. Jentsch, T. J. Neuronal KCNQ potassium channels: physiology and role in disease. Nat. Rev. Neurosci. 1, 21–30 (2000).
7. Bellocq, C. et al. Mutation in the KCNQ1 gene leading to the short QT-interval syndrome. Circulation 109, 2394–7 (2004).
8. Lee, M. P. et al. Targeted disruption of the Kvlqt1 gene causes deafness and gastric hyperplasia in mice. J. Clin. Invest. 106, 1447–1455 (2000).
9. Harchi, A. El et al. The S140G KCNQ1 atrial fibrillation mutation affects 'IKs' profile during both atrial and ventricular action potentials. J Physiol Pharmacol 1, 759–764 (2010).
10. Purtell, K. et al. The KCNQ1-KCNE2 K+ channel is required for adequate thyroid I- uptake. FASEB J. 26, 3252–3259 (2012).

11. Warth, R. et al. The role of KCNQ1/KCNE1 K(+) channels in intestine and pancreas: lessons from the KCNE1 knockout mouse. Pflugers Arch. 443, 822–8 (2002).
12. Abbott, G. W. et al. KCNQ1, KCNE2, and Na+-coupled solute transporters form reciprocally regulating complexes that affect neuronal excitability. Sci. Signal. 7, ra22 (2014).
13. Wang, H. S. et al. KCNQ2 and KCNQ3 potassium channel subunits: molecular correlates of the M-channel. Science 282, 1890–1893 (1998).
14. Tester, D. J., Will, M. L., Haglund, C. M. & Ackerman, M. J. Compendium of cardiac channel mutations in 541 consecutive unrelated patients referred for long QT syndrome genetic testing. Heart Rhythm 2, 507–17 (2005).
15. Chen, Y.-H. et al. KCNQ1 gain-of-function mutation in familial atrial fibrillation. Science 299, 251–4 (2003).
16. Unoki, H. et al. SNPs in KCNQ1 are associated with susceptibility to type 2 diabetes in East Asian and European populations. Nat. Genet. 40, 1098–102 (2008).
17. Yasuda, K. et al. Variants in KCNQ1 are associated with susceptibility to type 2 diabetes mellitus. Nat. Genet. 40, 1092–7 (2008).
18. Zhou, J.-B., Yang, J.-K., Zhao, L. & Xin, Z. Variants in KCNQ1, AP3S1, MAN2A1, and ALDH7A1 and the risk of type 2 diabetes in the Chinese Northern Han population: a case-control study and meta-analysis. Med. Sci. Monit. 16, BR179–83 (2010).
19. Roepke, T. K. et al. Targeted Deletion of Kcne2 Causes Gastritis Cystica Profunda and Gastric Neoplasia. PLoS One 5, e11451 (2010).
20. Than, B. L. N. et al. The role of KCNQ1 in mouse and human gastrointestinal cancers. Oncogene 33, 3861–8 (2014).

21. Frohlich, H. et al. Hypothyroidism of gene-targeted mice lacking Kcnq1. Pflugers Arch. 461, 45–52 (2011).

22. Grahammer, F. et al. The cardiac K+ channel KCNQ1 is essential for gastric acid secretion. Gastroenterology 120, 1363–1371 (2001).

23. Boini, K. M. et al. Enhanced insulin sensitivity of gene-targeted mice lacking functional KCNQ1. Am. J. Physiol. Regul. Integr. Comp. Physiol. 22–26 (2009). doi:10.1152/ajpregu.90839.2008.

24. Watanabe, H. et al. Disruption of the epilepsy KCNQ2 gene results in neural hyperexcitability. J. Neurochem. 75, 28–33 (2000).

25. Tinel, N., Lauritzen, I., Chouabe, C., Lazdunski, M. & Borsotto, M. The KCNQ2 potassium channel: Splice variants, functional and developmental expression. Brain localization and comparison with KCNQ3. FEBS Lett. 438, 171–176 (1998).

26. Rogawski, M. a. KCNQ2/KCNQ3 K+ channels and the molecular pathogenesis of epilepsy: Implications for therapy. Trends Neurosci. 23, 393–398 (2000).

27. Schroeder, B. C., Kubisch, C., Stein, V. & Jentsch, T. J. Moderate loss of function of cyclic-AMP-modulated KCNQ2/KCNQ3 K+ channels causes epilepsy. Nature 396, 687–690 (1998).

28. Jin, Z., Liang, G. H., Cooper, E. C. & Järlebark, L. Expression and localization of K channels KCNQ2 and KCNQ3 in the mammalian cochlea. Audiol. Neurotol. 14, 98–105 (2009).

29. Abbott, G. W. Biology of the KCNQ1 Potassium Channel. New J. Sci. 2014, 1–26 (2014).

30. Tristani-Firouzi, M. & Sanguinetti, M. C. Voltage-dependent inactivation of the human K + channel KvLQT1 is eliminated by association with minimal K + channel (minK) subunits. J. Physiol. 510, 37–45 (1998).

31. Sesti, F. & Goldstein, S. A. N. Single-Channel Characteristics of Wild-Type IKs Channels and Channels formed with Two MinK Mutants that Cause Long QT Syndrome. J. Gen. Physiol. 112, 651–663 (1998).

32. Sanguinetti, M. C. et al. Coassembly of KVLQT1 and minK (IsK) proteins to form cardiac IKS potassium channel. Nature 384, 80–83 (1996).

33. Barhanin, J. et al. K(V)LQT1 and lsK (minK) proteins associate to form the I(Ks) cardiac potassium current. Nature 384, 78–80 (1996).

34. Tinel, N. KCNE2 confers background current characteristics to the cardiac KCNQ1 potassium channel. EMBO J. 19, 6326–6330 (2000).

35. Schroeder, B. C. et al. A constitutively open potassium channel formed by KCNQ1 and KCNE3. Nature 403, 196–9 (2000).

36. Grunnet, M. et al. KCNE4 is an inhibitory subunit to the KCNQ1 channel. J. Physiol. 542, 119–130 (2002).

37. Angelo, K. et al. KCNE5 induces time- and voltage-dependent modulation of the KCNQ1 current. Biophys. J. 83, 1997–2006 (2002).

38. Roepke, T. K. et al. Kcne2 deletion uncovers its crucial role in thyroid hormone biosynthesis. Nat. Med. 15, 1186–94 (2009).

39. Roepke, T. K. et al. KCNE2 forms potassium channels with KCNA3 and KCNQ1 in the choroid plexus epithelium. FASEB J. 25, 4264–73 (2011).

40. Rundén-Pran, E., Haug, F. M., Storm, J. F. & Ottersen, O. P. BK channel activity determines the extent of cell degeneration after oxygen and glucose deprivation: A study in organotypical hippocampal slice cultures. Neuroscience 112, 277–288 (2002).

41. Marrion, N. V & Tavalin, S. J. Selective activation of Ca2+-activated K+ channels by co-localized Ca2+ channels in hippocampal neurons. Nature 395, 900–905 (1998).

42. Vergara, C., Latorre, R., Marrion, N. V & Adelman, J. P. Calcium-activated potassium channels. Curr. Opin. Neurobiol. 8, 321–329 (1998).

43. Toro, L. et al. MaxiK channel and cell signalling. Pflugers Arch. Eur. J. Physiol. 466, 875–886 (2014).

44. Ou, J. W. et al. Ca2+- and thromboxane-dependent distribution of MaxiK channels in cultured astrocytes: from microtubules to the plasma membrane. Glia 57, 1280–95 (2009).

45. Indriati, D. W. et al. Quantitative Localization of Cav2.1 (P/Q-Type) Voltage-Dependent Calcium Channels in Purkinje Cells: Somatodendritic Gradient and Distinct Somatic Coclustering with Calcium-Activated Potassium Channels. J. Neurosci. 33, 3668–3678 (2013).

46. Schneider, S. Inositol transport proteins. FEBS Lett. 589, 1049–1058 (2015).

47. Buccafusca, R. et al. Characterization of the null murine sodium/myo-inositol cotransporter 1 (Smit1 or Slc5a3) phenotype: myo-inositol rescue is independent of expression of its cognate mitochondrial ribosomal protein subunit 6 (Mrps6) gene and of phosphatidylinositol levels. Mol. Genet. Metab. 95, 81–95 (2008).

48. Holub, B. J. Metabolism and function of myo-inositol and inositol phospholipids. Annu. Rev. Nutr. 6, 563–97 (1986).

49. Hammami, S. et al. Cell volume and membrane stretch independently control K+ channel activity. J. Physiol. 587, 2225–2231 (2009).

50. Loussouarn, G. Phosphatidylinositol-4,5-bisphosphate, PIP2, controls KCNQ1/KCNE1 voltage-gated potassium channels: a functional homology between voltage-gated and inward rectifier K+ channels. EMBO J. 22, 5412–5421 (2003).

51. Berry, G. T. et al. The human osmoregulatory Na+/myo-inositol cotransporter gene (SLC5A3): molecular cloning and localization to chromosome 21. Genomics 25, 507–13 (1995).

52. Berry, G. T., Wang, Z. J., Dreha, S. F., Finucane, B. M. & Zimmerman, R. A. In vivo brain myo-inositol levels in children with Down syndrome. J. Pediatr. 135, 94–97 (1999).

53. Davanzo, P. et al. Decreased anterior cingulate myo-inositol/creatine spectroscopy resonance with lithium treatment in children with bipolar disorder. Neuropsychopharmacology 24, 359–69 (2001).

54. Harwood, A. J. Lithium and bipolar mood disorder: the inositol-depletion hypothesis revisited. Mol. Psychiatry 10, 117–26 (2005).

55. Willmroth, F. et al. Sodium-myo-inositol co-transporter (SMIT-1) mRNA is increased in neutrophils of patients with bipolar 1 disorder and down-regulated under treatment with mood stabilizers. Int. J. Neuropsychopharmacol. 10, 63–71 (2007).

56. Suh, B.-C. & Hille, B. PIP 2 Is a Necessary Cofactor for Ion Channel Function: How and Why? Annu. Rev. Biophys. 37, 175–195 (2008).

57. Hilgemann, D. W., Feng, S. & Nasuhoglu, C. The complex and intriguing lives of PIP2 with ion channels and transporters. Sci. STKE 2001, re19 (2001).

58. Loussouarn, G. Phosphatidylinositol-4,5-bisphosphate, PIP2, controls KCNQ1/KCNE1 voltage-gated potassium channels: a functional homology between voltage-gated and inward rectifier K+ channels. EMBO J. 22, 5412–5421 (2003).

59. Allison, J. H. & Stewart, M. A. Reduced Brain Inositol in Lithium-treated Rats. Nat. New Biol. 233, 267–268 (1971).

60. Shaltiel, G. et al. Valproate decreases inositol biosynthesis. Biol. Psychiatry 56, 868–874 (2004).

61. Lubrich, B. & van Calker, D. Inhibition of the high affinity myo-inositol transport system: a common mechanism of action of antibipolar drugs? Neuropsychopharmacology 21, 519–29 (1999).

62. Hayashi, E., Maeda, T. & Tomita, T. The effect of myo-inositol deficiency on lipid metabolism in rats. Biochim. Biophys. Acta - Lipids Lipid Metab. 360, 134–145 (1974).

63. Hegsted, D. M., Hayes, K. C., Gallagher, A. & Hanford, H. Inositol deficiency: an intestinal lipodystrophy in the gerbil. J. Nutr. 103, 302–7 (1973).

64. Kwon, H. M. et al. Cloning of the cDNA for a Na+/myo-inositol cotransporter, a hypertonicity stress protein. J. Biol. Chem. 267, 6297–301 (1992).

65. Hitomi, K. & Tsukagoshi, N. cDNA sequence for rkST1, a novel member of the sodium ion-dependent glucose cotransporter family. Biochim. Biophys. Acta - Biomembr. 1190, 469–472 (1994).

66. Coady, M. J., Wallendorff, B., Gagnon, D. G. & Lapointe, J. Y. Identification of a novel Na+/myo-inositol cotransporter. J. Biol. Chem. 277, 35219–35224 (2002).

67. Berry, G. T. et al. Loss of murine Na+/myo-inositol cotransporter leads to brain myo-inositol depletion and central apnea. J. Biol. Chem. 278, 18297–302 (2003).

68. Chau, J. F. L., Lee, M. K., Law, J. W. S., Chung, S. K. & Chung, S. S. M. Sodium/myo-inositol cotransporter-1 is essential for the development and function of the peripheral nerves. FASEB J. 19, 1887–9 (2005).

69. Porcellati, F. et al. Alternate splicing in human Na+-MI cotransporter gene yields differentially regulated transport isoforms. Am. J. Physiol. 276, C1325–C1337 (1999).

70. Porcellati, F. et al. Human Na(+)-myo-inositol cotransporter gene: alternate splicing generates diverse transcripts. Am. J. Physiol. 274, C1215–C1225 (1998).

71. Dohán, O. et al. The Sodium/Iodide Symporter (NIS): Characterization, Regulation, and Medical Significance. Endocr. Rev. 24, 48–77 (2003).

72. Vayre, L. et al. Immunohistochemical analysis of Na+/I- symporter distribution in human extra-thyroidal tissues. Eur. J. Endocrinol. 141, 382–386 (1999).

73. Spitzweg, C. et al. Expression of the sodium iodide symporter in human kidney. Kidney Int. 59, 1013–1023 (2001).

74. Morreale de Escobar, G., Obregon, M. J. & Escobar del Rey, F. Role of thyroid hormone during early brain development. Eur. J. Endocrinol. 151 Suppl , U25–37 (2004).

75. Carrasco, N. Iodide transport in the thyroid gland. Biochim. Biophys. Acta - Rev. Biomembr. 1154, 65–82 (1993).

76. Jin, X.-T., Galvan, A., Wichmann, T. & Smith, Y. Localization and Function of GABA Transporters GAT-1 and GAT-3 in the Basal Ganglia. Front. Syst. Neurosci. 5, 1–10 (2011).

77. Jin, X.-T., Paré, J. F. & Smith, Y. Differential localization and function of GABA transporters, GAT-1 and GAT-3, in the rat globus pallidus. Eur. J. Neurosci. 33, 1504–1518 (2011).

78. Borden, L. a. & Caplan, M. J. GABA transporter heterogeneity: pharmacology and cellular localization. Neurochem. Int. 29, 335–356 (1996).

79. Singh, H. et al. MaxiK channel interactome reveals its interaction with GABA transporter 3 and heat shock protein 60 in the mammalian brain. Neuroscience 317, 76–107 (2016).

Chapter I

KCNQ1, KCNE2 and Na+-coupled substrate transporters co-assemble to form co-regulatory macromolecular signaling complexes

Abstract

Na+-coupled solute transport is crucial for uptake of substrates including sugars such as *myo*-inositol, an important osmolyte and precursor for cell signaling molecules. Here, we discovered co-regulatory sugar transporter-ion channel complexes, in vivo and in vitro. Global metabolite profiling revealed that mice lacking the KCNE2 K^+ channel β subunit showed a deficiency in *myo*-inositol in cerebrospinal fluid (CSF) but not in serum. Increased stress responsiveness and seizure susceptibility in *Kcne2*–/– mice were alleviated by restoring normal CSF concentrations of *myo*-inositol. Suspecting a defect in *myo*-inositol transport in choroid plexus epithelium, we found that KCNE2 and the KCNQ1 voltage-gated potassium (Kv) channel α subunit co-assemble in the choroid plexus epithelium with SMIT1, a Na^+-coupled *myo*-inositol transporter. Heterologous co-expression demonstrated that *myo*-inositol transport by SMIT1 was specifically augmented by KCNQ1 but inhibited by the constitutively active, heteromeric KCNQ1-KCNE2 K^+ channel. SMIT1 and the related transporter SMIT2 were also inhibited by a constitutively active mutant KCNQ1, contrary to predicted driving-force effects, consistent with intimate channel-transporter coupling. Reciprocally, KCNQ1 and KCNQ1-KCNE2 activities were augmented by SMIT1 and glucose transporter SGLT1, but suppressed by SMIT2. Channel-transporter signaling complexes constitute a potentially widespread mechanism to facilitate solute transport and electrochemical crosstalk.

Introduction

Voltage-gated potassium (Kv) channel pore-forming α subunits form complexes with a range of ancillary (β) subunits, such as the single-transmembrane domain proteins encoded by the KCNE gene family (Fig. 2.1A), leading to various channel subunit compositions with diverse functional characteristics[1]. The KCNQ1 K+ channel β subunit is widely distributed in both excitable and non-excitable cells of vertebrates, and is unique among the S4 gene superfamily in that it forms either voltage-activated or constitutively active K^+-selective channels depending on its specific KCNE family β subunit partner[2]. KCNQ1 and KCNE gene disruption are linked to multiple pathologies, often with an unclear molecular etiology. A sequence variant in exon 2 of human KCNE2, a gene associated with the cardiac arrhythmia long QT syndrome (LQTS)[3], has been implicated in a human cardiocerebral phenotype comprising both neonatal seizures and LQTS[4]. In addition, duplication of a 200 kb region containing KCNE1 and KCNE2 has been detected in 16 individuals with schizophrenia, compared to 7 control subjects[5]. These findings suggested potential cerebral functions for KCNE2 (a protein we originally named MinK-related peptide 1). KCNE2 protein abundance is relatively low in neuronal tissue, but it is high in the fourth and lateral ventricles, in the apical membrane of the choroid plexus epithelium, where we have also detected KCNQ1[6]. KCNQ1, typically in complexes with either KCNE2 or KCNE3, which each render KCNQ1 constitutively active, is important in various non-excitable polarized epithelial cell types. In several of these epithelial tissues, KCNQ1-containing channels appear to be prerequisite for the function of ion transporters or

symporters, yet the molecular mechanisms for this necessity are unclear[6-8]. Here, while investigating the basis for the increase in neural excitability in *Kcne2*–/– mice, we discovered an ion channel-transporter signaling complex, the perturbation of which caused the CNS metabolite deficiency underlying increased excitability.

Results

Kcne2 deletion increased pentylenetetrazole-induced seizure susceptibility and mortality (Fig. 1B). Because intronic variants in human KCNE2 have also been associated with psychiatric disorders[5], we assessed the behavior of *Kcne2*–/– mice. *Kcne2* deletion reduced immobility time by ~40% in the tail suspension test (which measures despair and/or stress responsiveness) indicative of heightened stress response and/or reduced despair in *Kcne2*–/– mice compared to their *Kcne2*+/+ mice littermates[9-10] (Fig. 1C). *Kcne2* deletion did not affect motor function, balance (Fig. S1.1A) or overall activity (total locomotion or rearing) (Fig. S1.1 B,C).

KCNE2 abundance in the CNS is highest in the choroid plexus epithelium[6], which is the major site of CSF production and secretion, but *Kcne2* deletion does not significantly perturb CSF K^+ concentration or pH[6]. We therefore adopted an untargeted CSF metabolomics approach to discover potentially pathologic CSF milieu disturbances. Unsupervised principle component analysis (PCA) of liquid chromatography/mass spectrometry (LC/MS) findings demonstrated a robust and consistent difference between CSF from *Kcne2*–/– compared to *Kcne2*+/+ mice (Fig. 2.1D). Features that contributed

most significantly to this inter-genotype difference in CSF metabolites were identified based on loading plot values for the PCA analysis (Fig. 2.1E). The single greatest contributor to the observed PCA difference was tentatively identified as *myo*-inositol and affirmed by an indistinguishable LC retention time and MS/MS fragmentation pattern with that of a pure *myo*-inositol standard. Extracted ion counts verified that the 30% reduction in the concentration of *myo*-inositol in *Kcne2*–/– CSF was significant (Fig. 2.1F).

This finding was notable for two reasons. First, it was highly specific because *myo*-inositol was the only identified metabolite with a Kcne2-dependent abundance in the CSF. Second, *myo*-inositol is actively transported into the CSF from the blood primarily through the choroid plexus epithelium (to attain a CSF:blood *myo*-inositol ratio of >5:1[11]. In accord with perturbation of the *myo*-inositol concentration, an important osmolyte, *Kcne2* deletion altered choroid plexus epithelial cell shape and volume (Fig. S1.2). Strikingly, acute CSF supplementation of *myo*-inositol dose-dependently reversed behavioral abnormalities, and reduced pentylenetetrazole-induced seizure susceptibility, in *Kcne2*–/– but not *Kcne2*+/+ mice (Fig. 2.1G-J). This suggested that the CSF deficiency of *myo*-inositol was linked to the observed *Kcne2*–/– mouse CNS defects. The serum concentration of *myo*-inositol in *Kcne2*–/– mice was not significantly different from that of Kcne2+/+ mice (Fig. 1H), a finding recapitulated using a different system as confirmation (Fig. 2.2A). This was suggestive of local perturbation of *myo*-inositol active transport at the level of the choroid plexus rather than a systemic defect in *myo*-inositol homeostasis. Furthermore, *Kcne2* deletion did not alter total SMIT1 protein expression in mouse choroid plexus epithelium or kidney (Fig. 2.2B), ruling out a general reduction of SMIT1 (Slc5a3) protein expression.

Controversy surrounding the role of variations in the CSF concentration of *myo*-inositol in psychiatric disease notwithstanding[11-12], our data suggest that the perturbation in CSF *myo*-inositol content is linked with a pathological CNS excitability in the Kcne2-deficient mouse. Without affecting *Kcne2*+/+ mice, *myo*-inositol supplementation normalized two 'increased excitability' phenotypes in *Kcne2*–/– mice: increased seizure activity, and increased mobility in the tail suspension test, which probably reflects an increased responsiveness to stress[10] and if validated by antidepressants could potentially be further interpreted as decreased depressive or despair-type behavior[9].

Na^+-coupled *myo*-inositol transporter SMIT1 (SLC5A3) mRNA was previously detected in the choroid plexus epithelium[13]; here, we visualized SMIT1 protein in mouse choroid plexus epithelium, employing tissue from *Slc5a3*–/– mice as a negative control for immunofluorescence detection. SMIT1 protein was detectable in both the apical and basolateral membranes of the choroid plexus epithelium (Fig. 2.2C; see additional controls in Fig. S1.3A,B). Kcne2 deletion did not prevent membrane expression of SMIT1. In some sections SMIT1 apical membrane expression was less prominent (Fig. 2.2D), possibly reflecting regional variability in, or dynamic control of, SMIT1 localization, or simply variable antigen accessibility. The existence of SMIT1 on both basolateral and apical membranes of the choroid plexus epithelium suggests it could play a role both in *myo*-inositol uptake from the blood, and also in removing excess *myo*-inositol from the CSF.

We detected KCNQ1 and KCNE2 only on the apical membrane of the choroid plexus epithelium (Fig. 2.2E,F) as before[6]. We also detected choroid plexus epithelial KCNQ1-

KCNE2 and Kv1.3-KCNE2 protein complexes (Fig. 2.2G) as expected from our prior functional studies[6]. In addition, we made the surprising discovery that KCNE2 and KCNQ1 co-assemble with SMIT1 in the choroid plexus epithelium (Fig. 2.2G,H). KCNQ1-SMIT1 co-localization was observable in choroid plexus apical membrane (Fig. S1.3C).

SMIT1-KCNQ1 co-assembly was confirmed in heterologous co-expression studies (Fig. 2.3 A). When co-expressed in *Xenopus laevis* oocytes, SMIT1 doubled KCNQ1 outward K+ current (Fig. 2.3B,C) without affecting activation voltage dependence (Fig. S1.4A). The current doubling was independent of external *myo*-inositol (Fig. 2.3D) or Na^+ (Fig. S1.4B). SMIT1 similarly doubled KCNQ1-KCNE2 channel current density in a *myo*-inositol-independent manner (Fig. 2.3E,F). In contrast, SMIT1 neither co-immunoprecipitated with KCNQ4 (closely related to KCNQ1) (Fig. 2.3G) nor altered KCNQ4 current density, which was also unaffected by SMIT2 (Fig. 2.3H).

Reciprocally, KCNQ1 co-expression doubled steady-state *myo*-[2-3H(N)] inositol uptake by SMIT1, whereas KCNQ4 – despite similar voltage-dependent activation properties to KCNQ1 – had no effect (Fig. 2.4A). Surprisingly, however, KCNQ1-KCNE2 (but not KCNE2 alone) inhibited SMIT1 steady-state *myo*-[2-3H(N)] inositol uptake by ~70%, an effect that was not overcome by doubling the amount of SMIT1 cRNA injected while maintaining KCNQ1-KCNE2 cRNA constant (Fig. 2.4B). This was inconsistent with an exclusively electrochemical gradient-based explanation for KCNQ1 effects on SMIT1 given that KCNE2 converts KCNQ1 to a constitutively active K+ channel and therefore drives the membrane potential toward the equilibrium potential for K^+ (E_K). This membrane hyperpolarization

(compared to that of cells expressing the homomeric, voltage-dependent KCNQ1 channel) increases the driving force (under physiological conditions) for inward Na^+ movement such as occurs during electrogenic *myo*-inositol active transport, and would therefore be predicted to increase, rather than decrease, *myo*-inositol uptake by SMIT1[14]. Similarly, co-expression with SMIT1 of KCNQ1 harboring a voltage sensor point mutation (R231A) endowing constitutive channel activation[2] also strongly inhibited SMIT1 activity (~80%; Fig. 4A). With wild-type KCNQ1 co-expressed, SMIT1 activity was highly sensitive to KCNQ inhibitor XE991 (10 μM); the R231A mutation tempered this sensitivity (Fig. 4C). SMIT1 *myo*-[2-3H(N)] inositol uptake was still Na+-dependent with KCNQ1 co-expressed (Fig. 2.4D).

In contrast to SMIT1, SMIT2 decreased KCNQ1 current by 60% at +60 mV (without affecting KCNQ4, Fig. 3H), whereas SGLT1 augmented KCNQ1 current by 40% (Fig. 2.5A,B). Similar to SMIT1, effects of SMIT2 and SGLT1 on KCNQ1 did not involve altered voltage dependence and required neither external *myo*-inositol nor Na^+ (Fig. S1.4A,C-F). SMIT2 also inhibited KCNQ1-KCNE2 current (by ~50% at +60 mV; Fig. S5A,B). Effects on channel activity of the transporters studied were consistent over multiple oocyte batches (Fig. 2.5C).

Macroscopic (whole-oocyte) SMIT2 *myo*-[2-3H(N)] inositol uptake was suppressed by R231A-KCNQ1 but not altered by wild-type KCNQ1 (± KCNE2) (Fig. 2.5D). Wild-type KCNQ1 (± KCNE2) rendered SMIT2 susceptible to inhibition by KCNQ1-specific blocker (-)-

[3*R*,4*S*]-Chromanol 293B (20 μM) (Fig. 2.5E) without removing sensitivity to phlorizin addition or Na^+ removal (Fig. S1.5C,D).

Discussion

Our findings demonstrate the existence of co-regulatory ion channel-transporter signaling complexes in biological systems. While it is possible these complexes form to provide proximity such that K^+ efflux through the channel maintains a local electrical gradient facilitating electrogenic Na^+ influx, the observed sensitivity of transporter activity to KCNQ1 voltage sensor and/or pore status, together with functional effects counter to predicted driving force effects, suggest intimate functional and physical coupling.

Myo-inositol, an osmolyte involved in cell volume regulation, is also a precursor for cell signaling substrates including phosphatidylinositol and phosphatidylinositolphosphate lipids such as phosphatidylinositol 4,5-bisphosphate (PIP_2)[15]. As KCNQ1 is both PIP_2- and cell volume-sensitive[16-17], direct KCNQ1-SMIT1/2 interaction provides multiple potential feedback mechanisms to control cellular signaling and homeostasis. Notably, *Kcne2* deletion suppresses HCN channel function (Ih) in mouse thalamocortical circuits, increasing intrinsic excitability-enhanced burst firing in response to 4-aminopyridine, despite the relative paucity of neuronal KCNE2 expression[18]. Given that HCN activity is augmented by PIP_2 in vivo and in vitro[19], it is tempting to speculate that the increased seizure susceptibility of *Kcne2*-/- mice arises from HCN PIP_2 depletion because of reduced *myo*-inositol availability.

Mechanisms underlying the blood:CSF *myo*-inositol gradient and its disruption by *Kcne2* deletion remain incompletely understood. However, based on our data we suggest that choroid plexus *myo*-inositol uptake from the blood through basolateral SMIT1 is unaffected, whereas removal of KCNE2 from apical SMIT1-KCNQ1-KCNE2 complexes increases *myo*-inositol reuptake from the CSF into the choroid plexus epithelium (consistent with data in Fig. 2.4B), reducing CSF *myo*-inositol content. The newfound role of KCNQ1-KCNE2 in CSF *myo*-inositol homeostasis may impact multiple CNS disorders in which CSF *myo*-inositol levels have been implicated[20-22], including the cognitive deficits associated with Down's syndrome[23] – of particular interest given that *KCNE2* is located on human chromosome 21.

KCNQ1-KCNE2 is also required in vivo for normal activity of the sodium iodide symporter (NIS) and the gastric H^+/K^+-ATPase[7,8,24]. Furthermore, *KCNQ1* gene variants are linked to diabetes[25,26] yet the underlying mechanisms have been elusive. It remains to be determined if any or all of these processes necessitate KCNQ1-transporter complexes, whether KCNQ1 interacts with transporters in excitable cells such as cardiac myocytes, and the extent to which other ion channels and transporters participate in co-regulatory complexes.

Materials and Methods

Animal use

We generated and genotyped the *Kcne2*–/– mouse line as previously described[24] and housed and used mice according to the US National Institutes of Health Guide for the Care

and Use of Laboratory Animals. Animal procedures were approved by the Animal Care and Use Committee at Weill Medical College of Cornell University. The *Slc5a3*-/- mouse line was generated as previously described[31, 32]. Animal procedures were approved by the Institutional Animal Care and Use Committee at Boston Children's Hospital. All mice used in this study were generated from heterozygous crosses.

Data presentation and statistics

Continuous data are expressed as means ± standard error of the mean (SEM) of n independent measurements. Dichotomous data are presented as percent. Statistical comparisons were generally by 1 or 2-tailed, unpaired Student's t test or one-way analysis of variance (ANOVA) followed by Bonferroni's post hoc test, with two exceptions: seizure incidence percentages were compared using two-sided z-statistic test for proportions. In all cases, statistical significance was assumed with $P < 0.05$.

Seizure susceptibility measured by pentylenetetrazole test

Seizure susceptibility measurements were performed as previously described[27]. Briefly, pentylenetetrazole (Sigma-Aldrich) was dissolved in PBS and injected intraperitoneally to a concentration of 40-80 mg/kg bodyweight. Seizure events were observed over a period of 20 min. Mice were scored by an investigator blinded to genotype, for the sequence of four seizure behaviors produced: myoclonic jerks, clonic convulsions, tonic phase and death. Timing of the seizures and their duration after pentylenetetrazole injection was recorded. Myoclonus was defined as a single movement of the mouse that involved a downward motion of the head, combined with a single jerk of the body, and a brief upward extension

of the tail. Clonus was usually the second seizure behavior to occur chronologically after pentylenetetrazole injection and was defined as rapidly repetitive, often violent jerks of the mouse that involved the entire body, typically ending with the mouse falling to one side. The tonic stage of the seizure, when reached, was defined as a slow hind limb extension. Tonic stage was in some cases followed by death. Where appropriate, intraperitoneal injection of *myo*-inositol in vehicle (saline), or of vehicle alone, was performed by a non-scorer 30 min prior to intraperitoneal injection of pentylenetetrazole.

Behavioral tests

The tail suspension test (TST) was performed according to standard procedure[9], with the scorers blinded to genotype and content of injections. Where appropriate, intraperitoneal injection of *myo*-inositol or (-)-[3*R*,4*S*]-Chromanol 293B in vehicle (PBS), or of vehicle alone, was performed by a non-scorer 30 min prior to testing. Rotarod and open field tests were performed as previously described by M.T. and B.Z.[28]; rotarod performance was timed manually, and open field test performance quantified digitally, both by a scorer blinded to genotype.

CSF Metabolomics/mass spectrometry (MS)

CSF was isolated from the cisterna magna of 3-6 month old *Kcne2*+/+ and *Kcne2*–/– mice using a modification of a previously described technique[29]. Briefly, mice were initially anesthetized with 1% isoflurane in 100% oxygen in a Plexiglas chamber and then placed in a small animal stereotaxic apparatus (model 900, David Kopf Instruments, Tujunga, CA) fitted with a mouse anesthesia mask (David Kopf Instruments) with ear bars to minimize

movement of the head. With the head locked in place, the body of the mouse was allowed to drop, allowing access to the neck region. The neck was shaved, and an incision made using a sterile scalpel (no. 10 blade) and the muscles of the neck separated by blunt dissection to reveal the cisterna magna. Glass borosilicate capillary tubes (B100-78-10, Sutter Instrument, Novato, CA), pulled on a vertical micropipette puller (PP-830, Narishige, Japan) to generate a tapered tip with an inner diameter of roughly 0.6 mm, were then used to penetrate the cisterna magna and CSF was drawn into the capillary tubes. A 1 ml syringe with polyethylene tubing attached to the end (to allow tight connection with the capillary tube) was then used to remove the CSF from the capillary tube. CSF samples were then placed on dry ice and transferred to -80° C until analysis. Mice were then killed by CO2 asphyxiation. For MS data acquisition, CSF samples were extracted 1:20 in 70% acetonitrile (ACN) containing 0.2% acetic acid, vortexed, and centrifuged at 15,000 RPM for 10 min to remove cell debris. Supernatants were transferred to 250 µL conical polypropylene vials, capped and loaded into the liquid chromatography (LC) autosampler for analysis. Samples (2 µL) were analyzed using an LC-MS system and platform for untargeted metabolite profiling. A 1200 Series LC system (Agilent Technologies, Santa Clara, CA) with a 2.1 x 150 mm Cogent Diamond HydrideTM column (3.5 µm particle size, Microsolv Technology Corp, Eatontown, NJ) was utilized for chromatographic separation. MS analysis on post-column flow used Agilent Series 6230 Accurate Mass time-of-flight (TOF) mass spectrometer, equipped with dual spray electrospray ionization (ESI) source, operating in positive ion mode.

LC parameters for ANP separation were as follows: 2 µl injection volume, 25°C column temperature, and a 0.4 ml/min mobile phase flow rate. The mobile phase consisted of 0.2% acetic acid in ddH2O (solvent A) and 0.2% acetic acid in acetonitrile (solvent B) with gradient steps as follows: 0-2 min, 85% B; 2-3 min, to 80% B; 3-5 min, 80% B; 5-6 min, to 75% B; 6-7 min, 75% B, 7-8 min, to 70% B; 8-9 min, 70% B; 9-10 min, to 50% B; 10-11 min, 50% B, 11.0-11.1 min, 20% B; 11.1-14 min, 20% B; 14-14.1 min, 5% B; 14.1-24 min, 5% B; 24-24.1 min, 85% B and 24-34 min, 85% B. A separate isocratic pump delivered reference mass solution (ions m/z 121.0509 and 922.0093) for continuous mass calibration during sample analysis. Spectra were acquired in 2 GHz (extended dynamic range) mode with 1.71 spectra/sec sampled over a mass/charge (m/z) range of 50-1000 Daltons. The TOF capillary voltage was set at 4000 V, the fragmenter at 175 V, the nebulizer pressure was 35 psi, and 250°C nitrogen drying gas was delivered at a flow rate of 12 l/min.

MS Data Analysis

Raw data files were processed using Agilent MassHunter Qualitative Analysis Software (B346). Molecular feature extraction (MFE) generates information in features (compounds) that are stored in files for downstream comparative data analysis by MassProfiler Professional Software (Agilent). The analytical approach employs an algorithm for data alignment across multiple groups and treats all imported files as a single dataset. Following feature alignment and quality control , the unsupervised pattern recognition algorithm principal component analysis (PCA) was chosen to examine data sets for similarly changing features, expected and unexpected clusters, and the presence of outlying samples. Compounds determined to be differentially expressed based on

statistical criteria and PCA results were assigned tentative formulae by utilizing a molecular formula generator (MFG) algorithm in Massprofiler Professional or MassHunter Qualitative Analysis. The MFG algorithm assigned molecular formula based on an optimized goodness-of-fit, considering accurate measurements of mass defect, natural isotopic abundance rations, and spacing between isotope peaks. A putative compound ID was tentatively assigned based on the MFG score and confirmed by comparison with retention times and MS/MS fragmentation of pure chemical standards.

Confirmatory quantification of myo-inositol in serum

Myo-inositol was purchased from Sigma-Aldrich. LC-MS–grade acetonitrile, methanol, and sonic dismembrator model 100 were purchased from Fisher Scientific. The internal standard, [2H6]-*myo*-inositol (MID6), was purchased from Cambridge Isotope Laboratories Inc.

Mouse serum was obtained by cardiac puncture in anesthetized mice for the collection of whole blood. The serum was deproteinized by addition of 4 volumes of 20 μM MID6 prepared in acetonitrile/water (80:20, v/v) to 1 volume of serum samples. The samples were vortexed thoroughly and centrifuged at 14,000 rpm for 15 min. The supernatant was removed and diluted 10-fold with MQ water. Samples were vortexed and centrifuged again before LC-MS/MS analysis. All serum samples were prepared in duplicates.

For calibration standards, stock solutions of *myo*-inositol were prepared in MQ water at a final concentration of 10 mM. The calibration standard concentrations were 500, 125,

31.25, 7.81, and 1.95 µM of *myo*-inositol, also prepared in MQ water. Twenty microliters of each standard was mixed with 80 µl of 20 µM MID6 and 900 µl of MQ water.

A Shimadzu Prominence high-performance liquid chromatography (HPLC) system was used to separate samples and standards with a SUPELCOGEL Pb column (300 × 7.8 mm, 5 µm; Supelco). The injection volume was 20 µl, and the column temperature was set at 85°C. The HPLC protocol consisted of an isocratic gradient of 100% MQ water over a 45-min period. The flow rate was 0.5 ml/min and was diverted to waste from 0 to 16 min and from 28 to 45 min. The HPLC was coupled to a triple quadrupole tandem mass spectrometer equipped with an electrospray ionization source (AB Sciex QTRAP5500). It was operated in negative mode with the following settings: curtain gas 50, ion spray voltage −4500 V, dissolvation temperature 550°C, gas1 40, gas2 40, and declustering potential and collision energy −60, −23 for inositol transition 179.0/87.0 and −55, −15 for MID6 transition 185.1/167.0, respectively. LC-MS/MS peak areas were integrated using Analyst 4.0 software. Further data analysis was performed on Excel (Microsoft).

Electron microscopy

For electron microscopy, choroid plexus tissue from the fourth ventricle of *Kcne2*+/+ and *Kcne2*–/– mice (2/gender/genotype) was washed, fixed, stained, dehydrated and then infiltrated and embedded in Spurr's resin. Sections were cut, contrasted with lead citrate, and viewed on a JSM 100 CX-II electron microscope (JEOL USA Inc., Peabody, MA) operated at 80 kV. Images were recorded on Kodak 4489 Electron Image film and then digitized on an Epson Expression 1600 Pro scanner at 900 dpi.

Immunofluorescence detection

Tissue samples from *Kcne2*+/+ and *Kcne2*–/– mice were fixed in 4% paraformaldehyde solution (Electron Microscopy Sciences, Hatfield, PA, USA), followed by incubation in 30% sucrose overnight at 4°C. Embedding was performed in an optimal cutting temperature (OCT) compound (Tissue-Tek, Torrance, CA, USA), and embedded samples were stored at -80°C. Frozen samples were cut into 10 μm thick sections (Cryomicrotome CM 1850, Leica Microsystems, Bannockburn, IL, USA). Immunofluorescence detection of Kcnq1, Smit1 and Nkcc1 was performed by either of two methods. First, using a Discovery XT processor (Ventana Medical Systems), goat polyclonal anti-KCNQ1 (pan-species) primary antibody (Santa Cruz Biotechnology #SC-10646) was used at 1mg/ml; mouse monoclonal anti-NKCC1 (Santa Cruz Biotech) at 1:500 dilution; rabbit polyclonal anti-SMIT1 (1:500, Santa Cruz Biotechnology) at 1:500 dilution. Preceding the primary antibody incubation, tissue sections were blocked for 30 minutes in 10% normal goat, rabbit or mouse serum, 2% BSA in PBS, followed by 8 minutes Avidin/Biotin block. The primary antibody incubation (3 hours) was followed by incubation with biotinylated anti-rabbit, mouse or goat IgG as appropriate (ANC kit from Vector labs). The secondary detection was performed with Streptavidin-HRP D (Ventana Medical Systems), followed by incubation with Tyramide-Alexa Fluor secondary antibodies (Invitrogen). Alternatively, for images in Fig. 2.2C,D and Fig. S1.3, immunofluorescence detection was performed manually, with the experimenter blinded to the mouse genotype, after fixing/permeabilizing sections in ice-cold acetone for 10 minutes. Biotinylation was not employed for this approach; other experimental details

were similar. Immunostained slides were viewed with an Olympus BX51 microscope and pictures were acquired using CellSens software (Olympus).

Xenopus laevis oocyte preparation

cRNA transcripts encoding human KCNE2, KCNQ1, R231A-KCNQ1 (2), KCNQ4, SMIT1, SMIT2, SGLT1 and SMCT were produced from linearized cDNA templates using the T3 or T7 mMessage mMachine kit (Ambion, Austin, TX). SMIT1 cDNA was purchased from Origene (Rockville, MD); SMIT2 and SGLT1 clones were a kind gift from Dr. Michael J. Coady and Dr. Jean-Yves Lapointe (GÉPROM, Université de Montréal); SMCT cDNA was a kind gift from Dr. Nancy Carrasco (Yale University). Channel subunit and transporter cRNA was quantified by spectrophotometry and size integrity verified by gel electrophoresis. Defolliculated stage V and VI *Xenopus laevis* oocytes (Ecocyte Bioscience, Austin, TX) were injected with one or more of the cRNAs above (KCNQ1, 10 ng; KCNE2, 4 ng/oocyte; transporters, 5-25 ng/oocyte as described in text). Oocytes were incubated at 16 oC in ND96 solution containing penicillin and streptomycin with daily washing, for 4-5 days before functional or biochemical assays.

Two-electrode voltage clamp (TEVC) and myo-[2-3H(N)]-inositol flux assays

TEVC recordings were performed at room temperature using an OC-725C amplifier (Warner Instruments, Hamden, CT) and pClamp8 software (Molecular Devices, Sunnyvale, CA), 4-5 days after cRNA injection. Oocytes were bathed in a small-volume oocyte bath (Warner) and viewed with a dissection microscope. Bath solution was (in mM): 96 NaCl, 4 KCl, 1 MgCl2, 1 CaCl2, 10 HEPES (pH 7.6) ($4K^+/96Na^+$ solution) with/without Na^+

replacement by NMDG, and/or addition of phlorizin (500 µM) and/or *myo*-inositol (1 mM); bath chemicals were from Sigma Aldrich unless otherwise indicated. TEVC pipettes were of 8 MΩ resistance when filled with 3 M KCl. Currents were recorded with a Voltage protocol consisting of 3 s pulses between -120 mV and 60 mV at 20 mV intervals each followed by a 1 s tail pulse to -30 mV, from a holding potential of -80 mV.

TEVC data analysis was performed with pClamp8, Excel (Microsoft) and Origin 6.1 (OriginLab Corp., Northampton, MA). Values are stated as mean ± SEM. Normalized tail current was plotted versus prepulse voltage and fitted with a single Boltzmann function according to:

$$g = (A_1 - A_2) / \{1 + \exp[(V_{1/2} - V)/V_s]\} + A_2$$

where g is the normalized tail conductance, A_1 is the initial value at -∞, A_2 is the final value at +∞, $V_{1/2}$ is the half-maximal voltage of activation and V_s the slope factor. KCNQ1 current activation curves were fitted with a standard (zero-shift) double exponential function with Chebyshev 4-point smoothing filter.

Radiolabeled *myo*-inositol uptake assays using *myo*-[2-3H(N)] inositol (American Radiolabeled Chemicals, Inc, Saint Louis, MO, USA) were performed 5 days after oocyte cRNA injection. For each condition/expression group, 6-12 oocytes were placed in a round-bottomed, 10 ml culture tube, washed and resuspended in ND96 or NMDG-substituted ND96 (200 µl/tube) containing *myo*-[2-3H(N)] inositol (3 µCi/ml) with/without phlorizin (Sigma) (500 µM), XE991 (Sigma) (10 µM) or C293B (Tocris) (20 µM). After 30 minutes at room temperature, oocytes were washed 2-3 times in 3 ml ND96

or NMDG-substituted ND96 containing 1 mM cold *myo*-inositol (Sigma) followed by 1-2 washes in 3 ml ND96. Oocytes were next individually placed in wells of a 96-well plate, lysed in 100 µl 2% SDS in ND96, then each lysed oocyte was transferred to a scintillation vial (1 oocyte/vial) containing Ready Protein Plus scintillation fluid (Beckmann Coulter, Fullerton, CA) (6 ml). Vials were capped, shaken vigorously, then allowed to sit at room temperature for at least 30 minutes before scintillation counting in a Beckmann Coulter 6500. Repeat scintillation counts on the same sets of vials 24 h following the first count were never significantly different from the first count (data not shown). Each experiment was performed on several batches of oocytes from different deliveries as described in the figure legends; results presented are either raw data from a single representative batch, or in some cases pooled data from 2 or more batches normalized to the mean value of uptake of the intra-batch control group (either transporter alone, or in the absence of inhibitor).

Protein biochemistry

For choroid plexus epithelial studies, adult *Kcne2*+/+ and *Kcne2*–/– mice were killed by CO2 asphyxiation, and the choroid plexus removed from the fourth ventricle of the brain. Tissue samples were then snap-frozen in liquid N2 for use in western blot analysis. Whole choroid plexus cell lysates were isolated[30], resolved using SDS-PAGE and transferred to PVDF membranes for western blot analysis using standard techniques and equipment (Bio-Rad). Kidney tissue was similarly harvested and analyzed. PVDF membranes were incubated for 3 hours at room temperature in 5% milk with primary antibodies, diluted as follows: rabbit polyclonal anti-KCNE2 (in-house) 1:1000; goat polyclonal anti-KCNQ1 (Santa Cruz Biotech) 1:1000; GAPDH (Bio Rad) 1:100. For secondary detection,

horseradish peroxidase-conjugated species-appropriate anti-IgG antibodies (1:10,000, Bio-Rad) were used. Signals were detected with ECL-Plus chemiluminescence (Amersham Bioscience) and analyzed with a Gbox system using Gbox software (Syngene).

For *X. laevis* oocyte biochemistry, membrane fractions were prepared from oocytes injected with the appropriate cRNAs (see next section) as follows: 5-10 oocytes per group were homogenized in 1 ml lysis buffer containing: 0.3 M sucrose, 10 mM sodium phosphate and 1 mM EDTA supplemented with protease inhibitor cocktail (Sigma). The homogenate was subjected to a low spin centrifugation (4000 rpm; 15 min; 4 °C) to remove yolk protein and cell debris. Membrane fractions were then pelleted at 40,000 × g for 10 min for co-immunoprecipitation and/or western blot analysis. Protein concentrations were determined using the BCA method (Pierce, Rockford, IL, USA). For western blots, up to 5 µg of total protein was mixed with sample buffer and applied on 4–12% Bis-Tris SDS-PAGE gels (Invitrogen). Following electrophoresis, proteins were transferred onto nitrocellulose membranes (VWR). Membranes were incubated with goat anti-KCNQ1 polyclonal IgG (1:500, Santa Cruz Biotechnology), rabbit anti-SMIT1 (1:500, Santa Cruz Biotechnology), rabbit anti-SMIT2 (1:1000, MBL international) or rabbit anti-KCNQ4 (1:500, Santa Cruz Biotechnology). Horseradish peroxidase (HRP)-conjugated goat anti-rabbit or rabbit anti-goat IgG secondary antibody (Bio-Rad) was used for visualization with chemiluminescence ECL (Millipore). Signals were analyzed with a Gbox system using Gbox software (Syngene).

For co-immunoprecipitations, whole choroid plexus epithelial cell lysates or *X. laevis* oocyte crude membrane fractions were incubated with goat anti-KCNQ1 polyclonal IgG (1:500,

Santa Cruz Biotechnology), mouse monoclonal anti-Kv1.3 (1:500, NeuroMab), mouse monoclonal anti-NKCC1 (1:500, Santa Cruz Biotechnology), rabbit anti-SMIT1 (1:500, Santa Cruz Biotechnology), or rabbit anti-KCNQ4 (1:500, Santa Cruz Biotechnology) for 4-12 h before precipitation with Protein A/G agarose beads (Pierce). The reactions were washed 3-4 times and samples were eluted prior to immunoblotting as described above.

For Chinese hamster ovary (CHO) cell biochemistry, CHO cells were transfected with cDNAs for KCNQ1 and/or SMIT1-DDK-MyC (Origene). Two days post-transfection, cells were lysed in buffer containing 150 mM NaCl, 1% IGEPAL, 50 mM Tris (pH 8.0), 0.1% SDS. Lysates were centrifuged at 3,000 rcf for 15 minutes at 4°C and the pellets discarded. Lysates were normalized by total protein content (BCA Protein Assay kit, Pierce), mixed with NuPage LDS sample buffer (Life Technologies, Grand Island, NY) supplemented with 5% beta-mercaptoethanol, vortexed, heated at 37°C for 10 minutes, then briefly centrifuged at 1,000 g for 3 minutes at room temperature. Lysate samples were then separated using a NuPage 4-12% bis-tris gel with NuPage antioxidant (Life Technologies) in MOPS running buffer. Following electrophoresis, proteins were transferred to either PVDF or nitrocellulose membranes in the following buffer: 0.037% LDS, 20% MeOH, 48mM Tris base, 39 mM glycine. Membranes were then blocked in a solution of PBST (PBS + 0.1% Tween-20) + 5% nonfat milk powder; incubated at room temperature for 1-2 hours. Membranes were incubated overnight at 4°C in fresh PBST + 5% milk containing mouse monoclonal anti-DDK [1:2000] (Origene) or goat polyclonal KCNQ1 [1:1000] (Santa Cruz). After washing, membranes were incubated in PBST + 3% milk solution containing 1/5000-diluted HRP-conjugated secondary antibodies (Bio Rad) for 1 hour at room temperature.

After further washing, membranes were incubated with Luminata Forte Western HRP substrate for 5 minutes and imaged with a Syngene G Box.

For CHO cell co-immunoprecipitations, 100 µg total protein from each lysate sample was diluted with lysis buffer to 500 µl total volume and then pre-cleared with protein A/G PLUS agarose beads (Santa Cruz). Following the pre-clear step, beads were pelleted by a 5 minute spin at 1,000 rcf, 4°C, and the supernatant transferred to a new tube. Immunoprecipitating antibodies, goat polyclonal anti-KCNQ1 (Santa Cruz) or mouse monoclonal anti-DDK (Origene), were added to a dilution of 1/100 for overnight incubation at 4°C. The following day, fresh protein A/G PLUS agarose beads were washed in lysis buffer, pelleted, and reconstituted in lysis buffer to a 50% suspension (v/v). 40 µl of this suspension was added to each of the IP tubes and mixed end-over-end for 4 hours at 4°C. Beads were then pelleted, washed with lysis buffer (3x5 minutes), and then proteins eluted into NuPage LDS sample buffer for SDS-PAGE and western blotting as described above.

Figure 2.1: *Global metabolite profiling reveals that Kcne2−/− mice have depleted CSF myo-inositol, supplementation with which alleviates their neurological phenotypes.*

(**A**) Transmembrane topology of Kv channel α subunit (blue) and KCNE2 (red). (**B**) Mean seizure activity during the first 20 min after injection of pentylenetetrazole in *Kcne2*$^{+/+}$ and *Kcne2*$^{-/-}$ mice; $n = 22$ mice per genotype. *$P < 0.05$. (**C**) Mean immobility time and immobile-to-mobile switches during tail suspension test for *Kcne2*$^{+/+}$ and *Kcne2*$^{-/-}$ mice; $n = 15$ mice per genotype. *$P < 0.05$; **$P < 0.01$. (**D**) Unsupervised PCA of CSF metabolites acquired by LC-MS in positive ion mode. Relative quantification of 586 features (defined by an accurate mass and retention time pair) was obtained in CSF from all samples in at least one genotype (table S1). Data points are a three-dimensional projection that summarizes the variance of all CSF features (metabolites) from an individual mouse as three principal components, quantified as coordinates on each of three graphical projections. Results show consistent clustering of CSF metabolites for both *Kcne2*$^{+/+}$ and *Kcne2*$^{-/-}$ mice. These genotypes were distinguished by principal component 1 (PC1; quantified on the *x* axis), which accounted for >38% of total between-genotype variance. (**E**) Loading plot, depicting the relative contribution of individual features (metabolites) to the between-genotype variance observed for PC1 and PC2, as depicted in (D). The features that are most distant from the origin in PC1 are those that make the greatest contribution to distinguishing CSF in *Kcne2*$^{-/-}$ compared to *Kcne2*$^{+/+}$ mice. The single greatest contributor to PC1 variance (loading −0.948) (red arrow) was later identified as the Na^+ adduct of *myo*-inositol (RT, retention time). (**F**) Extracted ion chromatograms (EICs) for *myo*-inositol in CSF. Relative abundances for the Na^+ adduct of *myo*-inositol in CSF samples were calculated on the basis of the area under

EIC curves. The concentration of *myo*-inositol in CSF was significantly lower in*Kcne2*$^{-/-}$ compared to *Kcne2*$^{+/+}$ mice (30% decrease); n = 4 to 5 mice per genotype. ***P < 0.002. (**G**) Dose-dependent effects of intraperitoneal injection of *myo*-inositol on the immobility of *Kcne2*$^{-/-}$ mice during the final 4 min of the tail suspension test; n = 9 to 20 mice per dose. (**H**) Serum (left) and CSF (right) concentrations of *myo*-inositol in noninjected and *myo*-inositol–injected mice. No significant genotype-dependent differences (P > 0.05). (**I**) Comparison of effects of *myo*-inositol (n = 10 to 15 mice per group) on immobility time of *Kcne2*$^{+/+}$ and *Kcne2*$^{-/-}$ mice in the tail suspension test. *Significantly different from values obtained for noninjected and vehicle-injected *Kcne2*$^{-/-}$ mice only (P < 0.05). (**J**) Effects of *myo*-inositol on seizure incidence during the first 20 min after injection of pentylenetetrazole; n = 10 mice per group. Significant difference from same-genotype, vehicle-injected mice: *P < 0.05; **P < 0.01.

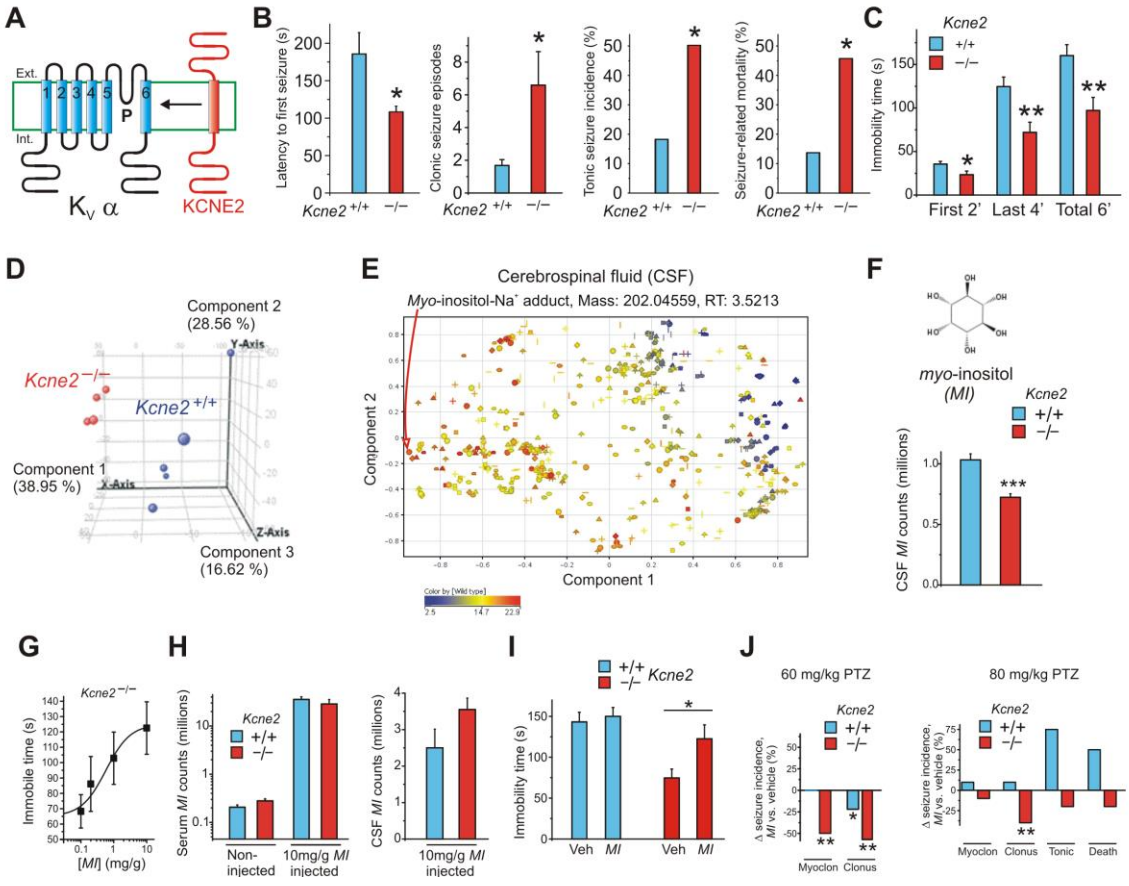
A
Ext.
1 2 3 4 5
6
P
Int.
K_V α
KCNE2
B
Latency to first seizure (s)
Clonic seizure episodes
Tonic seizure incidence (%)
Seizure-related mortality (%)
Kcne2 +/+
−/−
C
Kcne2
+/+
−/−
Immobility time (s)
First 2'
Last 4'
Total 6'
D
Component 2
(28.56 %)
Y-Axis
Kcne2 −/−
Kcne2 +/+
Component 1
(38.95 %)
X-Axis
Z-Axis
Component 3
(16.62 %)
E
Cerebrospinal fluid (CSF)
Myo-inositol-Na+ adduct, Mass: 202.04559, RT: 3.5213
Component 2
Component 1
F
myo-inositol
(MI)
Kcne2
+/+
−/−
CSF MI counts (millions)
G
Kcne2 −/−
Immobile time (s)
[MI] (mg/g)
H
Kcne2
+/+
−/−
Serum MI counts (millions)
Non-injected
10mg/g MI injected
CSF MI counts (millions)
10mg/g MI injected
I
+/+
−/−
Kcne2
Immobility time (s)
Veh
MI
Veh
MI
J
60 mg/kg PTZ
80 mg/kg PTZ
Kcne2
+/+
−/−
Δ seizure incidence, MI vs. vehicle (%)
Myoclon
Clonus
Tonic
Death

Figure 2.2: *Kcne2 and Kcnq1 co-assemble with Smit1 in mouse choroid plexus epithelium.*

(**A**) Mean serum myo-inositol concentration of *Kcne2*+/+ and *Kcne2*−/− mice (n = 5 mice per genotype). (**B**) Western blots of mouse *Kcne2*+/+ and *Kcne2*−/− choroid plexus epithelium and kidney lysates showing no appreciable effect of Kcne2 deletion on SMIT1 protein abundance, with glyceraldehyde-3-phosphate dehydrogenase (GAPDH) as a loading control (each lane using lysate from a different mouse). (**C**) Representative (of multiple sections from n = 2 mice per genotype) immunofluorescence images of adult *Slc5a3*+/+ and *Slc5a3*−/− mouse choroid plexus epithelium. White arrows, apically localized SMIT1. Scale bar, 40 μm. Green, SMIT1 antibody; blue, 4′,6-diamidino-2-phenylindole (DAPI). (**D**) Representative (of multiple sections from n = 2 mice per genotype) immunofluorescence images of adult *Kcne2*−/− mouse choroid plexus epithelium showing regions of apical membrane regions with (white arrows) or without (red arrow) SMIT1 signal. Scale bar, 40 μm. Green, SMIT1 antibody; blue, DAPI. (**E**) Immunohistochemistry of adult *Kcne2*+/+ mouse choroid plexus epithelium, showing apical localization of KCNQ1 (arrows). Scale bar, 80 μm. Brown, KCNQ1 antibody; representative of n = 3 mice. (**F**) Immunohistochemistry of adult Kcne2+/+ mouse choroid plexus epithelium, showing apical localization of KCNE2 (arrows). Scale bar, 40 μm. Brown, KCNE2 antibody; representative of n = 3 mice. (**G**) Western blots with immunoblotting (IB) antibodies as indicated, on adult Kcne2+/+ mouse choroid plexus epithelium lysates and immunoprecipitates (IP) using immunoprecipitation antibodies as indicated. Left, KCNE2 forms complexes with each of KCNQ1, Kv1.3, and SMIT1, but not NKCC1. Right, SMIT1 (arrow) forms complexes with KCNQ1 but not Kv1.3. Representative of n = 2 experiments. (**H**) Western blots with immunoblotting antibodies as indicated, on adult *Kcne2*+/+ and

Kcne2−/− mouse choroid plexus epithelium lysates and immunoprecipitates using immunoprecipitation antibodies as indicated. KCNQ1 (but not Kv1.3 or GAPDH) forms complexes with SMIT1 (but not NKCC1). Representative of n = 2 experiments. Arrow, higher exposure of blot directly above, to show KCNQ1 bands in the lysate.

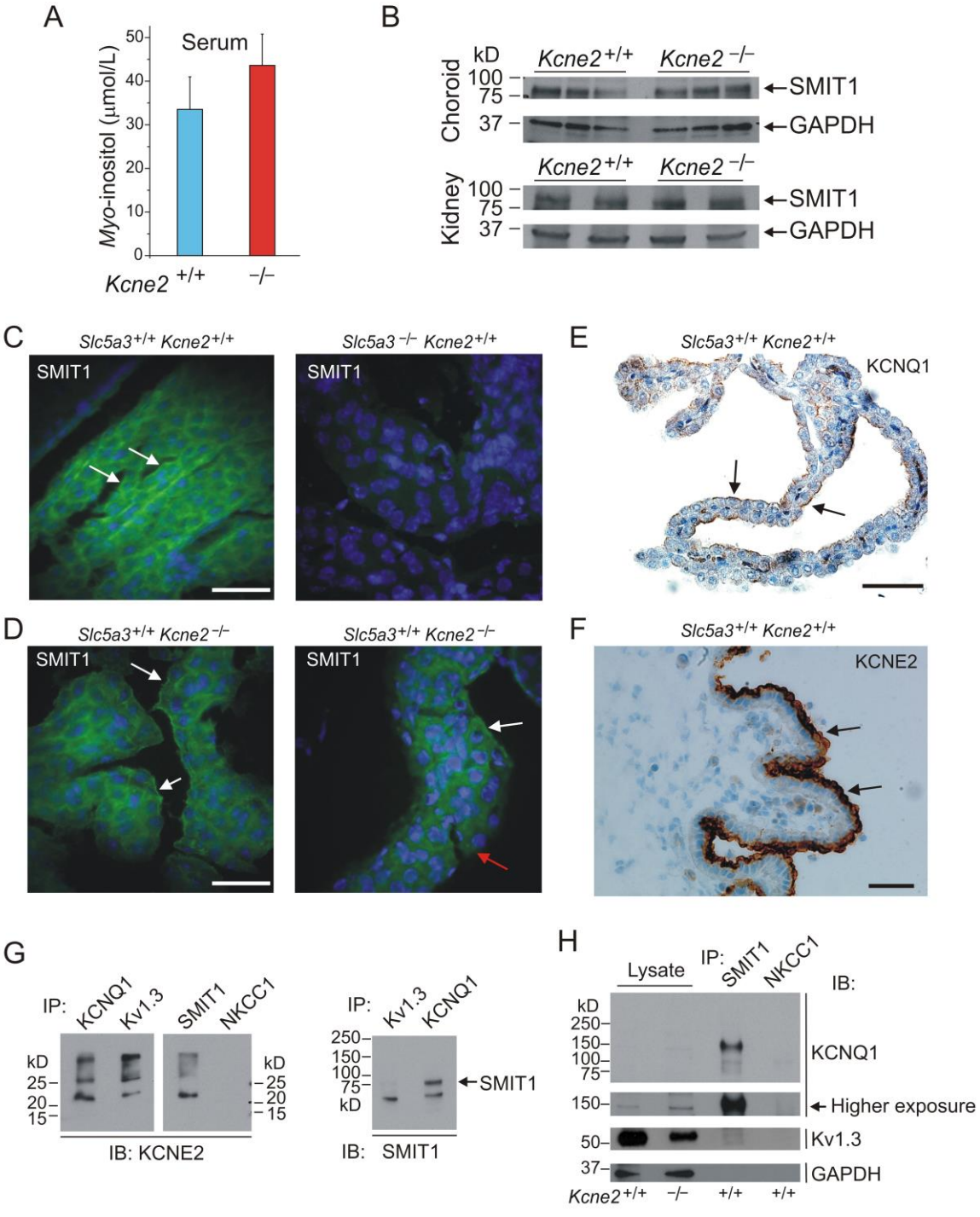
A
Serum
Myo-inositol (μmol/L)
50
40
30
20
10
0
Kcne2 +/+
−/−
B
kD
Kcne2+/+
Kcne2 −/−
Choroid
100
75
37
SMIT1
GAPDH
Kidney
C
Slc5a3+/+ Kcne2+/+
Slc5a3 −/− Kcne2+/+
SMIT1
D
Slc5a3+/+ Kcne2−/−
E
KCNQ1
F
KCNE2
G
IP:
KCNQ1
Kv1.3
SMIT1
NKCC1
IB: KCNE2
IB: SMIT1
H
Lysate
IB:
KCNQ1
Higher exposure
Kv1.3
GAPDH
Kcne2+/+ −/− +/+ +/+

Figure 2.3: *SMIT1 co-assembles with and augments activity of KCNQ1-KCNE2.*

(**A**) Western blots with immunoblotting antibodies as indicated on Chinese hamster ovary (CHO) cell lysates (upper blots) and immunoprecipitates (middle blots) using immunoprecipitation antibodies as indicated. Cells were transfected with KCNQ1 and/or Flag-tagged SMIT1 cDNA as indicated. Filled arrowheads indicate the characteristic monomer, dimer, and tetramer banding pattern of heterologously expressed KCNQ1. Single arrow indicates precipitating antibody detected by secondary antibody. Lower blots: GAPDH loading controls for lysates used in gels above. Results are representative of two independent experiments. (**B**) Exemplar current traces recorded in oocytes expressing SMIT1 and/or KCNQ1 using the standard voltage family protocol (inset). Scale bars: vertical, 1 μA; horizontal, 1 s. Zero current level is indicated by the dashed line. (**C**) Mean raw current-voltage relationships for oocytes co-injected with KCNQ1 cRNA without or with the indicated amount of SMIT1 cRNA; n = 21 (KCNQ1), 7 (SMIT1 + KCNQ1, 12.5 ng), 11 (SMIT1 + KCNQ1, 25 ng). †$P < 0.0005$ at 60 mV. N.S., nonsignificant ($P > 0.05$). (**D**) Mean raw macroscopic current-voltage relationships for oocytes in ND96 bath solution, with or without myo-inositol, co-injected with KCNQ1 cRNA and SMIT1 cRNA; n = 4 to 5 oocytes per group. (**E**) Exemplar current traces recorded in oocytes expressing SMIT1 and/or KCNQ1-KCNE2 using the standard voltage family protocol (B, inset). Scale bars: vertical, 0.5 μA; horizontal, 1 s. Zero current level is indicated by the dashed line. (**F**) Mean raw current-voltage relationships for oocytes as in (E), with or without myo-inositol in bath solution; n = 5 to 10 oocytes per group. †$P < 0.01$ at 60 mV. (**G**) Upper: Western blots of membrane-fractionated lysate (left) and KCNQ4 antibody–immunoprecipitated fraction (right) of *X. laevis* oocytes injected (Inj) with cRNA encoding KCNQ4 and/or SMIT1 and immunoblotted

with SMIT1 antibody. Arrow, the expected migration distance for SMIT1. Results are representative of two independent experiments. Middle: As above but immunoblotted with KCNQ4 antibody. Lower: Na^+- and K^+-dependent ATPase (left) and GAPDH (right) as loading controls for lysates. (**H**) Mean raw current-voltage relationships for oocytes expressing SMIT1 or SMIT2 and/or KCNQ4 using the standard voltage family protocol (B, inset); n = 9 to 12 oocytes per group.

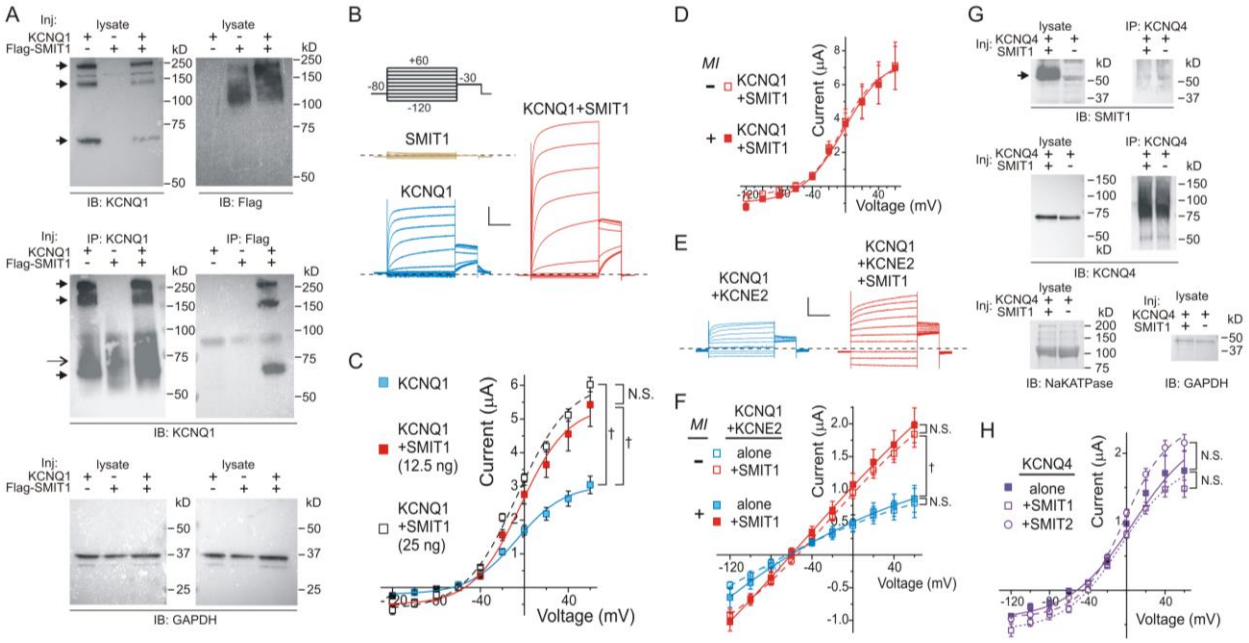

Figure 2.4: *KCNQ1 and KCNQ1-KCNE2 have differential effects on SMIT1 myo-inositol transport.*

(**A**) Mean *myo*-[2-3H(N)]inositol uptake by oocytes injected with cRNA encoding KCNQ1, KCNE2, SMIT1, KCNQ4, and/or R231A-KCNQ1 as indicated; n = 9 to 12. All SMIT1-injected groups gave mean values significantly different from those of non–SMIT1-injected groups ($P < 0.001$). (**B**) Mean *myo*-[2-3H(N)]inositol uptake by oocytes injected with cRNA encoding KCNQ1, KCNE2, and/or SMIT1 as indicated (black +, SMIT1; red +, doubled SMIT1 cRNA); n = 10 to 11. All SMIT1-injected groups gave mean values significantly different from those of the non–SMIT1-injected group ($P < 0.001$). (**C**) Effects of XE991 on myo-[2-3H(N)]inositol uptake by oocytes injected with cRNA encoding KCNQ1, R231A-KCNQ1, and/or SMIT1 as indicated, normalized to mean flux in the absence of XE991 (con); n = 9 to 12. (D) Effects of Na+ substitution with N-methyl-D-glucamine (NMDG) on mean *myo*-[2-3H(N)]inositol uptake by oocytes injected with cRNA encoding KCNQ1 and/or SMIT1 as indicated, normalized to mean flux in the presence of 96 mM NaCl; n = 12 to 13.

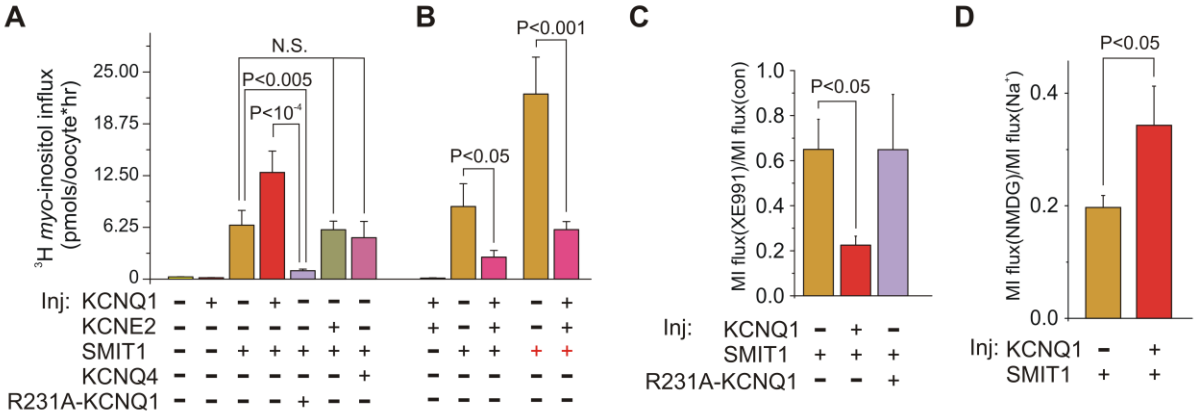

Figure 2.5: *Co-regulation of the KCNQ1 channel with SMIT2 and SGLT1 transporters.*

(**A**) Exemplar current traces recorded in oocytes expressing KCNQ1 and/or SMIT2, SMCT, and SGLT1, using the standard voltage family protocol (inset). Scale bars: vertical, 1 μA; horizontal, 1 s. Zero current levels are indicated by the dashed lines. (**B**) Mean raw current-voltage relationships for oocytes (and symbols) as in (A); n = 19 (KCNQ1), 13 (SMIT2 + KCNQ1), 12 (SMCT + KCNQ1), 16 (SGLT1 + KCNQ1). †$P < 0.0001$ at 60 mV. (**C**) Mean effects of the various transporters on KCNQ1 or KCNQ4 current density at 60 mV normalized to current density in the absence of coexpressed transporters, pooled from two to three batches of oocytes; n = 25 to 37. (**D**) Mean *myo*-[2-3H(N)]inositol uptake of oocytes injected with cRNA encoding KCNQ1, KCNE2, SMIT2, KCNQ4, and/or R231A-KCNQ1 as indicated. Data are pooled from four to five batches of oocytes and normalized to each intra-batch mean for SMIT2 alone (n = 45 to 51) except for KCNQ4 and R231A-KCNQ1 (each pooled and normalized from two batches, n = 16 to 19). (**E**) Mean *myo*-[2-3H(N)]inositol uptake by oocytes injected with cRNA encoding KCNQ1, KCNE2, and/or SMIT2 as indicated; n = 9 to 10.

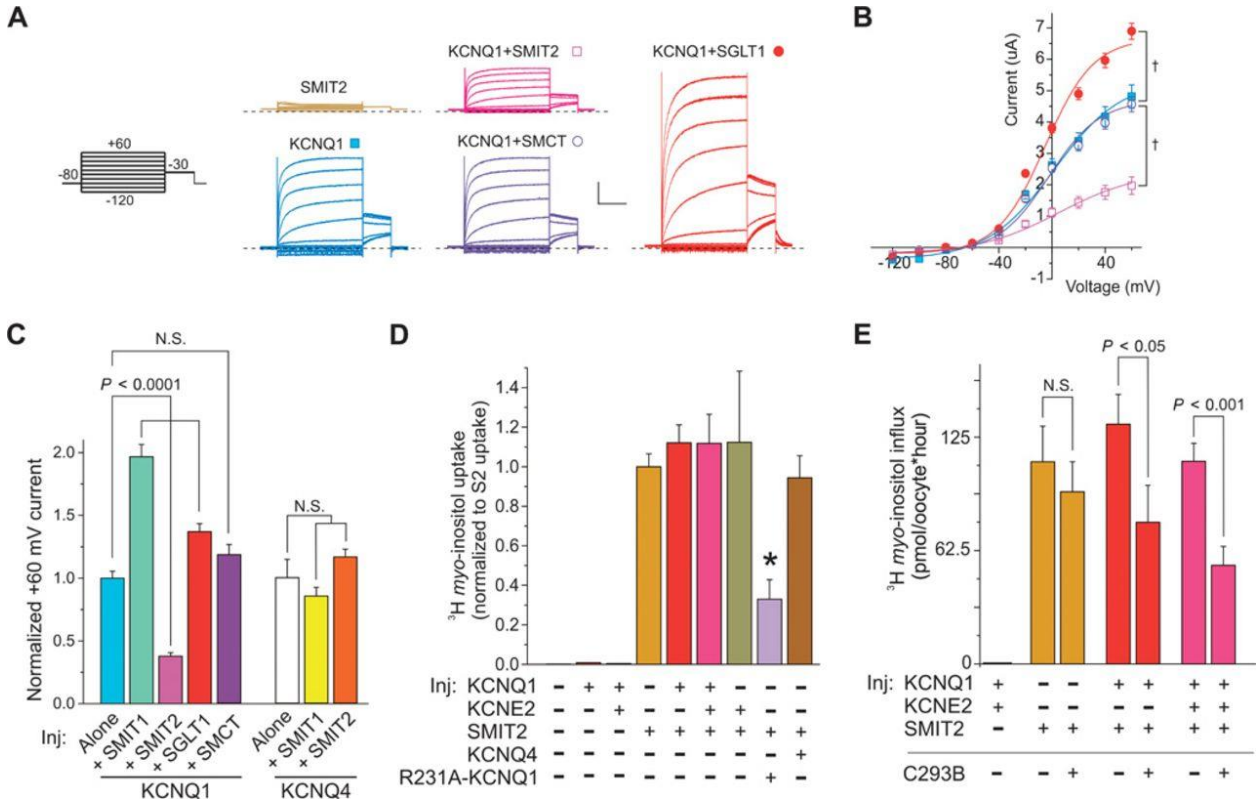
A
+60
-30
-80
-120
SMIT2
KCNQ1
KCNQ1+SMIT2
KCNQ1+SMCT
KCNQ1+SGLT1
B
Current (uA)
Voltage (mV)
-120
-80
-40
40
C
N.S.
P < 0.0001
N.S.
Normalized +60 mV current
Inj:
Alone
+ SMIT1
+ SMIT2
+ SGLT1
+ SMCT
Alone
+ SMIT1
+ SMIT2
KCNQ1
KCNQ4
D
3H myo-inositol uptake (normalized to S2 uptake)
Inj: KCNQ1
KCNE2
SMIT2
KCNQ4
R231A-KCNQ1
E
P < 0.05
P < 0.001
N.S.
3H myo-inositol influx (pmol/oocyte*hour)
Inj: KCNQ1
KCNE2
SMIT2
C293B

Figure S2.1: *Mouse motor function and activity assays*

(**A**) Mean rotarod performance of *Kcne2*+/+, *Kcne2*+/–, and *Kcne2*–/– mice; n = 7-10 mice per genotype (P>0.05 between groups).

(**B**) Mean distance covered during open field test by *Kcne2*+/+, *Kcne2*+/– and *Kcne2*–/– mice; n = 7-10 mice per genotype (P>0.05 between groups).

(**C**) Mean rearing during open field test by *Kcne2*+/+, *Kcne2*+/– and *Kcne2*–/– mice; n = 7-10 mice per genotype (P>0.05 between groups).

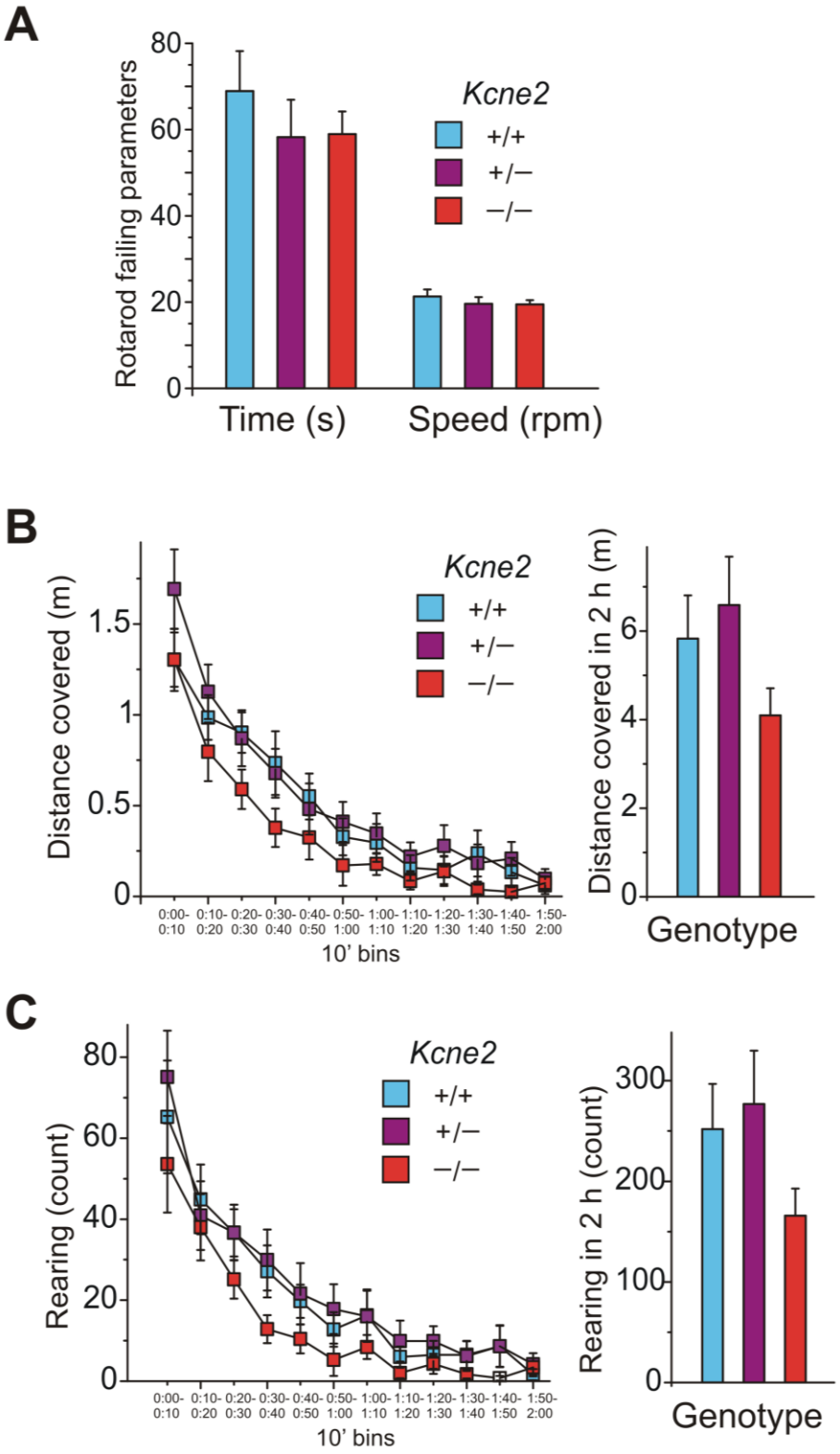
A
Rotarod failing parameters
80
60
40
20
0
Kcne2
+/+
+/–
–/–
Time (s)
Speed (rpm)
B
Distance covered (m)
1.5
1
0.5
0
Kcne2
+/+
+/–
–/–
0:00-0:10
0:10-0:20
0:20-0:30
0:30-0:40
0:40-0:50
0:50-1:00
1:00-1:10
1:10-1:20
1:20-1:30
1:30-1:40
1:40-1:50
1:50-2:00
10’ bins
Distance covered in 2 h (m)
6
4
2
0
Genotype
C
Rearing (count)
80
60
40
20
0
Kcne2
+/+
+/–
–/–
0:00-0:10
0:10-0:20
0:20-0:30
0:30-0:40
0:40-0:50
0:50-1:00
1:00-1:10
1:10-1:20
1:20-1:30
1:30-1:40
1:40-1:50
1:50-2:00
10’ bins
Rearing in 2 h (count)
300
200
100
0
Genotype

Figure S2.2: *Kcne2 deletion alters choroid plexus epithelium cell size and shape*

(**A**) Exemplar electron micrographs of CPe from *Kcne2*+/+ and *Kcne2*–/– mice. Black scale bars, 500 nm; gray scale bars, approximate thickness of CPe. MV, microvilli. Representative of n = 3 electron micrographs per genotype.

(**B**) Mean capacitance for CPe cells, n = 33-43 cells per genotype. *P<1x10-6

(**C**) Mean CPe cell height:width ratio, n = 90-92 cells per genotype. *P<0.001.

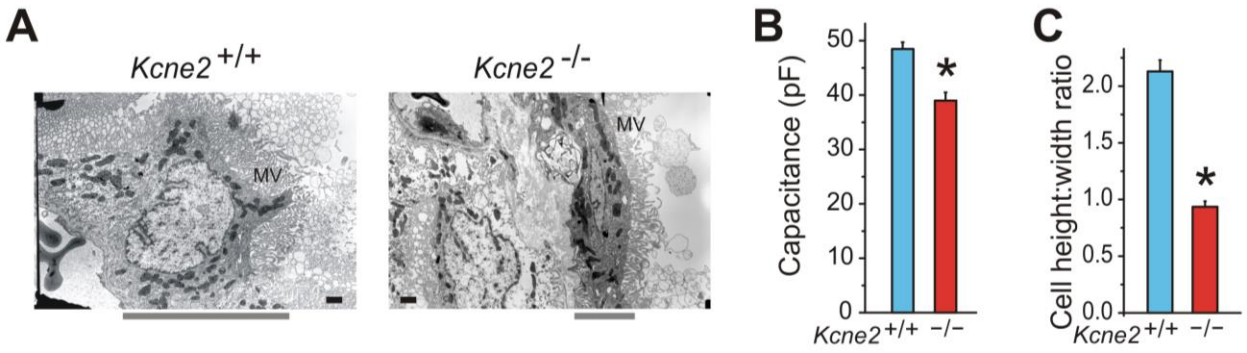

Figure S2.3: *SMIT1, NKCC1, and KCNQ1 expression in choroid plexus and kidney*

(**A**) Immunofluorescence images of adult *Slc5a3*+/+ (upper) and *Slc5a3*–/– (lower) mouse kidney, showing antibody specificity (no SMIT1 signal with *Slc5a3*–/– tissue). Red, anti-SMIT1 antibody. Representative of 2 sections from 1 mice per genotype).

(**B**) Immunofluorescence images of adult *Slc5a3*–/– mouse choroid plexus epithelium showing apical NKCC1 detection (red) but no SMIT1 signal (green, not visible). Scale bar: 40 µm. Blue, DAPI. Representative of 2 experiments on sections from one mouse.

(**C**) Immunofluorescence images of adult *Slc5a3*+/+ mouse choroid plexus epithelium showing apical KCNQ1(red) and SMIT1 (green) co-localization. Horizontal field of view: 80 µm. Blue, DAPI. Representative of 2 experiments on sections from one mouse.

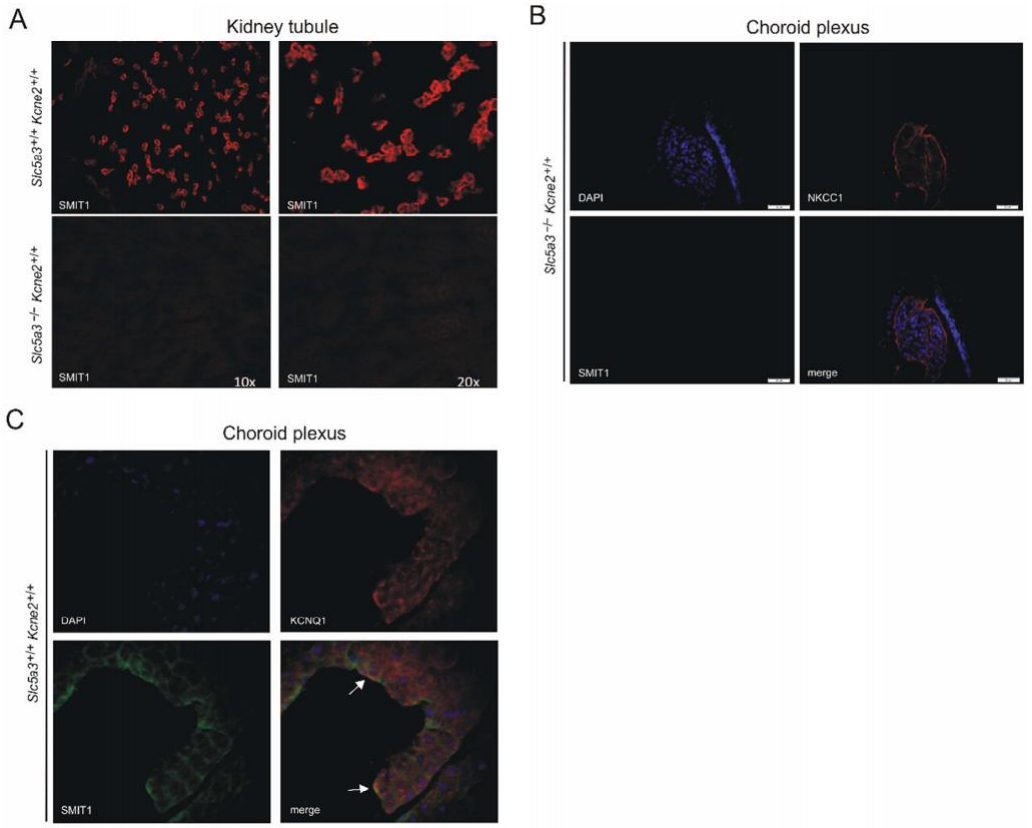

Figure S2.4: *KCNQ1 function with and without transporter coexpression*

(**A**) Mean normalized G/G_{max} (current measured at start of -30 mV tail pulse, protocol as in Fig. 2.3B) for currents generated by KCNQ1 (Q1) with/without SMIT1 (S1), SMIT2 (S2), SGLT1 or SMCT; n = 5-10 oocytes per group.

(**B**) Mean raw macroscopic current-voltage relationships for oocytes in ND96 bath solution or ND96 with NMDG replacing Na^+ (96 mM), co-injected with 10 ng KCNQ1 (Q1) cRNA and 25 ng SMIT1 (S1) cRNA per oocyte; n = 10 oocytes per group.

(**C**) Mean raw macroscopic current-voltage relationships for oocytes in ND96 bath solution with or without 1 mM MI, co-injected with 10 ng KCNQ1 (Q1) cRNA and 12 ng SMIT2 (S2) cRNA per oocyte; n = 5 oocytes per group.

(**D-F**). As for panel B but showing Q1 with SMIT2 (S2), SMCT and SGLT1, respectively; n = 5-6 oocytes per group.

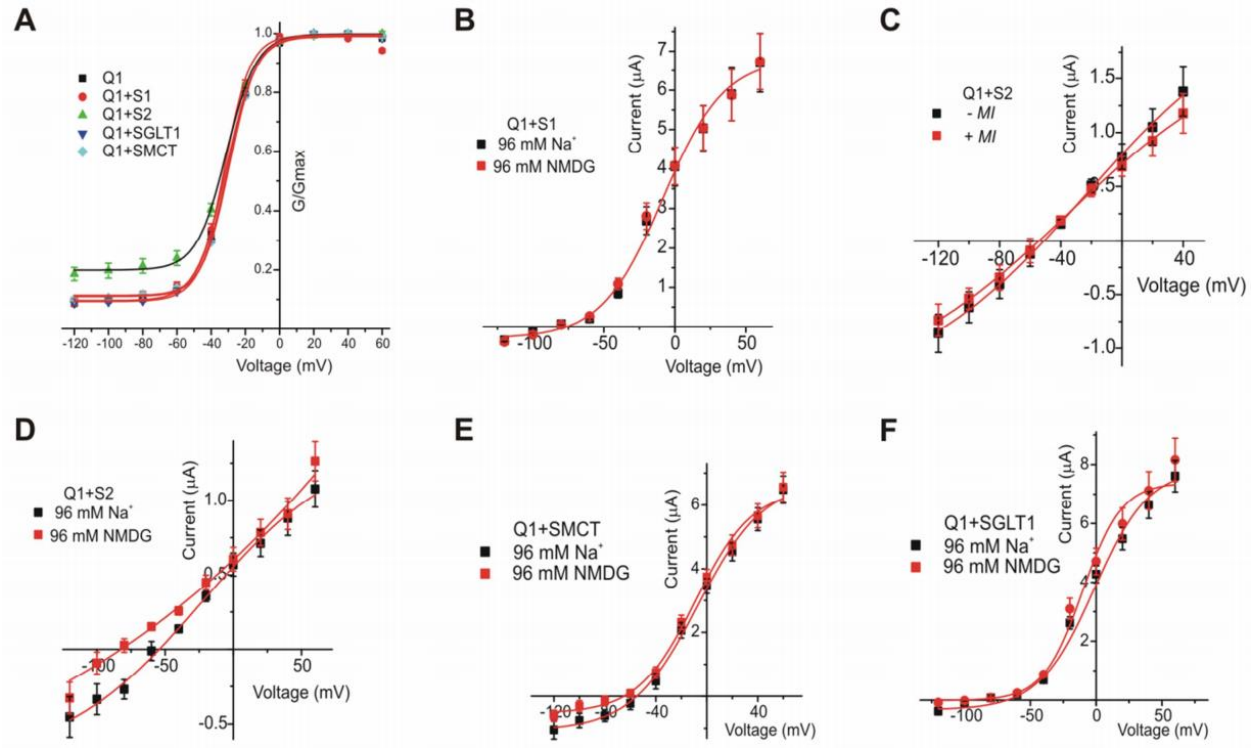

Figure S2.5: *Functional effects of SMIT2 interaction with KCNQ1-KCNE2*

(**A**) Exemplar current traces recorded in oocytes expressing SMIT1 (S2) and/or KCNQ1-KCNE2 (Q1+E2) using the standard voltage family protocol (Fig. 4B). Scale bars: vertical, 0.5 μA; horizontal, 1 s. Zero current level indicated by dashed line. (**B**) Mean raw current-voltage relationships for oocytes as in panel A; n = 7-10 oocytes per group. *P<0.05 at 60V. (**C**) Effects of phlorizin (500 μM) on *myo*-[2-3H(N)] inositol (MI) uptake by oocytes injected with cRNA encoding KCNQ1 (Q1) and/or SMIT2 (S2) as indicated, normalized to mean flux for same-batch oocytes in the absence of phlorizin (con); n = 7-9 oocytes per group. N.S., non-significant (P>0.05). (**D**) Effects of Na+ substitution with NMDG on mean *myo*-[2-3H(N)] inositol (MI) uptake by oocytes co-expressing SMIT2 with/without KCNQ1 and/or KCNE2, normalized to mean flux for same-batch oocytes in ND96 containing 96 mM NaCl (con); n = 10-11 oocytes per group.

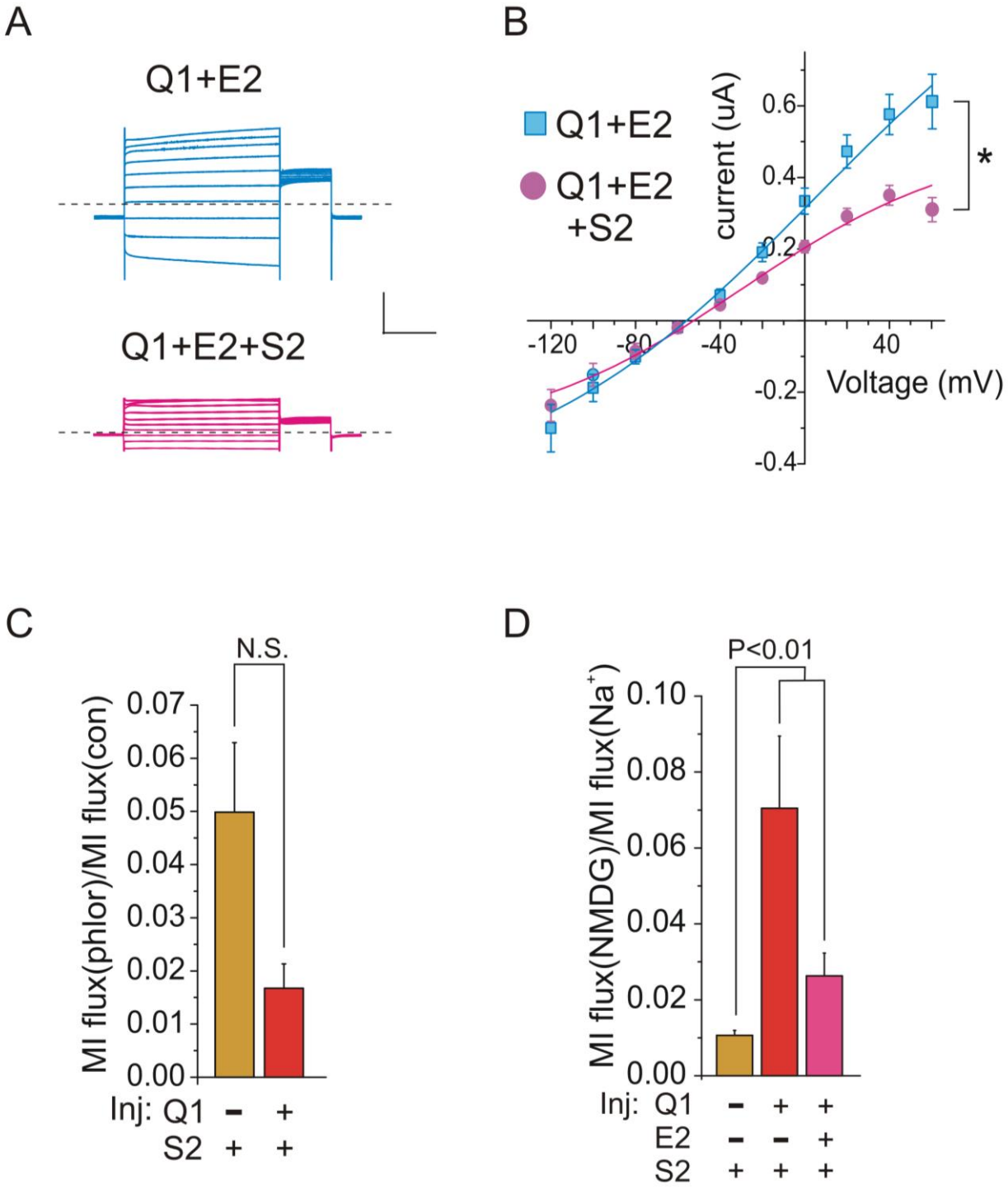
A
Q1+E2
Q1+E2+S2
B
Q1+E2
Q1+E2
+S2
current (uA)
0.6
0.4
0.2
-0.2
-0.4
-120
-80
-40
40
Voltage (mV)
*
C
N.S.
MI flux(phlor)/MI flux(con)
0.07
0.06
0.05
0.04
0.03
0.02
0.01
0.00
Inj: Q1 - +
S2 + +
D
P<0.01
MI flux(NMDG)/MI flux(Na+)
0.10
0.08
0.06
0.04
0.02
0.00
Inj: Q1 - + +
E2 - - +
S2 + + +

Acknowledgments: We thank N. Carrasco for the SMCT clone and M. Coady for the SMIT2 and SGLT1 clones. We are grateful to M. Anand for expert technical assistance, and N. Carrasco, I. Curtis, K. Duff, N. Harrison, and C. Inturrisi for advice and other resources.
Author contributions: All authors except D.J.L., M.T., G.T.B., and S.S.G. performed experiments. D.L.N was personally responsible for CHO studies. G.W.A., A.H., Z.H., Q.C., T.K.R., L.L., B.Z., M.T., S.S.G., D.J.L., D.D., X.H., R.H., R.B., G.T.B., and V.A.K. contributed to experimental design and/or data analysis.
Funding: G.W.A. is grateful for support from the NIH/National Heart, Lung, and Blood Institute (NHLBI) (R01 HL079275) and University of California, Irvine setup funds. S.S.G. is supported by a grant from the NIH/NHLBI (R37 HL87062) and a grant from the NIH (PO1 HD67244). G.T.B. is supported by a grant from the Manton Center for Orphan Disease Research.

References

1. McCrossan, Z.A. and G.W. Abbott, The MinK-related peptides. *Neuropharmacology* **47**, p. 787-821 (2004).
2. Panaghie, G. and G.W. Abbott, The role of S4 charges in voltage-dependent and voltage-independent KCNQ1 potassium channel complexes. *J Gen Physiol* **129**, p. 121-33 (2007).
3. Abbott, G.W., F. Sesti, I. Splawski, M.E. Buck, M.H. Lehmann, K.W. Timothy, M.T. Keating, and S.A. Goldstein, MiRP1 forms IKr potassium channels with HERG and is associated with cardiac arrhythmia. *Cell* **97**, p. 175-87 (1999).
4. Heron, S.E., M. Hernandez, C. Edwards, E. Edkins, F.E. Jansen, I.E. Scheffer, S.F. Berkovic, and J.C. Mulley, Neonatal seizures and long QT syndrome: a cardiocerebral channelopathy? *Epilepsia* **51**, p. 293-6 (2010).
5. Tam, G.W., L.N. van de Lagemaat, R. Redon, K.E. Strathdee, M.D. Croning, M.P. Malloy, W.J. Muir, B.S. Pickard, I.J. Deary, D.H. Blackwood, N.P. Carter, and S.G. Grant, Confirmed rare copy number variants implicate novel genes in schizophrenia. *Biochem Soc Trans* **38**, p. 445-51 (2010).
6. Roepke, T.K., V.A. Kanda, K. Purtell, E.C. King, D.J. Lerner, and G.W. Abbott, KCNE2 forms potassium channels with KCNA3 and KCNQ1 in the choroid plexus epithelium. *FASEB J* **25**, p. 4264-73 (2011).
7. Lee, M.P., J.D. Ravenel, R.J. Hu, L.R. Lustig, G. Tomaselli, R.D. Berger, S.A. Brandenburg, T.J. Litzi, T.E. Bunton, C. Limb, H. Francis, M. Gorelikow, H. Gu, K. Washington, P. Argani, J.R. Goldenring, R.J. Coffey, and A.P. Feinberg, Targeted disruption of the Kvlqt1 gene causes deafness and gastric hyperplasia in mice. *J Clin Invest* **106**, p. 1447-55 (2000).
8. Roepke, T.K., E.C. King, A. Reyna-Neyra, M. Paroder, K. Purtell, W. Koba, E. Fine, D.J. Lerner, N. Carrasco, and G.W. Abbott, Kcne2 deletion uncovers its crucial role in thyroid hormone biosynthesis. *Nat Med* **15**, p. 1186-94 (2009).
9. Cryan, J.F., C. Mombereau, and A. Vassout, The tail suspension test as a model for assessing antidepressant activity: review of pharmacological and genetic studies in mice. *Neurosci Biobehav Rev* **29**, p. 571-625 (2005).

10. Gleason, G., B. Liu, S. Bruening, B. Zupan, A. Auerbach, W. Mark, J.E. Oh, J. Gal-Toth, F. Lee, and M. Toth, The serotonin1A receptor gene as a genetic and prenatal maternal environmental factor in anxiety. *Proc Natl Acad Sci U S A* **107**, p. 7592-7 (2010).

11. Spector, R. and C. Johanson, Micronutrient and urate transport in choroid plexus and kidney: implications for drug therapy. *Pharm Res* **23**, p. 2515-24 (2006).

12. Bersudsky, Y., A. Shaldubina, G. Agam, G.T. Berry, and R.H. Belmaker, Homozygote inositol transporter knockout mice show a lithium-like phenotype. *Bipolar Disord* **10**, p. 453-9 (2008).

13. Guo, W., S. Shimada, H. Tajiri, A. Yamauchi, T. Yamashita, S. Okada, and M. Tohyama, Developmental regulation of Na+ / myo-inositol cotransporter gene expression. *Brain Res Mol Brain Res* **51**, p. 91-6 (1997).

14. Bourgeois, F., M.J. Coady, and J.Y. Lapointe, Determination of transport stoichiometry for two cation-coupled myo-inositol cotransporters: SMIT2 and HMIT. *J Physiol* **563**, p. 333-43 (2005).

15. Holub, B.J., The nutritional significance, metabolism, and function of myo-inositol and phosphatidylinositol in health and disease. *Adv Nutr Res* **4**, p. 107-41 (1982).

16. Loussouarn, G., K.H. Park, C. Bellocq, I. Baro, F. Charpentier, and D. Escande, Phosphatidylinositol-4,5-bisphosphate, PIP2, controls KCNQ1/KCNE1 voltage-gated potassium channels: a functional homology between voltage-gated and inward rectifier K+ channels. *EMBO J* **22**, p. 5412-21 (2003).

17. Hammami, S., N.J. Willumsen, H.L. Olsen, F.J. Morera, R. Latorre, and D.A. Klaerke, Cell volume and membrane stretch independently control K+ channel activity. *J Physiol* **587**, p. 2225-31 (2009).

18. Ying, S.W., V.A. Kanda, Z. Hu, K. Purtell, E.C. King, G.W. Abbott, and P.A. Goldstein, Targeted Deletion of Kcne2 Impairs HCN Channel Function in Mouse Thalamocortical Circuits. *PLoS One* **7**, p. e42756 (2012).

19. Pian, P., A. Bucchi, R.B. Robinson, and S.A. Siegelbaum, Regulation of gating and rundown of HCN hyperpolarization-activated channels by exogenous and endogenous PIP2. *J Gen Physiol* **128**, p. 593-604 (2006).

20. Talisman, I.J. and C.H. Marzabadi, Carbohydrate-based drugs in the treatment of epilepsy, depression and other affective disorders. *Curr Top Med Chem* **8**, p. 159-70 (2008).

21. Firbank, M.J., R.M. Harrison, and J.T. O'Brien, A comprehensive review of proton magnetic resonance spectroscopy studies in dementia and Parkinson's disease. *Dement Geriatr Cogn Disord* **14**, p. 64-76 (2002).

22. Kofman, O., W.R. Sherman, V. Katz, and R.H. Belmaker, Restoration of brain myo-inositol levels in rats increases latency to lithium-pilocarpine seizures. *Psychopharmacology (Berl)* **110**, p. 229-34 (1993).

23. Huang, W., G.E. Alexander, E.M. Daly, H.U. Shetty, J.S. Krasuski, S.I. Rapoport, and M.B. Schapiro, High brain myo-inositol levels in the predementia phase of Alzheimer's disease in adults with Down's syndrome: a 1H MRS study. *Am J Psychiatry* **156**, p. 1879-86 (1999).

24. Roepke, T.K., A. Anantharam, P. Kirchhoff, S.M. Busque, J.B. Young, J.P. Geibel, D.J. Lerner, and G.W. Abbott, The KCNE2 potassium channel ancillary subunit is essential for gastric acid secretion. *J Biol Chem* **281**, p. 23740-7 (2006).

25. Unoki, H., A. Takahashi, T. Kawaguchi, K. Hara, M. Horikoshi, G. Andersen, D.P. Ng, J. Holmkvist, K. Borch-Johnsen, T. Jorgensen, A. Sandbaek, T. Lauritzen, T. Hansen, S. Nurbaya, T. Tsunoda, M. Kubo, T. Babazono, H. Hirose, M. Hayashi, Y. Iwamoto, A. Kashiwagi, K. Kaku, R. Kawamori, E.S. Tai, O. Pedersen, N. Kamatani, T. Kadowaki, R. Kikkawa, Y. Nakamura, and S. Maeda, SNPs in KCNQ1 are associated with susceptibility to type 2 diabetes in East Asian and European populations. *Nat Genet* **40**, p. 1098-102 (2008).

26. Yasuda, K., K. Miyake, Y. Horikawa, K. Hara, H. Osawa, H. Furuta, Y. Hirota, H. Mori, A. Jonsson, Y. Sato, K. Yamagata, Y. Hinokio, H.Y. Wang, T. Tanahashi, N. Nakamura, Y. Oka, N. Iwasaki, Y. Iwamoto, Y. Yamada, Y. Seino, H. Maegawa, A. Kashiwagi, J. Takeda, E. Maeda, H.D. Shin, Y.M. Cho, K.S. Park, H.K. Lee, M.C. Ng, R.C. Ma, W.Y. So, J.C. Chan, V. Lyssenko, T. Tuomi, P. Nilsson, L. Groop, N. Kamatani, A. Sekine, Y. Nakamura, K. Yamamoto, T. Yoshida, K. Tokunaga, M. Itakura, H. Makino, K. Nanjo, T. Kadowaki, and M. Kasuga, Variants in KCNQ1 are associated with susceptibility to type 2 diabetes mellitus. *Nat Genet* **40**, p. 1092-7 (2008).

27. Donovan, G.P., C. Harden, J. Gal, L. Ho, E. Sibille, R. Trifiletti, L.J. Gudas, and M. Toth, Sensitivity to jerky gene dosage underlies epileptic seizures in mice. *J Neurosci* **17**, p. 4562-9 (1997).

28. Zupan, B. and M. Toth, Inactivation of the maternal fragile X gene results in sensitization of GABAB receptor function in the offspring. *J Pharmacol Exp Ther* **327**, p. 820-6 (2008).

29. Liu, L. and K. Duff, A technique for serial collection of cerebrospinal fluid from the cisterna magna in mouse. *J Vis Exp* (2008).

30. Speake, T., L.J. Freeman, and P.D. Brown, Expression of aquaporin 1 and aquaporin 4 water channels in rat choroid plexus. *Biochim Biophys Acta* **1609**, p. 80-6 (2003).

31. R. Buccafusca, C. P. Venditti, L. C. Kenyon, R. A. Johanson, E. Van Bockstaele, J. Ren, S. Pagliardini, J. Minarcik, J. A. Golden, M. J. Coady, J. J. Greer, G. T. Berry, Characterization of the null murine sodium/myo-inositol cotransporter 1 (Smit1 or Slc5a3) phenotype: Myo-inositol rescue is independent of expression of its cognate mitochondrial ribosomal protein subunit 6 (Mrps6) gene and of phosphatidylinositol levels in neonatal brain. Mol. Genet. Metab. **95**, 81–95 (2008)

32. G. T. Berry, S. Wu, R. Buccafusca, J. Ren, L. W. Gonzales, P. L. Ballard, J. A. Golden, M. J. Stevens, J. J. Greer, Loss of murine Na+/myo-inositol cotransporter leads to brain myo-inositol depletion and central apnea. J. Biol. Chem. **278**, 18297–18302 (2003).

Chapter II

KCNQ2 regulates sodium-dependent *myo*-inositol transporter expression and function

Abstract

Na+-coupled solute transport is crucial for uptake of a wide range of molecules including monovalent ions, glucose, and the cyclic polyol myo-inositol, an important substrate for the PIP2 signaling pathway. Recent studies have demonstrated regulation of substrate transport by formation of macromolecular complexes between ion channels and transporters, and reciprocal alteration of channel function by transporter and substrate status. In the present study, we discuss the discovery of SMIT1-KCNQ2 complex formation and the inhibition of SMIT1 and SMIT2 by KCNQ2. We show that this interaction is mediated by the S5-S6 pore-forming region of KCNQ2, and that KCNQ2 reduces SMIT1 activity approximately 70% by inhibiting SMIT1 surface expression an equal 70%. KCNQ2-SMIT2 myo-inositol uptake is sensitive to mutations in the KCNQ2 selectivity filter and voltage sensor. KCNQ2(G279S), a selectivity filter mutant rendering the channel impermeable to potassium, as well as double voltage sensor mutant KCNQ2(R210H, R214Q) each partially alleviate KCNQ2-mediated inhibition of SMIT2. By contrast, pharmacologically inhibiting the channel with the pore-binding KCNQ blocker XE991 further increases the inhibition of SMIT1 caused by KCNQ2-KCNQ3 co-expression. Last, we demonstrate that SMIT1 function is partially inhibited by cellular depolarization induced by elevated extracellular potassium levels and that co-expression of KCNQ2 alleviates this loss.

INTRODUCTION

Voltage-gated potassium channel (Kv) pore-forming (α) subunits are encoded by genes of a 40-member family in humans. They include a K+-selective pore region and a voltage sensor that permits response to changes in membrane potential. Previous investigations into Kv channels have revealed essential functions in numerous excitable cell types including neurons[1], cardiac[2] and skeletal muscle[3]. KCNQ gene family members are notable Kv channels given their diverse functions in many overlapping biological systems. Recent work has uncovered a rapidly growing number and diversity of ion channel-transporter complexes, including ATPases, secondary-active transporters, and a co-transporter [4–11]. Formation of these complexes allows a critical "crosstalk" between the two classes of proteins, facilitating physiological changes pertaining to gastric acid secretion[12–14], potassium efflux and myo-inositol transport[4], and thyroid hormone synthesis[8,9]. Additional systems have been demonstrated to form physical complexes[6,15], however functional changes remain to be quantified.

Each of the transporters studied here are associated with a variety of pathologies. Both SMIT1 (*SLC5A3*) and SMIT2 (*SLC5A11*) are 14-transmembrane domain membrane proteins which mediate cellular uptake of myo-inositol, an essential osmolyte that also acts as an important substrate for phosphatidylinositol (PI) signaling pathways that regulate a plethora of ion channels including those essential for human cardiac function[16–18]. Of some

controversy, alterations to SMIT1 expression and function in humans have also been implied in a variety of mood disorders[5]. In mice, *Slc5a3* deletion is fatal[19,20].
KCNQ complex formation has also been reported in drosophila, where upregulation or overexpression of the drosophila sodium/solute co-transporter-like SLC5A11 causes marked reductions in both expression and macroscopic current[21]. Drosophila KCNQ (dKCNQ), a functional amalgam of multiple mammalian KCNQ proteins, has properties similar to mammalian KCNQ2/KCNQ3 channel[22]. For this reason, we believe this data to be consistent with our previous finding that KCNQ1 current was significantly inhibited by co-expression of SMIT2, but not SMIT1[4]. This discovery of KCNQ-transporter complexes beyond mammalian organisms hints at a critical nature of the proteins' co-expression and interaction.

Recent data from the Hille lab have shown modulation of KCNQ2 channel kinetics by the myo-inositol (MI) transported by SMIT1[23]. In light of these findings and our original discovery of KCNQ1 interaction with SMIT1[4], we sought to identify and characterize the effects of KCNQ2 on SMIT1 and SMIT2. In stark contrast to KCNQ1, KCNQ2 strongly inhibits transporter function, decreasing MI transport through both SMIT1 and SMIT2. Here, we show that this effect is due to impaired trafficking of the transporter to the plasma membrane, and that physical complex formation requires the S5-S6 pore domain of the KCNQ2 channel. In CHO cells expressing SMIT1, myo-inositol transport appears to be partially inhibited by elevated extracellular potassium levels (e.g. cellular depolarization), however this effect is alleviated by co-expression of KCNQ2, suggesting a possible regulatory mechanism for cellular excitability.

RESULTS

Functional

KCNQ2 strongly inhibits SMIT1 (-70%, P < 0.0001, Fig 3.1A) and SMIT2 (-80%, P < 0.0001, Fig 3.2A) function in Xenopus laevis oocytes. KCNQ2 can also form a heterotetramer with KCNQ3, known as the M-channel, which is a key component of neuronal excitability and is a current antiepileptic drug target [24–26]. Therefore, we tested the effects of homomeric KCNQ2 vs. heteromeric KCNQ2/KCNQ3 channels and found that the activity of both SMIT1 and SMIT2 were most strongly inhibited by homomeric KCNQ2 channels. KCNQ3 inhibits SMIT1 68% (P < 0.0001); KCNQ2/KCNQ3 inhibits SMIT1 by 71% at 5+5 ng each channel RNA injected (P < 0.0001). Fig 1A also demonstrates the effects of varying the mass of RNA injected per oocyte; either 1ng each channel (Q2/Q3 1+1) (-53%, P < 0.01) or 5ng each channel (Q2/Q3 5+5), or 10ng for the homomeric conditions. SMIT1 inhibition was seen at RNA mass as low as 1+1 ng, with slightly stronger effect at 5+5 ng. Based on these data, we believe a total of 10ng channel per oocyte to be at, or very near to, the point of maximal effect. SMIT1 is inhibited by: KCNQ2 (70%, P ≤ 0.0001), KCNQ2(G279S) (77%, P ≤ 0.0001), KCNQ3 (68%, P ≤ 0.0001), 1 ng KCNQ2 + 1 ng KCNQ3 RNA (53%, P ≤ 0.01), and 5 ng KCNQ2 + 5ng KCNQ3 RNA (71% P ≤ 0.0001). KCNQ4, previously demonstrated not to form transporter complexes in oocytes4, and Kv from an alternate gene family, Kv1.1, served as negative controls.

To determine the mechanism by which this effect was occurring, we attempted to alleviate the inhibition of the transporters by KCNQ2 using a variety of methods. First, we examined the contribution of KCNQ2 K+ conductance by co-expressing SMIT1 with KCNQ2(G279S).

This mutant effects the selectivity filter of the channel, rendering it impermeable to potassium[27]. Because MI uptake is a sodium-dependent process, we hypothesized that KCNQ2-mediated potassium efflux might create a favorable electrical gradient for Na+-dependent MI uptake. This hypothesis, was, however, not supported by our findings; KCNQ2(G279S) suppressed SMIT1 function (77%, $P < 0.0001$), and effects were not significantly different from wild-type KCNQ2 effects on SMIT1 (Fig 3.1A).

We next examined the effects of KCNQ2 and related α subunits on SMIT2 (Fig 3.2A). SMIT2 was inhibited 79% ($P < 0.0001$) by KCNQ2, 51% ($P = 0.0004$) by KCNQ3, 70% by KCNQ2+KCNQ3 ($P < 0.0001$), but not by KCNQ4 (22%, $P > 0.9999$). Following this, we studied effects of two different KCNQ2 S4 domain mutants, R210H and R214Q, both individually and in combination. Each of these mutants strongly right-shifts the channels' voltage-dependence of activation[28]. While the single mutations in the KCNQ2 voltage sensor did not alleviate transporter inhibition, the double mutant doubled MI uptake through SMIT2 – although this did not reach statistical significance using multiple comparisons statistical analysis (Fig 3.2B). A similar doubling of MI uptake by SMIT2 co-expressed with KCNQ2 was observed with the KCNQ2 selectivity filter mutant, G279S (Fig 3.2B). These data suggest the possibility that SMIT2 transporter function is sensitive to the activity or conformation of co-expressed KCNQ2. We further investigated this idea by pharmacologically inhibiting KCNQ2 with pan-KCNQ channel blocker XE991 in SMIT1-expressing oocytes (Fig 3.1B-C). Consistent with earlier findings, XE991 strongly suppressed transporter function in oocytes injected with SMIT1 only (-57.5%, $P = 0.0007$) (Fig 3.1B). We hypothesize that this effect is due to native KCNQ1 expression in *X. laevis*

oocytes, an XE991-sensitive channel previously demonstrated to form complexes with SMIT1.[4] Similar to the effects of XE991 on SMIT1/KCNQ1 complexes, the co-expression of KCNQ2 and KCNQ3 further reduces SMIT1 function (-80%, P = 0.0033) (Fig 3.1C). We believe these effects to be demonstrative of KCNQ2/3-specific XE991 activity due to functional inhibition greater than that seen in oocytes expressing KCNQ1 and SMIT1, although further studies in a cell line that does not express endogenous KCNQ1, such as CHO cells, will be necessary to support or otherwise this hypothesis.

Next, we attempted to alter transporter function using known KCNQ2-inhibitor wortmannin[29]. Wortmannin exerts its effects by inhibition of PI3K and PI4K to reduce cellular PIP_2 levels, thereby inhibiting PIP_2-sensitive KCNQ2 channels. Although the drug strongly inhibited KCNQ2 currents (data not shown), we did not see an effect on MI uptake in SMIT1-alone (-19%, P = 0.3059) or SMIT1/KCNQ2/KCNQ3 (-40%, P = 0.1170) conditions (Fig 3.1D-E).

To determine if the KCNQ2 inhibition of SMIT transport activity was *X. laevis* oocyte-specific versus more general, we tested SMIT1-KCNQ2 function in mammalian Chinese hamster ovary (CHO) cells. First, we found that KCNQ2 inhibited SMIT1 function by approximately 70% in CHO cells (P < 0.0001), similar to our findings in oocytes (Fig 3.3A). We next tested the effects of a highly-selective KCNQ2-KCNQ3 channel opener, ICA-27243 (Fig 3.3B). ICA-27243 binds to the voltage sensor domain (VSD) of KCNQ2 and KCNQ3, strongly left-shifting the voltage dependence of activation[30–32]. ICA-27243 failed to alter SMIT1-KCNQ2 activity (0.02%, P = 0.6591); however, the effects of the drug may have been

masked by DMSO vehicle, which appeared to permeabilize the cell sufficiently to alter MI flux independent of drug application. The only conditions which cause functional changes of SMIT1-KCNQ2 with DMSO were those without either channel or transporter co-expressed: SMIT1 with DMSO (43%, $P < 0.0001$) and ICA-27243 (26%, $P = 0.0125$), as well as KCNQ2 with DMSO (24%, $P = 0.0228$) and ICA-27243 ($P = 0.0103$).

Next, we tested the effects of cellular depolarization by adding 50 mM K^+ to the extracellular solution (PBS) used during [3H]MI uptake assays (Fig. 3.3C-D). Using the Nernst equation, we estimate that CHO cells in this solution are held at approximately -20 mV; roughly 80% of KCNQ2 Vmax [33]. In cells expressing SMIT1 only, transporter function was reduced by 18% ($P = 0.0073$). In cells expressing SMIT1/KCNQ2, the addition of 50 mM potassium did not alter transporter function ($P = 0.7166$).

KCNQ2 reduces SMIT1 surface expression

Although we observed potentially interesting effects of specific KCNQ2 mutants, and of high extracellular K^+, on KCNQ2-SMIT1/2 activity, none of these manipulations came close to fully alleviating SMIT inhibition by KCNQ2. Thus, our next experiments were targeted toward determining the mechanism for the reduction in SMIT1 function by KCNQ2. We hypothesized that these effects may be the result of KCNQ2-mediated reductions in SMIT1 surface expression. As both oocytes and CHO cells exhibited similar levels of inhibition, we tested this hypothesis using CHO cells (a more suitable system than oocytes for studying protein trafficking and cell biology) for surface biotinylation assays followed by streptavidin pulldowns and western blots. Surface expression (-71%, $P = 0.0103$), but not

total expression (+30%, P = 0.1434), of SMIT1 was reduced by co-expression of KCNQ2. We find these results striking, as transporter function was similarly inhibited by approximately 70% in our earlier experiments. Interestingly, whole-cell KCNQ2 expression (-77%, P < 0.0001) and surface expression (-61%, P < 0.0001) were reduced by co-expression of SMIT1-FLAG (Fig 3.4A).

Based on these data, we sought to test KCNQ2-SMIT1 complex formation in CHO cells. By co-immunoprecipitation, we found that KCNQ2 physically interacts with FLAG-tagged SMIT1 (Fig 3.5A). We verified these findings by immunofluorescence and confocal microscopy, finding strong co-localization at the plasma membrane (Fig 3.5B).

KCNQ2 pore-forming region is required for SMIT1 binding

With the knowledge that KCNQ2-SMIT1 were forming complexes, and that the transporter inhibition appeared to be primarily a surface trafficking effect, we set out to determine which region, or regions, of KCNQ2 were mediating an interaction with SMIT1. We generated and expressed KCNQ2 fragments tagged with either YFP or GFP in CHO cells and tested for interaction with co-expressed SMIT1-FLAG using co-immunoprecipitation and western blots (Fig 3.6D). We started with cytosolic N and C terminal fragments of KCNQ2, with the knowledge that these intracellular domains are often protein-binding sites[34] (Fig 3.6A). However, neither the N-terminal (1-97) nor C-terminal (321-852) fragments demonstrated interaction with SMIT1. We then generated the KCNQ2(1-224) construct, which includes the entire KCNQ2 N-terminus and voltage sensor domain through the S4-S5 linker (Fig. 3.6B, top), again finding no interaction with SMIT1. Next, we tested a slightly

longer construct, starting at the N-terminus and ending early in the C-terminal sequence, KCNQ2(1-549) (Fig 3.6B, bottom), and this time observed an interaction with SMIT1 by coIP. By the process of elimination, it seemed that the addition of the pore-forming S5-S6 region restored KCNQ2 interaction with SMIT1. To verify this, we generated the KCNQ2(222-323) fragment, which encodes only for the pore-forming region, from the S4-S5 linker through the first few amino acids of the C-terminus. As predicted, the 222-323 construct did interact with SMIT1 (Fig. 3.6C), confirming that the pore-forming region was necessary and sufficient for SMIT1 binding. Due to a comparatively strong Kozak consensus sequence for the YFP tag 3' of the Q2 fragment, cells expressed YFP both with the Q2 fragment (solid arrow) and without (dashed arrow) (Fig. 3.6C). In FLAG pulldown experiments, only the Q2-YFP protein precipitated along with the transporter; YFP-alone was not pulled down by FLAG, further confirming specificity of complex formation with the Q2 pore fragment. The results are summarized in Figure 3.6D.

METHODS

X. laevis oocyte preparation and [3H]MI uptake

cRNA were generated from linearized plasmids containing target cDNA. In vitro cRNA synthesis was performed using T3, T7, or SP6 mMessage mMachine kits (Ambion). SMIT1 cDNA was purchased from Origene; SMIT2 cDNA was a gift from M. J. Coady and J.-Y. Lapointe (GÉPROM, Université de Montréal). cRNA quality was verified by spectrophotometry and gel electrophoresis. *Xenopus laevis* oocyte microinjection and radiolabeled *myo*-inositol uptake assays were performed as previously described4. Briefly, stage IV and V defollliculated oocytes were injected with 50 nl containing variable mass of

cRNA as indicated in each figure caption. Total channel RNA mass per oocyte totaled 10 ng, except where otherwise indicated. Transporter injections per oocyte were 20 ng. Injected oocytes were incubated for 5 days at 16C in ND96 storage solution, supplemented with penicillin and streptomycin. For each group, oocytes were placed in a round-bottomed, 10-ml culture tube, washed with ND96. For drug-treated groups, oocytes were resuspended in ND96 containing either 10 uM wortmannin (Alomone), or 20 uM XE991 (Santa Cruz) for 30 minutes. All oocytes were then washed with ND96 and resuspended in ND96 containing 3 μCi/ml *myo*-[2-3H(N)]inositol (American Radiolabeled Chemicals Inc.) for a 30 minute incubation at room temperature, with or without drug where indicated. Oocytes were washed with 1 mM cold myo-inositol (Sigma Aldrich), followed by three washes in ND96. Oocytes were transferred to individual wells in a 96 well plate and lysed in 0.2% SDS in ND96. Lysates were transferred to individual scintillation vials containing 5 ml Cytoscint scintillation cocktail fluid (MP Biomedicals). Vials were capped, shaken, then allowed to sit at room temperature for at least 30 min before scintillation counting in a Beckmann Coulter LS6500 liquid scintillation counter.

Protein biochemistry

CHO cells were cultured, transfected, and lysed as previously reported 4. In brief, cells were transfected using Mirus LT-1 transfection reagent with a total of 15 ug cDNA per 10 cm plate and allowed 36-48 hrs expression at 37°C before lysis. Lysis buffer was composed of 1% IGEPAL, 0.1% SDS, 50 mM Tris (pH 8.0), 150 mM NaCl, and a protease-inhibitor cocktail tablet (Thermo Fisher). Total protein was quantified by the BCA method (Thermo Fisher). Proteins were resolved by SDS-PAGE and transferred onto PVDF membranes for

immunoblotting with the following antibodies, as noted: KCNQ2 (Santa Cruz), DDK (Origene), FLAG (Sigma Aldrich), SMIT1 (Santa Cruz), YFP (Santa Cruz), GFP (Santa Cruz; Rockland Immunochemicals. For secondary detection, horseradish peroxidase (HRP)-conjugated antibodies (BioRad) were used in conjugation with Luminata Forte HRP substrate (Millipore). Imaging was performed using Syngene Gbox hardware and software. For murine brain study, *Slc5a3* (-/-) mice were bred from *Slc5a3* (+/-) pairs. Mice were sacrificed by CO2 asphyxiation, tissues were collected and snap frozen in chilled isopentane for use in later experiments. Tissue was minced and homogenized in a buffer containing 150 mM NaCl, 50 mM Tris-HCl (pH 7.4), 1% IGEPAL, 1% CHAPS, 1% Triton X-100, 1% sodium dodecyl sulfate, and one mini protease-inhibitor cocktail tablet per 10 ml (Thermo Fisher) and mixed at 4°C for 2 hours. Samples were cleared of insoluble fractions by centrifugation before western blotting as above.

For co-immunoprecipitation study, all samples were first pre-cleared of non-specific interaction by incubating the total lysate with protein A/G PLUS-coated agarose beads (Santa Cruz) for 1 hr. Beads were then pelleted and discarded. Total protein was quantified by BCA, as above. Immunoprecipitating antibodies were then added at a concentration of [1:100] for overnight pulldown at 4°C. The following day, antibody-antigen complexes were pulled down with fresh protein A/G PLUS agarose beads.

Surface expression experiments were performed by culturing and transfecting CHO cells, as above, followed by PBS wash and 30 minute incubation at 4°C in a PBS solution containing 1 mg/ml EZ-Link Sulfo-NHS-SS-Biotin (Thermo Fisher). The reaction was then quenched by subsequent wash with 50 mM Tris (pH 8.0) and PBS. Cells were then lysed, total protein quantified, and western blotted as described above.

CHO transporter assay

CHO cells were cultured in 12-well dishes and transfected with 2 ug cDNA per well, otherwise as described above. After 36-48 hrs of expression, dishes were rinsed with PBS, and then covered with a PBS solution containing 2 μCi/ml *myo*-[2-3H(N)]inositol (American Radiolabeled Chemicals Inc.) for a 30 minute incubation at room temperature, with or without 100 uM ICA-27243 (Alomone Labs) where indicated. Wells were then washed with PBS four times, and then lysed in a 0.2% SDS in PBS solution for 15 minutes at room temperature. Lysate from each well was then collected and transferred to individual scintillation vials, prepared and analyzed as above.

For experiments utilizing altered extracellular solution (Fig. 3.3C-D), cells were incubated with either 100 mM NaCl for 24 priors to uptake assay or 50 mM K^+ for 30 minutes prior to uptake assay. Elevated ion concentrations were maintained throughout each uptake experiment.

Immunocytochemistry

CHO cells were transfected as described above. Tissue preparation and immunocytochemistry techniques were performed as previously reported [4,35]. SMIT1-FLAG was detected using anti-DDK (Origene). KCNQ2-GFP was observed directly without additional antibody. Images were captured on a Leica SP8 confocal microscope. A z-stack of the entire cell depth was captured, allowing isolation of the bottom layer to best

visualize the boundaries of the plasma membrane. Analyses were performed with ImageJ and Volocity (PerkinElmer).

KCNQ2 fragment generation

KCNQ2-YFP, (1-97)-GFP, (321-852)-GFP, and (1-549)-YFP were gifts from Naoto Hoshi (UC Irvine). KCNQ2(1-224)-YFP was constructed from KCNQ2(1-549)-YFP by excising the undesired fragments using a single AccI digest, and re-ligation with T4 DNA ligase. KCNQ2(222-323)-YFP was constructed using KCNQ2(1-549)-YFP as template and later backbone as well. The target fragment was amplified by PCR and added restriction sites for EcoRI and KpnI using the following primer pair: GAATTCCTGGGATACGTGGTCTACGCTCACA and GGGTACCCTGCTCTTGGACTTTCA. PCR products were re-amplified with the following primer pairs to improve the 5' Kozak sequence: GGATCCACCGGTCCCACCATGGTGAG and CTCACCATGGTGGGACCGGTGGATCC. PCR products and backbone (KCNQ2(1-549)-YFP) were then digested with EcoRI and KpnI, and then ligated using T4 DNA ligase before transformation into DH5α cells and subsequent purification by Maxiprep (QIAGEN).
KCNQ2(G279S) was made from full-length KCNQ2 in pCDNA3 using the QuikChange mutagenesis kit (Agilent) with the following primers: AGATCTCGAGCTCAAGCTTCGCCRCCATGGGATCGGTGGTCTACGCTC and GAGCGTAGACCACCGATCCCATGGYGGCGAAGCTTGAGCTCGAGATCT. The mutated plasmids were transformed and purified as per QuikChange kit instructions.

Data presentation and statistics

Statistical calculations were made using GraphPad Prism statistical software. Data were calculated using one-way ANOVA with multiple comparisons and Bonferroni's correction.

DISCUSSION

Our findings expand the rapidly-growing ion channel-transporter field, with evidence of novel complex formation in vitro and in vivo. Although the effects of KCNQ1 and KCNQ2 on SMIT1 activity are diametrically opposed, our data highlight the complicated role of potassium efflux through the channel with regards to MI transport through SMIT1. The complicated relationship between K^+ conductance and MI transport was demonstrated by voltage-sensor mutant KCNQ1(R231A). Whereas wild-type KCNQ1 greatly increased SMIT1 function, the KCNQ1(R231A) mutant, which locks the voltage sensor into an "open" conformation, strongly inhibited SMIT1 function[4]. These effects were in stark contrast to our initial hypothesis that potassium efflux through the channel created a favorable electrochemical gradient for the sodium-dependent MI transport by SMIT1. These data suggested that SMIT1 augmentation by KCNQ1 occurred through a mechanism, or mechanisms, independent of potassium current. Similarly, our present data demonstrate that inhibition of KCNQ2 function by KCNQ2(R210H) or KCNQ2(R214Q) single mutations or PIP_2 depletion via wortmannin are insufficient to alter the pronounced inhibition of SMIT1 by KCNQ2.

Although the R210H and R214Q KCNQ2 mutations failed to alter transporter function individually, the double R210H+R214Q KCNQ2 S4 mutant roughly doubled transporter function compared to the effects of wild-type KCNQ2 on SMIT2. Similarly, although

KCNQ2(G279S) did not completely alleviate the inhibition of SMIT2 by KCNQ2, this pore mutation did roughly double transporter function when compared to wild-type KCNQ2-SMIT2. Although neither of these effects reached statistical significance, we believe that these effects, along with the effects of KCNQ1(R231A)-SMIT1 transporter function, may be demonstrative of the effects of channel conformation on complexed SMIT2 function. Future studies of KCNQ2 and KCNQ1 mutations altering voltage sensor and/or pore conformation will continue to elucidate the effects of channel conformation on transporter function.

In contrast to the KCNQ2(G279S) and wortmannin data, we did find that cellular depolarization by the addition of 50 mM K^+ to the extracellular CHO solution did significantly inhibit SMIT1, and that a resistance to this effect was conferred by co-expression of KCNQ2 (Fig 3.3D). We hypothesize that this may reflect an ability of the KCNQ2-complexed transporter to maintain its function during rapid, or frequent, cellular depolarizations. This effect may prove to be cumulative over an extended period of depolarization, providing a sort of handbrake to maintain MI influx and thereby maintain PIP_2 levels sufficient to keep the repolarizing currents of the PIP_2-sensitive M-channel open[18]. Our hypothesis is strengthened by the recent work of the Hille lab, who showed augmentation of neuronal KCNQ2 activity by myo-inositol transported intracellularly through SMIT1. Hille and colleagues also suggest that myo-inositol dialyzed directly into the cell takes approximately 10 minutes to incorporate into PIP_2[23]. Given such a slow system, the "handbrake" function of KCNQ2 to maintain MI influx during extended periods

of depolarization seems quite important, potentially minimizing the downtime of PIP_2-sensitive channels, such as KCNQ2, during cellular depolarization.

The channel-conformation as mechanism hypothesis is particularly striking given that the pore-forming region of KCNQ2 was found to be the keystone for KCNQ2-SMIT1 complex formation. However, our surface biotinylation experiments revealed inhibition of both SMIT1 surface trafficking and total MI uptake by approximately 70% each. It seems less likely that channel conformation would play a role in SMIT1 trafficking from ER to surface, however it is possible that the changes in channel conformation induced by shifts in V_m align in such a way to encourage transporter endocytosis or otherwise alter surface expression.

The question remains, however – why form a complex? To what end does KCNQ2 inhibit transporter function? We propose that complex formation may promote the constituents' targeting to specific cell regions, and that this highly specific targeting may be critically important for rapidly and/or frequently activating systems such as a neuron, as discussed above. Furthermore, if the "handbrake" hypothesis of KCNQ2 upon SMIT2 is correct, this function may serve to regulate highly localized PIP2 and PIP2-sensitive channels such as KCNQ2, present in the axon initial segment.

Figure 3.1: *KCNQ2 and XE991 strongly inhibit myo-inositol influx through SMIT1 in X. laevis oocytes.*

Mean *myo*-[2-3H(N)]inositol uptake by oocytes injected with cRNA encoding KCNQ2 (Q2), SMIT1 (S1), pore-mutant KCNQ2(G279S), KCNQ3 (Q3), and/or Kv1.1 as indicated. (1+1) and (5+5) indicate ng of RNA injected, each channel. Drug names appear in brackets. Wort = wortmannin. All bars normalized to mean SMIT1 activity alone. N for each group indicated in white text, representing number of injected oocytes over a minimum of three repeated experiments. (A,B,D) values normalized to SMIT1 uptake. (C,E) values normalized to S1/Q2/Q3 uptake. **** P < 0.0001; *** P < 0.001; ** P <0.01; n.s. = not significant

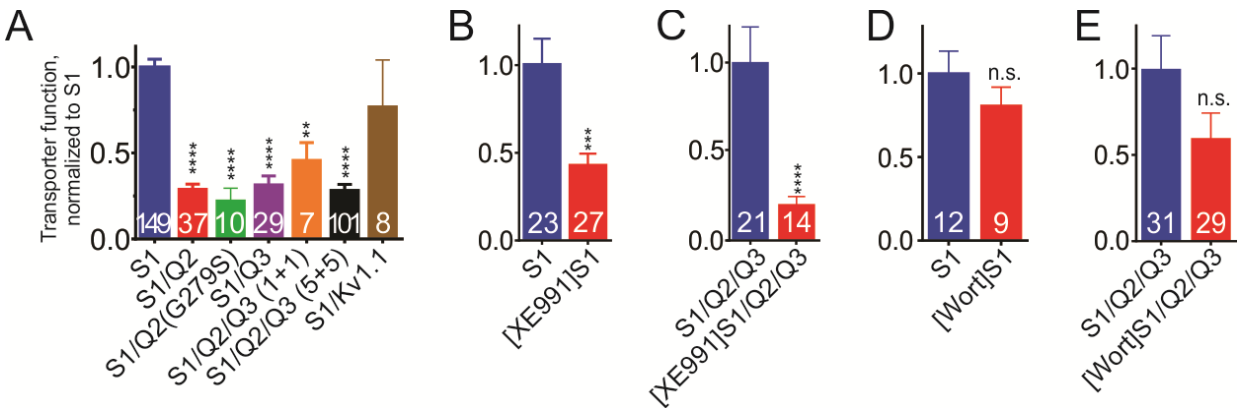

Figure 3.2: *KCNQ2 strongly inhibits myo-inositol influx through SMIT2 in X. laevis oocytes.* Mean *myo*-[2-3H(N)]inositol uptake by oocytes injected with cRNA encoding KCNQ2 (Q2), SMIT2 (S2), pore-mutant KCNQ2(G279S), KCNQ3 (Q3), KCNQ4 (Q4), voltage sensor mutants KCNQ2(R210H) and KCNQ2(R214Q), as indicated. All bars normalized to mean SMIT2 activity alone. N for each group indicated in white text, representing number of injected oocytes over a minimum of two repeated experiments. **** P < 0.0001; *** P < 0.001

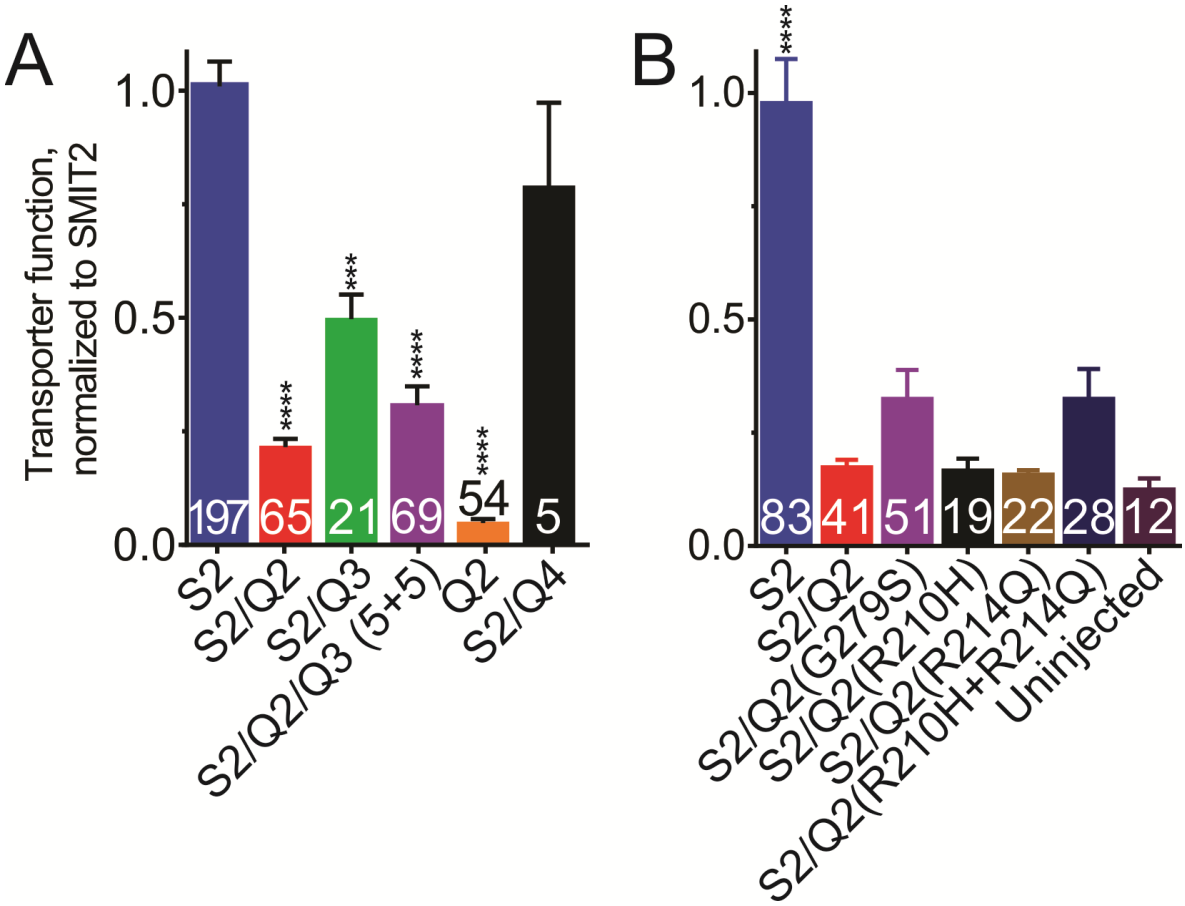

Figure 3.3: *KCNQ2 strongly inhibits myo-inositol influx through SMIT1 in CHO cells.*
Mean *myo*-[2-3H(N)]inositol uptake by CHO cells transfected with cDNA encoding KCNQ2 (Q2), and/or SMIT1 (S1) as indicated. All bars normalized to same-group mean SMIT1 activity alone. N for each group indicated in white text, representing number of transfected dishes over repeated experiments. (A) Statistical comparisons made to SMIT1 baseline. (B) Statistical comparisons made to SMIT1/Q2[DMSO]. **** P < 0.0001; ** P <0.01; * P <0.05

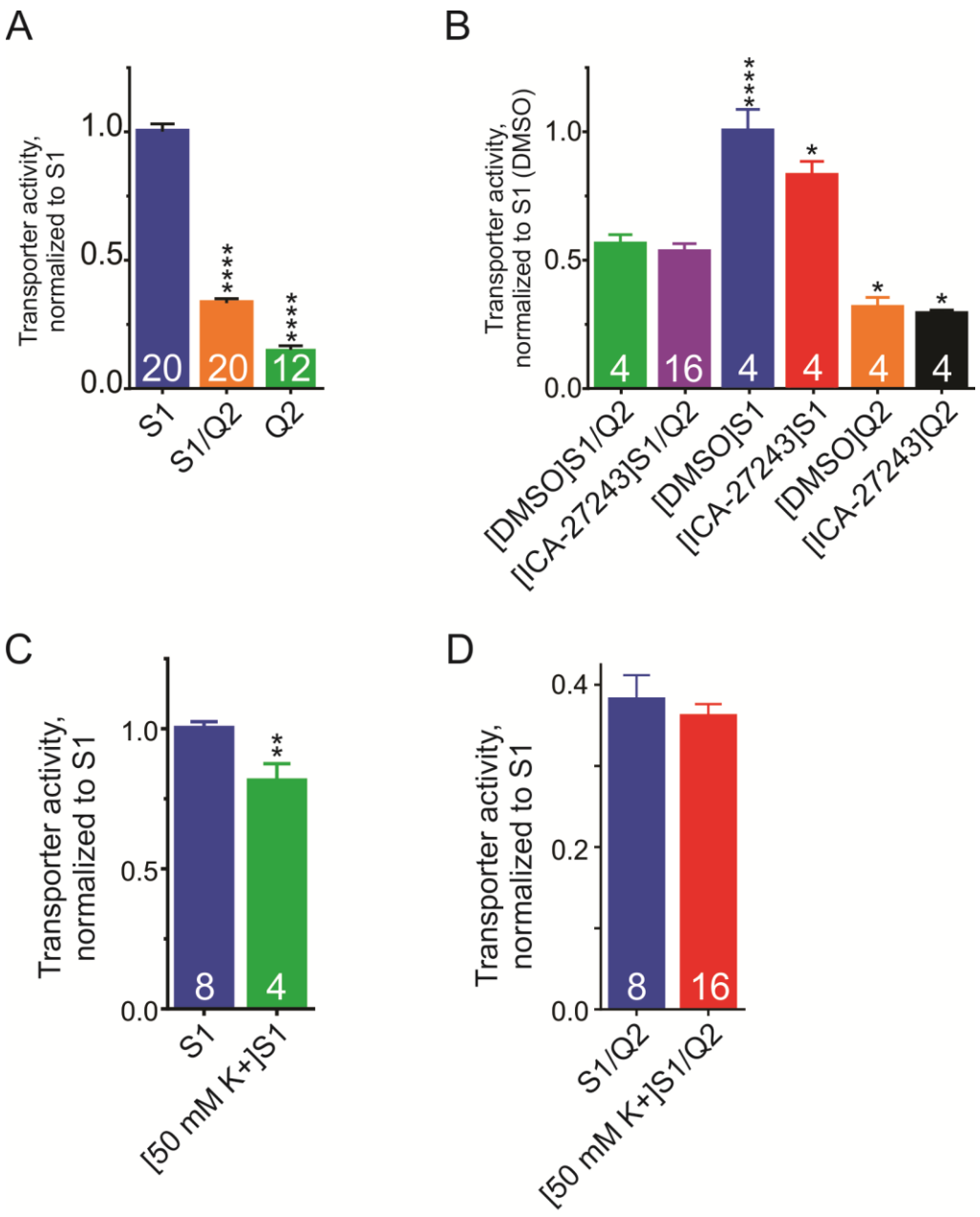

Figure 3.4: *KCNQ2 and SMIT1 expression and surface trafficking are reciprocally altered in CHO cells.*

CHO cells transfected with KCNQ2 and/or SMIT1-FLAG as indicated, blots representative of n=4 transfections. (**A**) *Left:* whole cell lysates and surface fractions of CHO cells transfected with KCNQ2 +/- SMIT1-FLAG, as indicated, immunoblotted for KCNQ2 (Q2). *Right,* quantified data from surface biotinylation experiments. Arrow indicates SMIT1-FLAG band. (**B**) *Left:* whole cell lysates and surface fractions of CHO cells transfected with SMIT1-FLAG +/- KCNQ2, as indicated, immunoblotted for FLAG. *Right,* quantified data from surface biotinylation experiments.

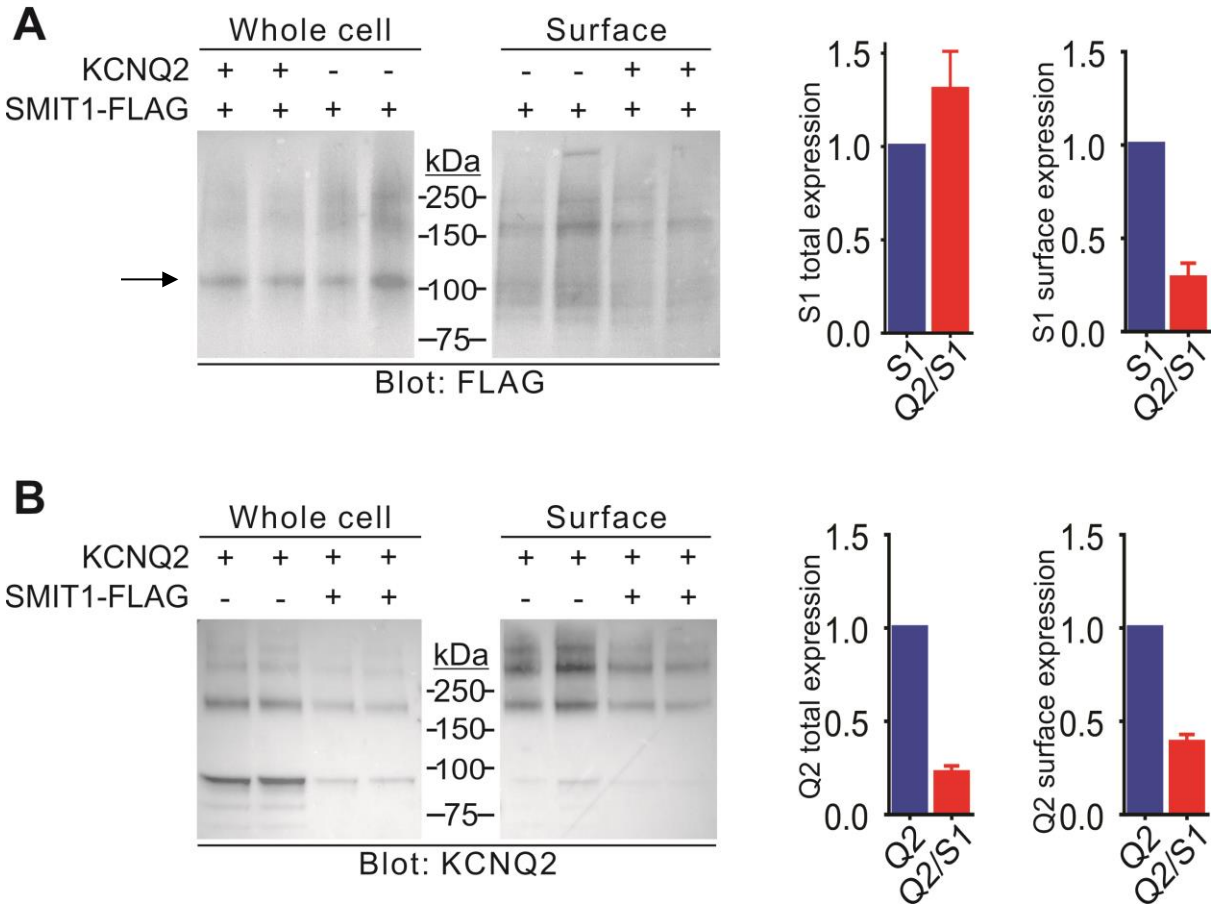

Figure 3.5: *KCNQ2 and SMIT1 form complexes and co-localize at cell periphery in CHO cells.* (**A**) CHO cells transfected with KCNQ2 and/or SMIT1-FLAG as indicated. Proteins were immunoprecipitated (IP) using the indicated antibodies, and immunoblotted (IB) as labeled beneath each blot. Arrows indicate characteristic multimeric SMIT1 or KCNQ2 band patterns as indicated. (**B**) Representative CHO cell transfected with KCNQ2-GFP and SMIT1-FLAG. Cells were stained for FLAG in red channel, KCNQ2-GFP was visualized using native fluorescence in green. DAPI nuclear staining shown in blue. Imaging performed using confocal microscopy. Image is representative of n=3 transfections.

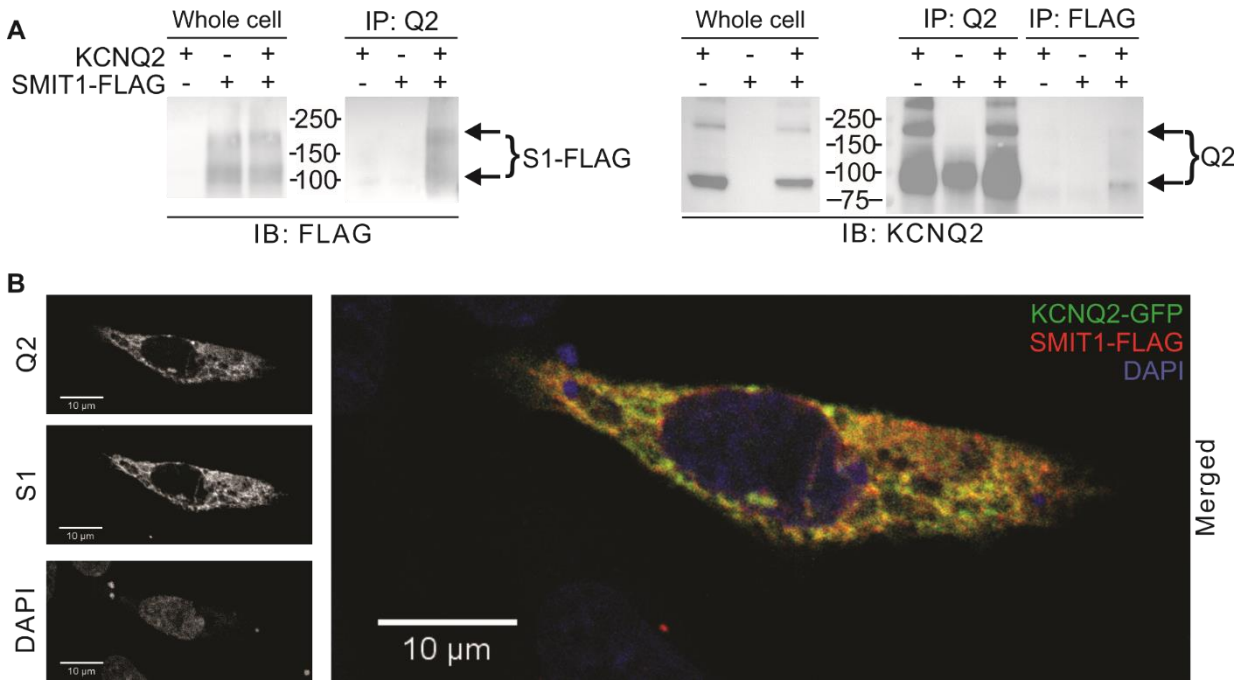

Figure 3.6: *The KCNQ2 pore-forming region is required for binding to SMIT1.*
CHO cells transfected with KCNQ2 fragments and/or SMIT1-FLAG as indicated. All blots representative of n=2 experiments. Immunoprecipitating (IP) antibodies as labeled; FLAG, YFP, or GFP. Immunoblot (IB) as labeled; GFP or FLAG. Red "X" denotes fragments which did not bind to SMIT1. Green check mark signifies SMIT1-binding fragments (**A**) Cytosolic Q2 fragments. *Top,* N-terminal fragment KCNQ2(1-97) does not bind to SMIT1-FLAG. *Bottom*, C-terminal fragment KCNQ2 (321-852) does not bind to SMIT1-FLAG. (**B**) Transmembrane Q2 fragments. *Top,* the N-terminal through S4-S5 linker fragment (KCNQ2(1-224)) does not bind to SMIT1. *Bottom,* the extension of the previous fragment to include the pore-forming S5-S6 region (KCNQ2(1-549)) enables binding to SMIT1-FLAG. (**C**) The S5-S6 pore-forming region fragment (KCNQ2(222-323)) binds to SMIT1-FLAG.

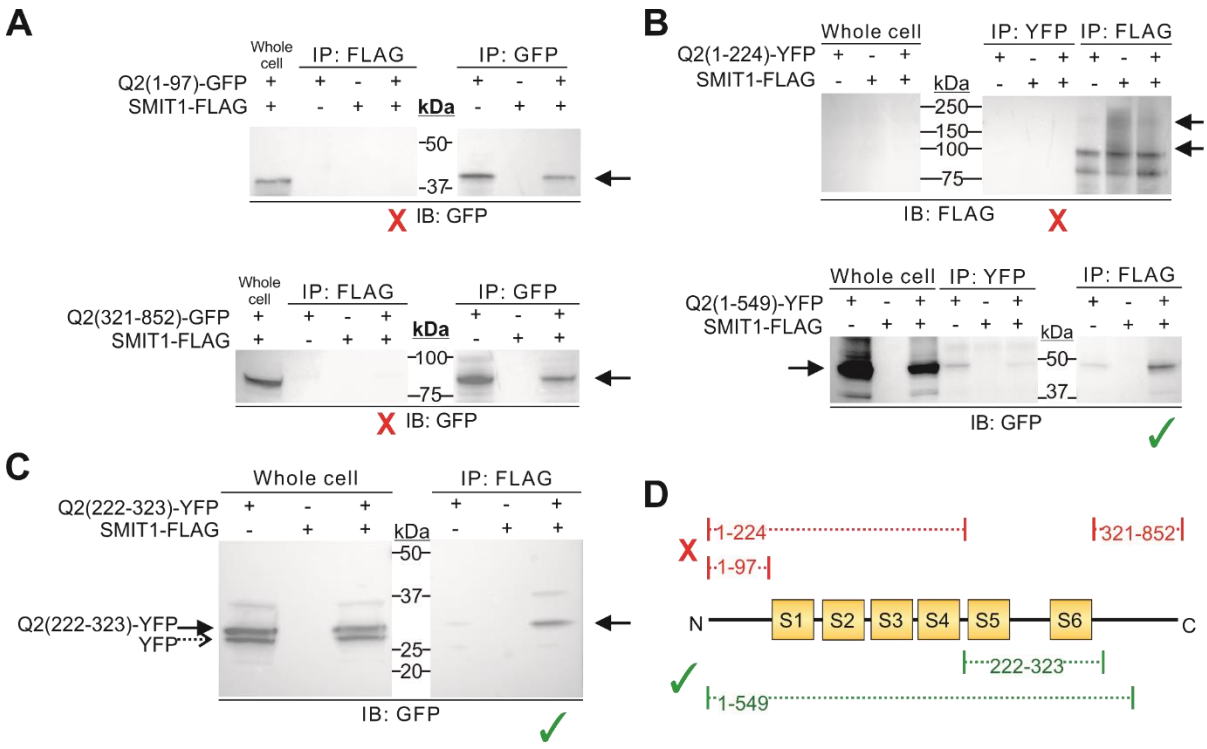

Acknowledgements: We thank N. Hoshi for his generous gift of KCNQ2-YFP, (1-97)-GFP, (321-852)-GFP, and (1-549)-YFP cDNA, and M. Coady for the SMIT2 clone. This work was funded by the American Heart Association (Predoctoral fellowship #14PRE20040013 to DLN) and National Institutes of Health (R01GM115189 to GWA).

References

1. Goldman, A. M. et al. Arrhythmia in heart and brain: KCNQ1 mutations link epilepsy and sudden unexplained death. Sci. Transl. Med. 1, 2ra6 (2009).
2. Wu, D.-M. et al. KCNE2 is colocalized with KCNQ1 and KCNE1 in cardiac myocytes and may function as a negative modulator of I(Ks) current amplitude in the heart. Heart Rhythm 3, 1469–80 (2006).
3. Boini, K. M. et al. Enhanced insulin sensitivity of gene-targeted mice lacking functional KCNQ1. Am. J. Physiol. Regul. Integr. Comp. Physiol. 22–26 (2009). doi:10.1152/ajpregu.90839.2008.
4. Abbott, G. W. et al. KCNQ1, KCNE2, and Na+-coupled solute transporters form reciprocally regulating complexes that affect neuronal excitability. Sci. Signal. 7, ra22 (2014).
5. Neverisky, D. L. & Abbott, G. W. Ion channel–transporter interactions. Crit. Rev. Biochem. Mol. Biol. 9238, 1–11 (2016).
6. Singh, H. et al. MaxiK channel interactome reveals its interaction with GABA transporter 3 and heat shock protein 60 in the mammalian brain. Neuroscience 317, 76–107 (2016).
7. Grahammer, F. et al. The cardiac K+ channel KCNQ1 is essential for gastric acid secretion. Gastroenterology 120, 1363–1371 (2001).
8. Roepke, T. K. et al. Kcne2 deletion uncovers its crucial role in thyroid hormone biosynthesis. Nat. Med. 15, 1186–94 (2009).
9. Purtell, K. et al. The KCNQ1-KCNE2 K+ channel is required for adequate thyroid I- uptake. FASEB J. 26, 3252–3259 (2012).
10. Feng, M. et al. Store-Independent Activation of Orai1 by SPCA2 in Mammary Tumors. Cell 143, 84–98 (2010).
11. Mistry, A. C. et al. The Sodium Chloride Cotransporter (NCC) and Epithelial Sodium Channel (ENaC) Associate. Biochem. J. (2016). doi:10.1042/BCJ20160312
12. Vucic, E. et al. Kir1.1 (ROMK) and Kv7.1 (KCNQ1/KvLQT1) are essential for normal gastric acid secretion: importance of functional Kir1.1. Pflügers Arch. - Eur. J. Physiol. 467, 1457–1468 (2015).
13. Heitzmann, D. et al. Heteromeric KCNE2/KCNQ1 potassium channels in the luminal membrane of gastric parietal cells. J. Physiol. 561, 547–57 (2004).

14. Roepke, T. K. et al. The KCNE2 potassium channel ancillary subunit is essential for gastric acid secretion. J. Biol. Chem. 281, 23740–7 (2006).

15. Cross, B. M., Hack, A., Reinhardt, T. a & Rao, R. SPCA2 regulates Orai1 trafficking and store independent Ca2+ entry in a model of lactation. PLoS One 8, e67348 (2013).

16. Hilgemann, D. W., Feng, S. & Nasuhoglu, C. The complex and intriguing lives of PIP2 with ion channels and transporters. Sci. STKE 2001, re19 (2001).

17. Loussouarn, G. Phosphatidylinositol-4,5-bisphosphate, PIP2, controls KCNQ1/KCNE1 voltage-gated potassium channels: a functional homology between voltage-gated and inward rectifier K+ channels. EMBO J. 22, 5412–5421 (2003).

18. Suh, B.-C. & Hille, B. PIP 2 Is a Necessary Cofactor for Ion Channel Function: How and Why? Annu. Rev. Biophys. 37, 175–195 (2008).

19. Berry, G. T. et al. Loss of murine Na+/myo-inositol cotransporter leads to brain myo-inositol depletion and central apnea. J. Biol. Chem. 278, 18297–302 (2003).

20. Chau, J. F. L., Lee, M. K., Law, J. W. S., Chung, S. K. & Chung, S. S. M. Sodium/myo-inositol cotransporter-1 is essential for the development and function of the peripheral nerves. FASEB J. 19, 1887–9 (2005).

21. Park, J.-Y. et al. Drosophila SLC5A11 mediates hunger by regulating K+ channel activity. Curr. Biol. ?, ? (2016).

22. Cavaliere, S. & Hodge, J. J. L. Drosophila KCNQ channel displays evolutionarily conserved electrophysiology and pharmacology with mammalian KCNQ channels. PLoS One 6, (2011).

23. Dai, G., Yu, H., Kruse, M., Traynor-kaplan, A. & Hille, B. Osmoregulatory inositol transporter SMIT1 modulates electrical activity by adjusting PI(4,5)P 2 levels. Proc. Natl. Acad. Sci. 201606348 (2016). doi:10.1073/pnas.1606348113

24. Gunthorpe, M. J., Large, C. H. & Sankar, R. The mechanism of action of retigabine (ezogabine), a first-in-class K+ channel opener for the treatment of epilepsy. Epilepsia 53, 412–24 (2012).

25. Lange, W. et al. Refinement of the Binding Site and Mode of Action of the Anticonvulsant Retigabine on KCNQ K ς Channels. 75, 272–280 (2009).

26. Rogawski, M. A. Diverse mechanisms of antiepileptic drugs in the development pipeline. Epilepsy Res. 69, 273–294 (2006).

27. Schroeder, B. C., Kubisch, C., Stein, V. & Jentsch, T. J. Moderate loss of function of cyclic-AMP-modulated KCNQ2/KCNQ3 K+ channels causes epilepsy. Nature 396, 687–690 (1998).

28. Panaghie, G. & Abbott, G. W. The Role of S4 Charges in Voltage-dependent and Voltage-independent KCNQ1 Potassium Channel Complexes. J. Gen. Physiol. 129, 121–133 (2007).

29. Zhang, H. et al. PIP2 activates KCNQ channels, and its hydrolysis underlies receptor-mediated inhibition of M currents. Neuron 37, 963–975 (2003).

30. Padilla, K., Wickenden, A. D., Gerlach, A. C. & McCormack, K. The KCNQ2/3 selective channel opener ICA-27243 binds to a novel voltage-sensor domain site. Neurosci. Lett. 465, 138–42 (2009).

31. Wickenden, A. D. et al. N-(6-Chloro-pyridin-3-yl)-3,4-difluoro-benzamide (ICA-27243): A Novel, Selective KCNQ2/Q3 Potassium Channel Activator. Mol. Pharmacol. 73, 977–986 (2007).

32. Roeloffs, R. et al. In Vivo Profile of ICA-27243 [N-(6-Chloro-pyridin-3-yl)-3,4-difluoro-benzamide], a Potent and Selective KCNQ2/Q3 (Kv7.2/Kv7.3) Activator in Rodent Anticonvulsant Models. J. Pharmacol. Exp. Ther. 326, 818–828 (2008).

33. Selyanko, A. A., Hadley, J. K. & Brown, D. A. Properties of single M-type KCNQ2/KCNQ3 potassium channels expressed in mammalian cells. J. Physiol. 534, 15–24 (2001).

34. Schwake, M., Jentsch, T. J. & Friedrich, T. A carboxy-terminal domain determines the subunit specificity of KCNQ K+ channel assembly. EMBO Rep. 4, 76–81 (2003).

35. Kanda, V. a, Lewis, A., Xu, X. & Abbott, G. W. KCNE1 and KCNE2 inhibit forward trafficking of homomeric N-type voltage-gated potassium channels. Biophys. J. 101, 1354–63 (2011).

Discussion and conclusion

The chansporter complexes discussed in this thesis expand the rapidly growing field of channel-transporter complexes. In order to best present the complicated and diverse collection of proteins participating in chansporter complex formation, we will here discuss each known complex sorted by constituent protein class.

K^+ channel-SLC transporter interactions

Physical interaction between KCNQ1-KCNE2 and SMIT1

As shown in Chapter I, phenotypic assessment of the *Kcne2* knockout mouse line lead the Abbott lab to discover that *Kcne2* disruption in mice reduces the seizure threshold and causes behavioral abnormalities[12]. In the CNS, KCNE2 is most highly expressed in the choroid plexus epithelium, the primary site of cerebrospinal fluid (CSF) production and secretion [39], where it regulates KCNQ1 and KCNA3 (Kv1.3) channels. The Abbott lab suspected a role for KCNQ1-KCNE2 in regulating CSF composition. After exhausting other hypothesis-based alternatives, they performed unbiased mass spectrometry-based metabolomics analysis of the CSF and found that *Kcne2* deletion altered the concentration of just one identifiable CSF metabolite: *myo*-inositol. The Abbott lab determined that, under normal conditions, KCNQ1-KCNE2 channels physically interact with SMIT1 to form chansporter complexes in which the two protein classes reciprocally regulate one another. KCNQ1 doubled the *myo*-inositol uptake activity of SMIT1, but addition of KCNE2 to the complex had the opposite effect, inhibiting SMIT1. SMIT1 augmented the activity of both KCNQ1 channels and KCNQ1-KCNE2 channels.

Early attempts to determine the mechanism for channel-transporter feedback yielded interesting but not yet definitive results. Co-expression of KCNQ1 with SMIT1 roughly doubled SMIT1 activity versus SMIT1 alone. One might surmise that the increase in SMIT1 activity is a product of the potassium efflux through KCNQ1 channels, thereby increasing the electrical gradient to favor sodium-coupled *myo*-inositol transport. Consistent with this, Abbott and colleagues found that when co-expressed with KCNQ1, SMIT1 function was suppressed by XE991, a pore-binding KCNQ channel-blocker [12]. These data provided a basis for targeting transporter activity through a novel drug approach: ion channel manipulation. In addition, they also suggested that K^+ flux through KCNQ1 is seemingly important for augmentation of SMIT1 activity. However, the channel-blocking effect is specific to KCNQ1-SMIT1, because when the non-interacting and non-augmenting KCNQ4 and SMIT1 were co-expressed, XE991 had no effect, even though XE991 inhibits KCNQ4, as a pan-KCNQ blocker. This, then, suggests that merely having K^+ flux through a channel in the same cell is not sufficient to augment SMIT1 activity – arguing that either the electrical gradient hypothesis is incorrect, or the effect requires close physical proximity between channel and transporter (e.g. physical interaction).

Further suggesting that the chansporter inter-subunit cooperation is more complex than merely electrical gradient enhancement, Abbott and colleagues found unexpected results when studying the KCNQ1-R231A S4 mutant that locks the voltage sensor of the channel into an open, or "on", state, forming a constitutively active channel [95]. Following the increased driving force hypothesis, this would be theorized to increase Na^+-linked *myo*-inositol influx, yet the addition of KCNQ1-R231A to SMIT1 greatly *inhibits* transporter

function[12]. Within the context of the driving force hypothesis these findings are in diametric opposition to each other, and instead suggest the possibility that KCNQ1 voltage sensor conformation, independent of actual conductance, might influence SMIT1 activity. This could also be the reason that KCNE2 inhibits *myo*-inositol uptake of KCNQ1-SMIT1 complexes, because KCNE2 also holds KCNQ1 open, although KCNE2 also greatly reduces outward current through KCNQ1 despite favoring its open state. Future investigations will be targeted at understanding exactly how KCNQ1 augments SMIT1 and NIS activity and whether there are underlying mechanistic commonalties. Intriguingly, we also found that KCNQ1 and SMIT2 functionally interact, and that SMIT2 inhibits KCNQ1 activity, but we do not yet know the mechanistic basis for these effects either [12].

Physical interaction between SMIT1-KCNQ2, and functional effects of KCNQ2 and/or KCNQ3 on SMIT1 and SMIT2

As demonstrated in Chapter II, M-channel constituents KCNQ2 and KCNQ3 each independently, and in presumed heterotetramers, inhibit SMIT1 and SMIT2 *myo*-inositol uptake *in vitro.* These findings are highly unexpected given the Abbott lab's previous study which found KCNQ1-SMIT1 complexes to reciprocally double each other's function[12]. These importance of these findings are bolstered by the very recent findings on KCNQ2-SMIT1 reported by Hille and colleagues, who demonstrated that SMIT1 and *myo*-inositol can modulate KCNQ2 function via alterations to intracellular PIP_2 levels[91]. In our present studies, however, reductions in PIP_2 via wortmannin administration did not alter KCNQ2-KCNQ3-complexed SMIT1 *myo*-inositol uptake, suggesting that PIP_2 levels may be a one-

way form of communication to alter KCNQ2 function, but have not yet been demonstrated to act as a feedback loop linking SMIT1 and KCNQ2 function reciprocally.

KCNQ2 double voltage sensor mutant R210H+R214Q, as well as the potassium-impermeable KCNQ2(G279S) selectivity filter mutant, each exhibited modest, though not statistically significant effects, on KCNQ2-mediated inhibition of SMIT2 function. In concert with the KCNQ1(R231A) voltage sensor mutant discussed in Chapter I, these data suggest the possibility of a structurally-linked regulation of transporter activity by channel conformation.

Given the vital importance of M-channel formation and function in neurons, it is tempting to speculate on the nature of KCNQ2-KCNQ3-SMITx complex formation within the brain. *Kcnq2* and *Slc5a3* deletions are each fatal (though the latter may be ameliorated by supplementing mother and pup with additional *myo*-inositol), each hypothesized to exert their fatal effects by respiratory distress. The respiratory distress may be a product of neural hyperexcitability due to excess catecholamine release from uninhibited adrenal chromaffin cells[24,67]. We hypothesize that overlapping nature of these syndromes belies KCNQ2-SMIT1 complex formation *in vivo*, however further studies of subcellular localization will be required to determine with more precision where the complexes are forming.

Functional interaction between KCNQ1-KCNE2 and NIS

The importance of KCNQ1-KCNE2 complexes for efficient thyroid hormone synthesis were first reported in 2009 when, together with the Carrasco lab, Roepke and colleagues discovered that *Kcne2*-/- mice are hypothyroid [38]. Using positron emission tomography they found that disruption of KCNQ1-KCNE2 complexes, discovered in thyroid epithelial cells, impairs iodide accumulation in the thyroid gland [38]. Subsequently, the Lang group confirmed this, using *Kcnq1*-/- mice[21]. It was later delineated which of the processes involved in thyroid iodide accumulation (focusing on iodide uptake versus organification) was disrupted by *Kcne2* deletion, discovering it to be iodide uptake by NIS[10].

In the thyroid, I^- uptake is mediated by NIS (Fig. 1.3)[103]. NIS-mediated I^- uptake can be strongly inhibited by the KCNQ1-selective antagonist [3*R*,4*S*]-chromanol 293B. This effect was selective to I^- transport, without directly altering organification, and occurred both *in vivo* (in the mouse), and *in vitro* (in the rat thyroid cell line, FRTL-5) [10]. The effects of chromanol 293B on I^- transport are only apparent when KCNQ1-KCNE2 and NIS are co-expressed, providing strong support for KCNQ1-KCNE2 mediation of NIS function.

Regarding the mechanism of KCNQ1-NIS interaction, there is not yet have confirmation of a physical interaction, although complex formation seems likely. The KCNQ1-KCNE2 channel is constitutively active at weakly negative potentials because KCNE2 modifies the voltage-dependent gating of KCNQ1 such that its current voltage relationship is linear rather than outwardly rectifying[34]. The related β subunit KCNE3 achieves a similar effect on KCNQ1 by directly locking its VSD in the activated position via acidic residues in the membrane proximal KCNE3 extracellular segment [95,104], but this mechanism has not yet been

confirmed for KCNQ1-KCNE2 (which is a more difficult channel to study, because KCNE2 also shrinks macroscopic current density). One might predict that the relatively constant outward K^+ flux that KCNQ1-KCNE2 would be predicted to provide in thyroid cells at weakly negative potentials might facilitate NIS function by enhancing the electrical gradient required for sodium entry (with other pumps etc. redistributing Na^+ and K^+ ions to take care of the chemical part of the gradient), yet the NIS-related sodium-dependent monocarboxylate transporter (SMCT) is not affected by KCNQ1-KCNE2 status [10], possibly suggesting against the electrical gradient hypothesis. However, it may be that for the outward movement of K^+ through KCNQ1-KCNE2 to have any effect on sodium-dependent transporters, they need to be localized close to one another, or even tightly coupled; a hypothesis to be tested in the future. Either way, KCNQ1-KCNE2 is critical in the thyroid for its regulation of NIS activity, and an excellent example of biologically important functional interaction between an ion channel and a transporter. Accordingly, disruption of *Kcnq1* or *Kcne2* genes causes hypothyroidism, and in the case of *Kcne2* other phenotypic hallmarks of insufficient THs including dwarfism, alopecia, and cardiomegaly [21,38]. These findings exemplify the critical functions of chansporter crosstalk, if not necessarily physical interaction, *in vivo*. Although KCNQ1-NIS physical interaction seems likely, complex formation has yet to be proven.

Physical interaction between MaxiK and GAT3

Very recently, Singh and colleagues uncovered an additional K^+ channel-transporter interaction in the brain [79]. MaxiK channels – voltage- and Ca^{2+}-activated channels named for their large conductance – were demonstrated to physically interact with GABA

transporter 3 (GAT3). As both GAT3 and MaxiK channels are localized in glia, the authors propose that the complexes may serve to limit GABA release, although no functional experiments have been published to date on this very recently discovered chansporter complex. Interestingly, GAT3 is encoded by *SLC6A11* – adding yet another member of the *SLC* superfamily to the list of transporters regulated functionally and/or physically by K^+ channels.

Ion channel-ATPase interactions

Several examples are known of ion channels functionally interacting with transporters in the transmembrane ATPase family (and to our knowledge just one known case of physical interaction). Transmembrane ATPases are primary active transporters that use ATP hydrolysis to provide the energy to transport ions up their electrochemical gradient. In many cell types, ion channels and pumps are involved in activities such as maintaining ion homeostasis, that require one or more of the proteins to support function of one or more of the others. One broad example is the Na^+/K^+-ATPase. This ubiquitous protein eliminates 3 Na^+ ions while bringing in 2 K^+ ions, thus helping to restore the appropriate concentrations of K^+ and Na^+ ions, and also the negative membrane potential, following action potentials in excitable cells so that the cell is ready for future action potentials. Here, however, we will focus on just two contrasting examples. First we discuss facilitation of gastric H^+/K^+-ATPase activity by K^+ channels. As one of many examples of channels cooperating with pumps to ensure favorable cellular/extracellular ion balance or specific ion secretion but probably without the necessity for direct physical coupling, we focus on this example because it involves KCNQ1, which we also discussed above in the context of its ability to co-

assemble with the SLC transporters. Second, we cover physical interaction of the unusual Orai1 Ca^{2+} channel with the SPCA2 ATPase – we chose this example because it involves formation of one of the thus-far few known examples of a macromolecular channel-transporter complex.

Functional interactions between K^+ channels and the gastric H^+/K^+-ATPase

Under normal conditions, gastric acid secretion is coordinated by a small symphony of cellular events. In response to gastric parietal cell stimulation, H^+/K^+-ATPase is trafficked to the apical surface of the acid-secreting cells where it can begin the process of H^+ efflux in exchange for K^+ influx[105]. The gastric acid secretion process would stagnate here, were it not for the presence of potassium-normalizing K^+ channels KCNQ1–KCNE2[106] and KCNJ1 (*ROMK*)[85]. Together, these channels coordinate the "resetting" of intracellular and luminal K^+ levels to enable prolonged H^+/K^+-ATPase function and further gastric acid secretion. Thus, in addition to its roles in the thyroid and choroid plexus, KCNQ1–KCNE2 acts as a "team player" within the parietal cells of the gastric glands of the stomach. Here, the KCNQ1–KCNE2 complex acts to counterbalance and functionally reset the high intracellular K^+ levels accumulated by the H^+/K^+-ATPase (Fig4.1)[8,29,87]. Although KCNQ1 channels are typically inhibited by extracellular protons, the formation of the KCNQ1–KCNE2 complex enables constitutive activation of the channel as well as an augmentation of the channel's current and function at low extracellular pH [86,107]. This last attribute is critical to maintaining the function of this channel in the very low pH of the stomach. Gastric acid secretion can be strongly inhibited by application of the KCNQ1 blocker chromanol 293B [22], thereby inhibiting potassium efflux and maintaining a hyperpolarized parietal cell by way

of intracellular potassium accumulation. Also crucial is that KCNE2 helps ensure that KCNQ1 is localized at the apical membrane where it can assist the H^+/K^+-ATPase. Deletion of *Kcne2* results in aberrant localization of KCNQ1 to the basolateral membrane of parietal cells, because in this pathologic state KCNE3 is upregulated and hijacks KCNQ1, taking it to the wrong side of the cell and disenabling it from assisting the H^+/K^+-ATPase. However, even concomitant *Kcne3* deletion does not restore gastric acid secretion in *Kcne2*-/- mice, illustrating the importance of the effects of KCNE2 on KCNQ1 gating and pH sensitivity for the parietal cell function of KCNQ1[108] 2011. It is of no surprise, then, that *Kcne2* and *Kcnq1* knockout mice each display profound hypochlorhydria and altered gastric morphology[8,87].

KCNJ1, also known as $K_{ir}1.1$, is an inward-rectifier potassium channel comprised of intracellular N- and C-terminals, two transmembrane segments (M1, M2) and one pore-forming region (H5). Like Kv channels, four of the KCNJ1 proteins must tetramerize to form a membrane protein with a functional pore. KCNJ channels are regulated by multiple pathways, including protein kinase A (PKA), protein kinase C (PKC), intracellular pH and PIP_2[109]. Well-known for its role in potassium recycling in the kidney, KCNJ1 is also expressed in gastric parietal cells[85,109]. Like KCNQ1–KCNE2, KCNJ1 channels on the parietal cell apical membrane appear to help facilitate gastric acid secretion by recycling K^+ for later participation in ion exchange by the H^+/K^+-ATPase. Selective blockade of KCNJ1 channels by application of K_{ir}-selective blocker tertiapin-Q (TPNQ), and/or application of KCNQ blocker XE991, to the gastric lumen suggests the requirement of both KCNQ1-KCNE2 and KCNJ1 channel function for maintenance of normal gastric acid secretory responses. These

findings are validated in *Kcnj1* knockout mouse studies, which demonstrated reductions in gastric acid secretion independent of any other developmental or morphological changes to the stomach[85]. Likewise, Roepke and colleagues previously showed that although *Kcne2*−/− mice exhibit abnormal parietal cell morphology in addition to achlorhydria, *Kcne2*+/- mice exhibit hypochlorhydria in the absence of morphological changes to parietal cells, suggesting KCNQ1-KCNE2 channels are directly involved in supporting H^+/K^+-ATPase function rather than their disruption causing achlorhydria indirectly via disruption of cell architecture[87].

H^+/K^+-ATPase is not a member of the *SLC* gene superfamily, and in fact functions as an antiporter – transporting H^+ out of the cell, to participate in gastric acid formation, in exchange for drawing K^+ into the cell. This pump operates in stark contrast to the SLC5A proteins which operate as symporters, drawing both sodium and their substrate (MI, glucose, etc.) into the cell. Although crosstalk between K^+ channels and the gastric H^+/K^+-ATPase has been functionally demonstrated, physical interaction of the transporter with KCNQ1–KCNE2 or any of the channels discussed above has not. In the case of KCNQ1–KCNE2, it is considered unlikely that it operates by direct physical interact with H^+/K^+-ATPase, because while apical membrane expression of the latter is thought to occur only after signaling by secretagogues (which stimulate trafficking of H^+/K^+-ATPase-containing vesicles to the apical membrane), KCNQ1–KCNE2 is thought to reside in the apical membrane at rest – although this has not yet been fully investigated.

Physical interaction between Orai1 and SPCA2

Previous research has demonstrated Orai1 to be a vital component of store-operated calcium channel activation[110]. Orai1 channels (Figure 1.1A), which consist of four-transmembrane segment proteins forming a functional hexamer at the plasma membrane (PM), are activated by the depletion of internal calcium stores, generally referred to as a "store-operated" mechanism [110,111]. The activity of these channels is greatly increased when co-expressed with STIM proteins – endoplasmic reticulum (ER)-bound Ca^{2+} store sensors that possess no channel activity on their own [110,112]. Together, the STIM1-Orai1 complex forms a unique Ca^{2+} sensor-channel pairing between the PM and ER [110]. Perturbations to Orai channel function may cause diverse problems, including immune deficiency [113] and myopathy [114].

Secretory pathway Ca^{2+}-ATPase isoform 2 (SPCA2), encoded by (*ATP2C2*) is a P-type calcium transporter localized to the Golgi [115]. The SPCA proteins, spanning 10 transmembrane segments, use ATP to transport Ca^{2+} and Mn^{2+} from the cytoplasm and into the Golgi and are critical in their role as Ca^{2+} signal terminators [83,116]. Although SPCA1 is ubiquitously expressed, SPCA2 expression is restricted to brain and secretory and absorptive epithelial tissues [88,117] and is highly upregulated in the mammary epithelium during lactation [83]. Recently, SPCA2 has been highlighted as a critical component in human breast tissue and tumorigenicity, by way of intracellular Ca^{2+} level regulation [83]. In the same study, SPCA2 was demonstrated to form a complex with calcium channel Orai1 (Figure 5 B) [83]. When physically associated, SPCA2-Orai1 complexes enable Ca^{2+} signaling independent of Ca^{2+} stores, STIM sensors, or SPCA2 pump activity, revealing a previously

unknown mechanism of Orai1 operation [83]. These findings provide the first evidence for non-K^+ channel participation in chansporter complex crosstalk or formation.

Conclusions

It is striking that many of the transporters demonstrated to complex with Kv channels are, to date, from the *SLC* gene families. In addition to SMIT1, we found that SMIT2 and SGLT1 (*SLC5A11* and *SLC5A1,* respectively) exerted effects when co-expressed with KCNQ1 [12], however in-depth characterization remains to be pursued. Our most recent studies have shown additional Kv, KCNQ2 and KCNQ3, to functionally interact with *SLC5A* members SMIT1 and SMIT2, and, in the case of KCNQ2-SMIT1, even form physical complexes. Further exploration of *SLC* members is warranted and may yield additional Kv-SLC complexes.

The potential connections between SMIT1, states of mania, inositol status, and lithium present a tantalizing cluster of biological phenomena. We know that both SMIT1 mRNA levels and brain inositol levels are acutely responsive to lithium treatment, though the latter is of little surprise given the well-established use of lithium to inhibit IMPase in many *in vitro* experiments[118]. We also know that inositol levels roughly correspond to manic symptom presentation in humans[53]. Together, these data suggest the possibility of altered inositol pathways constituting elements of the etiology of manic disorders, although there have been no pharmaceutical interventions to test or leverage this concept aside from lithium[119,120]. Given the ability of ion channel-targeted drugs to manipulate co-assembled SMIT1 activity, as described in this thesis, it is interesting to consider the possibility that

novel interventions for mania could come in the form of re-purposed, or structurally modified, ion channel drugs. However, it is important to remember that many potassium channels, and KCNQ1 in particular, are widely expressed and fulfil a wide spectrum of physiological roles. Targeting a Kv such as KCNQ1 would therefore present significant challenges with respect to side effects. Increased specificity might potentially be achieved if a drug could target only chansporter complexes, particularly if they could also be tailored for specific transporter-channel-KCNE subunit combinations.

Perhaps most critically, the findings discussed here demonstrate the emergence of a potentially broad paradigm in cell signaling, that of direct channel-transporter crosstalk and co-regulation facilitated by direct physical coupling. There are a number of research directions that should now be pursued to flesh out this idea. First, the scope of chansporter complexes that exist *in vivo* must be catalogued in order to define the generality of this new principle. Second, mechanistic questions must be addressed, including how channels can augment transporter function, what signaling information is exchanged within chansporter complexes, what is the directionality of this information, and why the necessity for direct interaction – is it merely proximity to limit the distance through which ions must diffuse, or are their intimate interactions between the moving parts of channels and transporters that convey information of a higher order than solely ion movement?

Figure 4.1: *Channel-transporter crosstalk in gastric parietal cells facilitates gastric acid secretion.*

Sodium-hydrogen exchanger (NHE) draws Na+ into the cell and expels H^+. The sodium–potassium ATPase (Na^+/ K^+) releases Na^+ and draws in K^+. $Na^+/K^+/Cl^-$ cotransporter 1 (NKCC1) draws Na^+,K^+ and Cl^- into the cell. The anion exchanger (AE) exchanges Cl^- and HCO_3^-. H^+/K^+-ATPase (HKA) expels H^+ into the stomach lumen accompanied by an unknown Cl^- channel or transporter to participate in gastric acid formation. KCNQ1–KCNE2 (Q1-E2) and KCNJ1 channels expel potassium from the cell in order to ''reset'' the high intracellular K^+ accumulated by HKA activity.

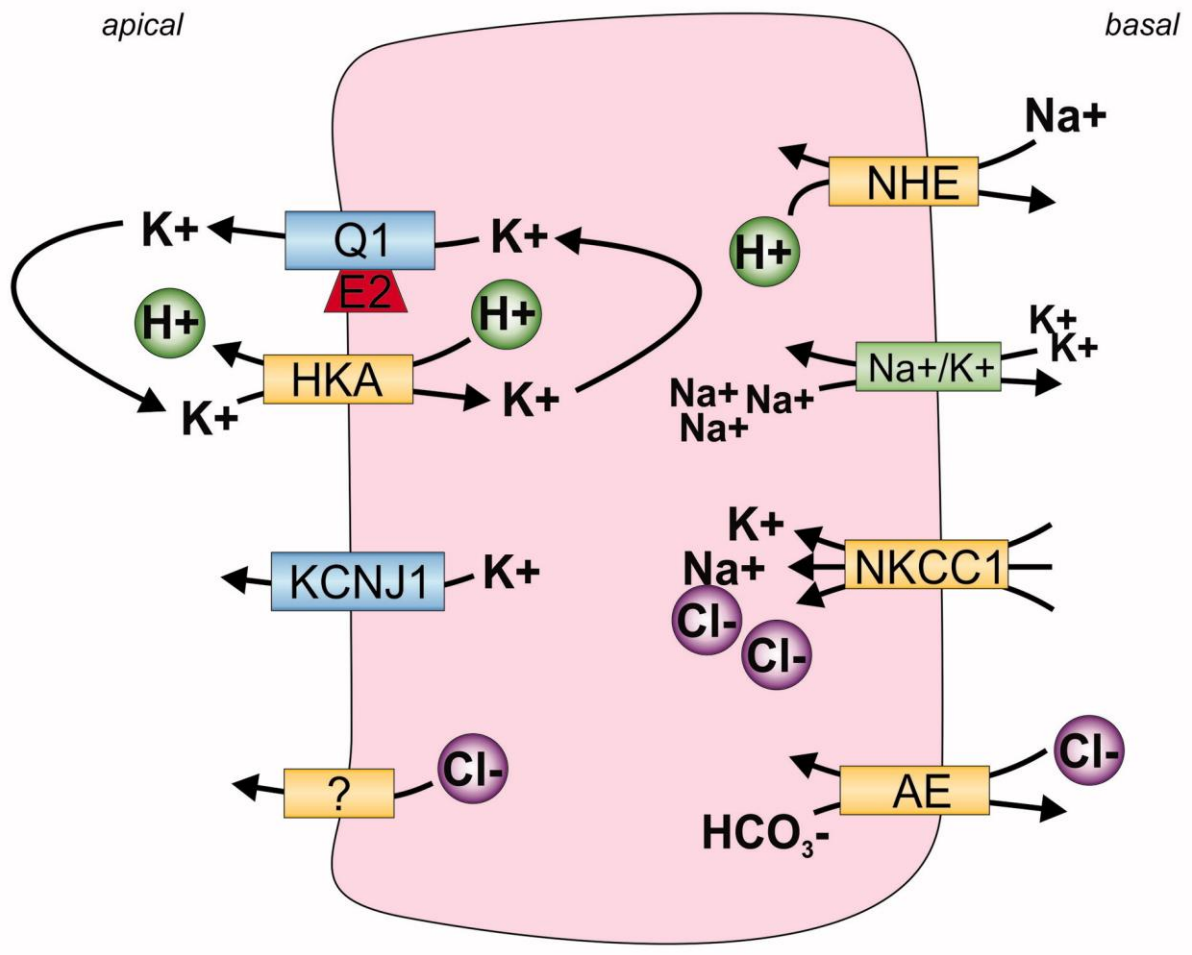

REFERENCES

1. Abbott, G. W. et al. KCNQ1, KCNE2, and Na+-coupled solute transporters form reciprocally regulating complexes that affect neuronal excitability. Sci. Signal. 7, ra22 (2014).
2. Roepke, T. K. et al. KCNE2 forms potassium channels with KCNA3 and KCNQ1 in the choroid plexus epithelium. FASEB J. 25, 4264–73 (2011).
3. Panaghie, G. & Abbott, G. W. The Role of S4 Charges in Voltage-dependent and Voltage-independent KCNQ1 Potassium Channel Complexes. J. Gen. Physiol. 129, 121–133 (2007).
4. Dai, G., Yu, H., Kruse, M., Traynor-Kaplan, A. & Hille, B. Osmoregulatory inositol transporter SMIT1 modulates electrical activity by adjusting PI(4,5)P 2 levels. Proc. Natl. Acad. Sci. 201606348 (2016). doi:10.1073/pnas.1606348113
5. Watanabe, H. et al. Disruption of the epilepsy KCNQ2 gene results in neural hyperexcitability. J. Neurochem. 75, 28–33 (2000).
6. Berry, G. T. et al. Loss of murine Na+/myo-inositol cotransporter leads to brain myo-inositol depletion and central apnea. J. Biol. Chem. 278, 18297–302 (2003).
7. Roepke, T. K. et al. Kcne2 deletion uncovers its crucial role in thyroid hormone biosynthesis. Nat. Med. 15, 1186–94 (2009).
8. Frohlich, H. et al. Hypothyroidism of gene-targeted mice lacking Kcnq1. Pflugers Arch. 461, 45–52 (2011).
9. Purtell, K. et al. The KCNQ1-KCNE2 K+ channel is required for adequate thyroid I-uptake. FASEB J. 26, 3252–3259 (2012).
10. Dai, G., Levy, O. & Carrasco, N. Cloning and characterization of the thyroid iodide transporter. Nature 379, 458–460 (1996).
11. Tinel, N. KCNE2 confers background current characteristics to the cardiac KCNQ1 potassium channel. EMBO J. 19, 6326–6330 (2000).
12. Choi, E. & Abbott, G. W. A shared mechanism for lipid- and beta-subunit-coordinated stabilization of the activated K+ channel voltage sensor. FASEB J. 24, 1518–1524 (2010).

13. Singh, H. et al. MaxiK channel interactome reveals its interaction with GABA transporter 3 and heat shock protein 60 in the mammalian brain. Neuroscience 317, 76–107 (2016).
14. Hersey & Sachs. Gastric acid secretion. Physiol. Rev. 75, 155–189 (1995).
15. Roepke, T. K. et al. KCNE2 forms potassium channels with KCNA3 and KCNQ1 in the choroid plexus epithelium. FASEB J. 25, 4264–73 (2011).
16. Vucic, E. et al. Kir1.1 (ROMK) and Kv7.1 (KCNQ1/KvLQT1) are essential for normal gastric acid secretion: importance of functional Kir1.1. Pflügers Arch. - Eur. J. Physiol. 467, 1457–1468 (2015).
17. Abbott, G. W. Biology of the KCNQ1 Potassium Channel. New J. Sci. 2014, 1–26 (2014).
18. Lee, M. P. et al. Targeted disruption of the Kvlqt1 gene causes deafness and gastric hyperplasia in mice. J. Clin. Invest. 106, 1447–1455 (2000).
19. Roepke, T. K. et al. The KCNE2 potassium channel ancillary subunit is essential for gastric acid secretion. J. Biol. Chem. 281, 23740–7 (2006).
20. Heitzmann, D. et al. KCNE Beta Subunits Determine pH Sensitivity of KCNQ1 Potassium Channels. Cell. Physiol. Biochem. 19, 21–32 (2007).
21. Heitzmann, D. et al. Heteromeric KCNE2/KCNQ1 potassium channels in the luminal membrane of gastric parietal cells. J. Physiol. 561, 547–57 (2004).
22. Grahammer, F. et al. The cardiac K+ channel KCNQ1 is essential for gastric acid secretion. Gastroenterology 120, 1363–1371 (2001).
23. Roepke, T. K. et al. Genetic dissection reveals unexpected influence of subunits on KCNQ1 K+ channel polarized trafficking in vivo. FASEB J. 25, 727–736 (2011).
24. Huang, C. L. Regulation of ROMK trafficking and channel activity. Curr. Opin. Nephrol. Hypertens. 10, 693–8 (2001).
25. Soboloff, J. et al. Orai1 and STIM reconstitute store-operated calcium channel function. J. Biol. Chem. 281, 20661–20665 (2006).
26. Prakriya, M. et al. Orai1 is an essential pore subunit of the CRAC channel. Nature 443, 230–233 (2006).

27. Mercer, J. C. et al. Large Store-operated Calcium Selective Currents Due to Co-expression of Orai1 or Orai2 with the Intracellular Calcium Sensor, Stim1. J. Biol. Chem. 281, 24979–24990 (2006).
28. Feske, S. et al. A mutation in Orai1 causes immune deficiency by abrogating CRAC channel function. Nature 441, 179–185 (2006).
29. Nesin, V. et al. Activating mutations in STIM1 and ORAI1 cause overlapping syndromes of tubular myopathy and congenital miosis. Proc. Natl. Acad. Sci. U. S. A. 111, 4197–4202 (2014).
30. Vanoevelen, J. et al. The secretory pathway Ca2+/Mn2+-ATPase 2 is a Golgi-localized pump with high affinity for Ca2+ ions. J. Biol. Chem. 280, 22800–22808 (2005).
31. Durr, G. et al. The medial-Golgi Ion Pump Pmr1 Supplies the Yeast Secretory Pathway with Ca2+ and Mn2+ Required for Glycosylation, Sorting, and Endoplasmic Reticulum-Associated Protein Degradation. Mol. Biol. Cell 9, 1149–1162 (1998).
32. Feng, M. et al. Store-Independent Activation of Orai1 by SPCA2 in Mammary Tumors. Cell 143, 84–98 (2010).
33. Cross, B. M., Hack, A., Reinhardt, T. a & Rao, R. SPCA2 regulates Orai1 trafficking and store independent Ca2+ entry in a model of lactation. PLoS One 8, e67348 (2013).
34. Xiang, M., Mohamalawari, D. & Rao, R. A novel isoform of the secretory pathway Ca2+,Mn 2+-ATPase, hSPCA2, has unusual properties and is expressed in the brain. J. Biol. Chem. 280, 11608–11614 (2005).
35. Willmroth, F. et al. Sodium-myo-inositol co-transporter (SMIT-1) mRNA is increased in neutrophils of patients with bipolar 1 disorder and down-regulated under treatment with mood stabilizers. Int. J. Neuropsychopharmacol. 10, 63–71 (2007).
36. Davanzo, P. et al. Decreased anterior cingulate myo-inositol/creatine spectroscopy resonance with lithium treatment in children with bipolar disorder. Neuropsychopharmacology 24, 359–69 (2001).
37. Harwood, a J. Lithium and bipolar mood disorder: the inositol-depletion hypothesis revisited. Mol. Psychiatry 10, 117–26 (2005).
38. Atack, J. R., Broughton, H. B. & Pollack, S. J. Inositol monophosphatase — a putative target for Li+ in the treatment of bipolar disorder. Trends Neurosci. 18, 343–349 (1995).